

**THE ROLE OF LIPOPROTEIN LIPASE IN THE GROWTH AND  
PROGRESSION OF BREAST CANCER**

by © Alexandria J. Tobin

A thesis submitted to the School of Graduate Studies in partial fulfillment of the  
requirements for the degree of

**Master of Science**

**Department of Biochemistry, Faculty of Science**

Memorial University of Newfoundland

**August 2020**

St. John's Newfoundland and Labrador

## **Abstract**

Lipoprotein lipase (LPL) is an extracellular lipase that hydrolyzes triglycerides and phospholipids from circulating lipoproteins to promote the delivery of hydrolyzed lipids to cells. LPL is highly expressed in the adipose tissue surrounding breast tumors and reported to be expressed in breast cancer cells. The hydrolysis products generated by LPL are used by cells as components of the cell membrane, as an energy supply, and as signaling molecules. Therefore, the presence of LPL on or around cancer cells may contribute to the growth and progression of breast cancer tumors. We hypothesized that the hydrolysis products generated by LPL from lipoproteins can promote increased cell viability and pro-inflammatory cytokine secretion from breast cancer cells. My results show that the lipoprotein hydrolysis products generated by LPL from total lipoproteins significantly increased the metabolic activity of multiple breast cancer cell lines and the normal MCF10A breast cell line. Using cytokine arrays, a significant increase in the secretion of some cytokines and chemokines of 2- to 10-fold was observed in MDA-MB-231 cells treated with lipoprotein hydrolysis products compared to control. In contrast, MCF-7 cells showed a decrease in the secretion of fewer cytokines. These results were verified by ELISA. The results of this study provide information on how LPL within the tumor microenvironment could affect breast cancer cell viability to potentially influence the progression of breast cancer.

## **Acknowledgements**

First, I would like to thank my supervisors Dr. Robert Brown and Dr. Sherri Christian for their constant support and guidance throughout this process. I am very grateful to have had excellent supervisors that gave me the experience to grow both academically and professionally. I would also like to thank my supervisory committee member Dr. Sheila Drover for her invaluable contributions to this work, including the thorough review of this manuscript. I was lucky to have many great lab mates over the past couple of years including Jenika Marshall, Erin O'Brien, and Mallory Pitts, who taught me techniques and assisted in this study. Additionally, I would like to thank the many undergraduate researchers that supported this work. Finally, I would like to thank my parents, friends, and partner for always encouraging me.

## Table of Contents

Abstract	ii
Acknowledgements	iii
Table of Contents	iv
List of Tables	ix
List of Figures	x
List of Abbreviations	xii
Chapter 1 Introduction	1
1.1 Breast cancer	1
1.1.1 Incidence and prevalence of breast cancer	1
1.1.2 Overview of breast cancer	2
1.1.3 Breast tumor evaluation and characterization	5
1.1.4 Breast cancer classification and prognosis	9
1.1.5 Overview of the tumor microenvironment	12
1.2 Overview of lipoproteins	23
1.3 Lipoprotein lipase	26
1.3.1 Overview of the <i>sn</i> -1 lipases	26
1.3.2 LPL synthesis and processing	29
1.3.3 Regulation of LPL activity	32
1.4 LPL hydrolysis products and their relevance to breast cancer	33

1.5 Hypothesis	35
1.6 Objectives	35
Chapter 2 Materials and Methods	37
2.1 Mammalian cell culture	37
2.1.1 HEK-293 cell culture and maintenance	37
2.1.2 MCF-7 and T47D cell culture and maintenance	37
2.1.3 MDA-MB-231, MDA-MB-468, and SKBR3 cell culture and maintenance	38
2.1.4 MCF-10a cell culture and maintenance	38
2.2 HEK-293 transfection with recombinant LPL plasmid	39
2.2.1 HEK-293 cell transfection	39
2.2.2 Lysis and collection of LPL-transfected and mock HEK-293 cells	40
2.3 Qualitative and quantitative analysis of LPL	41
2.3.1 SDS-PAGE and western blot	41
2.3.2 Lipase activity assay	42
2.4 Lipoprotein isolation and quantification	43
2.4.1 Total lipoprotein isolation	43
2.4.2 Phospholipid quantification in total lipoproteins	44
2.5 Lipoprotein hydrolysis product generation, quantification, and treatment of breast cancer and MCF-10a cells	45

2.5.1 Hydrolysis of total lipoproteins by LPL	45
2.5.2 Quantification of the FFA content of lipoprotein hydrolysis products	45
2.5.3 Treatment of breast cancer and MCF-10a cells with lipoprotein hydrolysis products	46
2.6 Analyses of breast cancer and MCF-10a cell metabolic activity and cytokine secretion	47
2.6.1 Measurement of cell metabolic activity by MTT assay	47
2.6.2 Analysis of cytokine expression by cytokine array	48
2.6.3 ELISA to measure the concentration of TNF- $\alpha$ , IL-4, and IL-6 cytokines	49
2.6.4 Western blot of breast cancer cell lysates	51
2.6.5 Analysis of endogenous LPL activity in heparinized media from breast cancer and MCF-10a cells	51
2.7 Bioinformatics gene expression analysis of LMF1 in breast cancer and normal breast tissue	52
2.8 Statistical analysis	52
Chapter 3 Results	53
3.1 Assessment of recombinant human LPL following HEK-293 transfection	53
3.1.1 Western blot and lipase activity assay	53

3.1.2 Hydrolysis of total lipoproteins	53
3.2 The effect of total lipoprotein hydrolysis products on the metabolic activity of breast cancer and MCF-10a cells	56
3.3 The effect of total lipoprotein hydrolysis products on the cytokine secretion profile of MDA-MB-231 and MCF-7 breast cancer cells	58
3.3.1 The effect of total lipoprotein hydrolysis products on MDA-MB-231 cell cytokine secretion	58
3.3.2 The effect of total lipoprotein hydrolysis products on MCF-7 cell cytokine secretion	62
3.4 The effect of total lipoprotein hydrolysis products on TNF- $\alpha$ , IL-4, and IL-6 cytokine secretion in breast cancer and MCF-10a cells	62
3.4.1 TNF- $\alpha$ cytokine secretion in breast cancer and MCF-10a cells following hydrolysis products treatment	64
3.4.2 IL-4 cytokine secretion in breast cancer and MCF-10a cells following hydrolysis products treatment	64
3.4.3 IL-6 cytokine secretion in breast cancer and MCF-10a cells following hydrolysis products treatment	64
3.5 Assessment of LPL expression in breast cancer cells	68
3.6 Assessment of endogenous LPL activity in breast cancer cells	68
3.7 LMF1 expression in breast cancer cell lines, breast cancer patient samples, and normal breast tissue	70

Chapter 4 Discussion	73
4.1 Total lipoprotein hydrolysis products generated by LPL modulate breast cancer cell metabolic activity	73
4.2 Total lipoprotein hydrolysis products generated by LPL cause subtype-specific cytokine secretion from breast cancer cells	79
4.3 Endogenous LPL expressed by breast cancer cells is not enzymatically active and may be a result of dysregulated LMF1 expression	83
4.4 Future perspectives	85
4.5 Overall conclusion	87
References	88
Appendix I: Supplementary data	105

## List of Tables

Table 1: Cytokines detected by the Proteome Profiler™ Human Cytokine Array	59
Supplemental Table 1: Summarized data from the cytokine array analysis of MDA-MB-231 breast cancer cell supernatant	107
Supplemental Table 2: Summarized data from the cytokine array analysis of MCF-7 breast cancer cell supernatant	109

## List of Figures

Figure 1.1: Structure of a breast duct or lobule	3
Figure 1.2: Overview of breast cancer subtypes by IHC markers	13
Figure 1.3: Interactions in the breast tumor microenvironment	21
Figure 1.4: The <i>sn</i> -1 cleavage point of a general phospholipid and triglyceride	27
Figure 1.5: Transport of LPL from parenchymal cells to the vascular endothelial surface	31
Figure 1.6: Total lipoprotein hydrolysis products generated by LPL could influence breast cancer progression	36
Figure 3.1: Analysis of LPL protein expression and enzymatic activity following HEK-293 cell transfection with LPL plasmid	54
Figure 3.2: FFA quantification of total lipoprotein hydrolysis products after incubation with LPL or mock-transfected heparinized media	55
Figure 3.3: MTT assay of breast cancer and MCF-10a cells after treatment with LPL hydrolysis products (HP) or mock hydrolysis products	57
Figure 3.4: Cytokine array analysis of MDA-MB-231 breast cancer cell supernatant treated with total lipoprotein hydrolysis products	60

Figure 3.5: Cytokine array analysis of MCF-7 breast cancer cell supernatant treated with total lipoprotein hydrolysis products	63
Figure 3.6: ELISA analysis of TNF- $\alpha$ cytokine expression in supernatant collected from breast cancer and MCF-10a cells	65
Figure 3.7: ELISA analysis of IL-4 cytokine expression in supernatant collected from breast cancer and MCF-10a cells	66
Figure 3.8: ELISA analysis of IL-6 cytokine expression in supernatant collected from breast cancer and MCF-10a cells	67
Figure 3.9: Representative image of a western blot for detection of LPL in breast cancer cell lysates	69
Figure 3.10: Analysis of endogenous LPL activity in breast cancer cells	71
Figure 3.11: Analysis of LMF1 mRNA expression in breast cancer cell lines, primary breast tumor samples, and normal breast tissue	72
Figure 4.1: Proposed positive-feedback loop in breast cancer cells	78
Supplemental Figure 1: Western blot to detect LPL protein expression	106
Supplemental Figure 2: Western blot to detect LPL protein expression in breast cancer cell lysates, additional replicates	111

## List of Abbreviations

A/A	Antibiotic/antimycotic
ABCA1	ATP-binding cassette transporter 1
ABCG1	ATP-binding cassette subfamily G member 1
AJCC	The American Joint Committee on Cancer
Akt	Protein kinase B
apoB	Apolipoprotein B
ATGL	Adipose triglyceride lipase
ATP	Adenine triphosphate
BCA	Bicinchonic acid
BL1	Basal-like 1
BL2	Basal-like 2
BSA	Bovine serum albumin
CAA	Cancer-associated adipocytes
CAF	Cancer-associated fibroblast
CCL	chemokine ligand

CD36	Cluster of differentiation 36
coA	Coenzyme A
Cpeb1	Cytoplasmic polyadenylation element-binding protein 1
CPT1A	Carnitine palmitoyltransferase 1A
CSF1	Colony stimulating factor 1
DCIS	Ductal carcinoma <i>in situ</i>
DMEM	Dulbecco's Modified Eagle Medium
DMSO	Dimethyl sulfoxide
ECM	Extracellular matrix
EDTA	Ethylenediaminetetraacetic acid
EGF	Epidermal growth factor
EGFR	Epidermal growth factor receptor
EL	Endothelial lipase
EMT	Epithelial-mesenchymal transition
ER	Endoplasmic reticulum
ER	Estrogen receptor
ERK	Extracellular signal-related kinase

FAF	Fatty acid-free
FAO	Fatty acid $\beta$ -oxidation
FASN	Fatty acid synthase
FBS	Fetal bovine serum
FFA	Free fatty acid
GEO	Gene Expression Omnibus
GES	Gene expression signature
GPCR	G protein-coupled receptor
GPIHBP1	Glycosylphosphatidylinositol-anchored high-density lipoprotein-binding protein 1
hASC	Human adipose tissue derived stem cell
HDL	High-density lipoprotein
HEK-293	Human embryonic kidney-293 cells
HER2	Human epidermal growth factor receptor 2
HER2-E	HER2-enriched
HL	Hepatic lipase
HP	Hydrolysis products
HRP	Horseradish peroxidase

HSPG	Heparan sulfate proteoglycan
ICAM	Intracellular adhesion molecule
IDC	Invasive ductal carcinoma
IDL	Intermediate-density lipoprotein
IFN- $\gamma$	Interferon gamma
IHC	Immunohistochemistry
IL	Interleukin
IM	Immunomodulatory
JAK	Janus kinase
LAR	Luminal androgen receptor
LCIS	Lobular carcinoma <i>in situ</i>
LDL	Low-density lipoprotein
LMF1	Lipase maturation factor 1
LPA	Lysophosphatidic acid
LPL	Lipoprotein lipase
MAPK	Mitogen-activated protein kinase
M-CSFR	Macrophage-CSF receptor

miRNA	microRNA
MMP	Matrix metalloproteinases
MSC	Mesenchymal stem cell
MSL	Mesenchymal stem-like
mTORC	Mechanistic target of rapamycin complex
MTT	3-(4, 5-dimethylthiazolyl-2)-2,5-diphenyltetrazolium bromide
NF- $\kappa$ B	Nuclear factor- $\kappa$ B
PBS	Phosphate-buffered saline
PDGFR	Platelet-derived growth factor receptor
PDGR	Platelet-derived growth factor
PDK1	Phosphatidylinositol-dependent kinase 1
PD-L1	Programmed death-ligand 1
PI3K	Phosphoinositide 3-kinase
PIP <sub>2</sub>	Phosphatidylinositol (4,5) bisphosphate
PIP <sub>3</sub>	Phosphatidylinositol (3,4,5) triphosphate
PL	Pancreatic lipase
PL	Phospholipid

PLA <sub>1</sub>	Phospholipase A <sub>1</sub>
PLIN2	Perilipin 2
PR	Progesterone receptor
PTEN	Phosphatase and tensin homolog
RMA	Robust multi-chip average
ROS	Reactive oxygen species
RPMI	Roswell Park Memorial Institute
RTK	Receptor tyrosine kinase
SDS-PAGE	Sodium dodecyl sulfide polyacrylamide gel electrophoresis
SEER	Surveillance, Epidemiology, and End Results Program
SR-BI	Scavenger receptor class-B type 1
STAT	Signal transducer of activation
TAM	Tumor-associated macrophage
TBS	Tris-buffered saline
TCA	Tricarboxylic acid cycle
TG	Triglyceride
TGF- $\beta$	Transforming growth factor beta

TGS	Tris-glycine-SDS
Th1	T helper 1
Th2	T helper 2
THL	Tetrahydrolipstatin
TIL	Tumor-infiltrating lymphocytes
TNBC	Triple-negative breast cancer
TNF- $\alpha$	Tumor necrosis factor- $\alpha$
TNM	Tumor, lymph node, metastasis
VEGF	Vascular endothelial growth factor
VLDL	Very low-density lipoprotein

## **Chapter 1 Introduction**

### **1.1 Breast cancer**

#### **1.1.1 Incidence and prevalence of breast cancer**

Despite advances in detection, treatment, and prevention, breast cancer remains the second leading cause of death from cancer among Canadian women. In 2020, it is estimated that approximately 28,000 breast cancer diagnoses will be made, representing 25% of all new cancer cases in women [1]. Breast cancer in men can occur, but it is very rare and it accounts for less than 1% of all breast cancer cases [1]. While the incidence of breast cancer has remained relatively consistent, breast cancer mortality has declined significantly by 49% since its peak in 1986. This decline is primarily attributed to early-detection and progress in treatment [2]. Breast cancer signs and symptoms usually do not present until the tumor has progressed to a palpable lump in the breast or until the cancer spreads to surrounding tissues. When symptoms do appear, they are often reported as physical changes to the breast, such as lumps, size and shape differences, skin irritation, nipple discharge, and pain [3]. Prognosis largely depends on the stage that the cancer is detected; the 5-year relative survival for breast cancer begins at 100% for stage 1 and declines to 22% at stage 4. In addition to the impact on patients, cancer care is costly for the Canadian health care system. The cost of cancer care rose from \$2.9 billion in 2005 to \$7.5 billion in 2012, and with an aging population and increasing number of cancer diagnoses, the cost will continue to rise [2]. Because of this, it is essential that new

methods of breast cancer detection and treatment are developed to achieve the best prognosis and reduce the burden on health care systems [2, 3]. The identification of novel targets to treat breast cancer is necessary to accomplish this.

### **1.1.2 Overview of breast cancer**

Breast tissue covers the area between the collarbone, lower ribs, and armpit, and consists of functional glandular tissue, connective tissue, and subcutaneous adipose tissue. Each breast contains approximately 15-20 lobes and multiple smaller lobules which produce milk in lactating women. The milk is then carried from the lobes to the nipple through a series of ducts [4]. The ducts and lobes are lined with two types of epithelial cells: luminal epithelial cells, which produce milk, and myoepithelial cells, which are attached to the basement membrane and have contractile properties to assist in milk ejection (Figure 1.1) [5].

Most breast cancer cases arise from cells within the ducts and lobes and is categorized as pre-invasive (*in situ*) or invasive. The classification depends on whether the cancer is confined to the area of initiation or spread to surrounding tissues. Tumors that originate in the glandular tissue are called carcinomas. Ductal carcinoma *in situ* (DCIS) arises in the cells of the ducts and accounts for approximately 20% of all breast cancer cases [6, 7]. Similarly, lobular carcinoma *in situ* (LCIS) arises in the epithelial cells of the lobes and is considered a precancerous condition. LCIS is thought to increase the risk of developing invasive carcinoma by approximately 30-40% [8, 9]. An important feature of LCIS is the downregulation of the adhesion molecule E-cadherin, which is

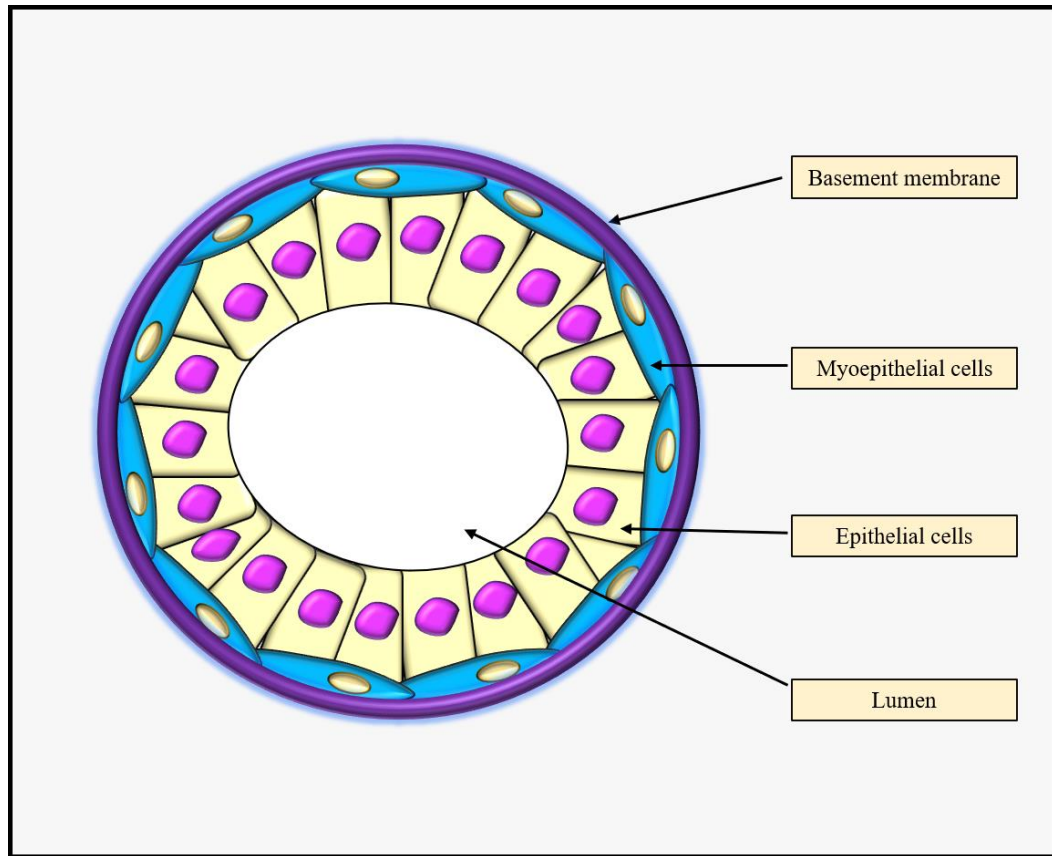


**Figure 1.1:** Structure of a breast duct or lobule

Breasts are comprised of ducts and lobes. Lobes are divided into multiple smaller lobules which produce milk in lactating women, which is then carried to the nipple through a series of ducts. The ducts and lobes are lined with two types of epithelial cells: luminal epithelial cells, which produce milk, and myoepithelial cells, which are attached to the basement membrane and have contractile properties to assist in milk ejection.

normally present on all epithelial cells to attach to other cells and the basement membrane. This loss of adhesion is considered an important step toward developing invasive carcinoma [5]. Both DCIS and LCIS increase the risk of developing invasive breast cancer by approximately 1-2% per year. Because of this, DCIS and LCIS have often been treated by conventional methods such as surgical intervention, radiation, and chemotherapy. However, many cases of DCIS and LCIS will not progress to invasive carcinoma, and since 2012 it has been suggested that the current therapeutic strategies are too aggressive [6, 10, 11].

The most recent World Health Organization (WHO) classification of breast tumors outlines 21 major and 14 rare carcinoma subtypes. Invasive ductal carcinoma (IDC) accounts for approximately 70-75% of invasive breast cancer cases, whereas invasive lobular carcinoma accounts for 10-14% [12, 13]. Rare breast carcinomas, such as tubular carcinoma and inflammatory carcinoma, have a range of clinical features and can be mild or highly aggressive [13]. In addition, breast cancer can also arise from other tissues within the breast structure. Breast sarcomas and lymphomas, originating from the connective and lymph tissue, respectively, account for less than 1% of all breast cancer cases. Breast sarcomas are particularly rare and hence poorly understood, with an annual incidence estimated at 45 cases per 10 million women [14, 8]. There is little agreement on the best course of treatment and prognosis of breast sarcomas and lymphomas due to the rarity of these tumors [15, 16].

### **1.1.3 Breast tumor evaluation and characterization**

Once a diagnosis of breast cancer is made, the tumor characteristics are evaluated to guide decisions on the best course of treatment. The American Joint Committee on Cancer (AJCC) Staging Manual defines the criteria by which tumors are assessed, and it has been widely adopted to estimate prognosis. The eighth edition has expanded from previous versions to include two staging systems for breast cancer: the anatomic stage and the prognostic stage [17, 18]. The anatomic stage is based on the classic tumor, lymph node, metastasis (TNM) grading system. The TNM system evaluates the size of the primary tumor, lymph node involvement, and distant metastasis before and after cancer treatment based on specific criteria. Each TNM component is ranked and then combined to give an overall anatomic stage ranging from stage 0 to stage IV, with stage IV having the worst prognosis [17].

The prognostic stage of grading was introduced in the newest staging manual to address the importance of evaluating the histologic grade, hormone receptor expression, and gene expression, to accurately determine the extent of disease and treatment options [19]. A histologic grade is assigned to breast carcinomas based on the degree of differentiation from normal breast epithelial cells. The most common grading system is the Nottingham Grading System, which assigns a grade of 1-3 to three morphological features: the degree of tubule formation, nuclear pleomorphism, and mitotic count [19]. The scores are then combined to give an overall tumor grade of I, II, or III, with grade III tumors having the worst prognosis [20]. Previously, the histologic grade was not considered to be an important prognostic factor in cases where there is significant lymph

node involvement [17, 18]. However, a study using data obtained by the Surveillance, Epidemiology, and End Results Program (SEER) of the National Cancer Institute demonstrated that tumor grade is strongly associated with patient outcome [21]. It is now known that tumor grade is an essential prognostic measure that is independent of anatomic features of the tumor and is therefore included in the latest AJCC Staging Manual [18].

The hormone receptor status of breast tumors provides critical information about the treatment course and overall prognosis. The estrogen receptor (ER) and progesterone receptor (PR) are regularly expressed by breast cells to respond to hormone stimulation. However, in malignant conditions, ER/PR expression promotes breast cancer cell growth and resistance to chemotherapeutic-induced apoptosis [22, 23]. The ER/PR status is evaluated by immunohistochemistry (IHC), where nuclear staining for ER or PR in greater than 1% of the tumor cells is considered positive. The standard of care for ER/PR positive breast tumors is endocrine therapy, which works by blocking the ER or the production of estrogen [12]. The PR gene, *PGR*, is a direct target of the ER in response to estrogen. Therefore, endocrine therapies targeting estrogen also affect PR expression. Some studies report the detection of single hormone receptor-positive subtypes, specifically ER-negative/PR-positive, but this remains controversial [24]. In addition to serving as a predictive factor of endocrine therapy response, ER/PR expression also provides information on the overall prognosis. It has been shown that patients with ER/PR positive tumors have better outcomes, regardless of treatment type. Additionally, tumors with high expression of ER/PR determined via IHC are associated with better

outcomes than those with lower ER/PR expression. Unfortunately, ER/PR positive breast tumors often develop resistance to endocrine therapy and have a recurrence risk of 10-41% over a 20 year period [24, 25].

Since its identification in 1985 as an oncogene, the status of the human epidermal growth factor receptor 2 (HER2) has become crucial to consider when making treatment decisions [26]. HER2 is overexpressed in approximately 15-20% of breast tumors and is associated with a poor prognosis and reduced relapse-free survival. A higher degree of *HER2* amplification confers a worse prognosis [27]. HER2 is found in the presence or absence of ER/PR expression. The HER2 receptor belongs to the epidermal growth factor receptor (EGFR) family of receptor tyrosine kinases (RTK), but it has a constitutively active conformation. HER2 does not have a ligand-binding domain, so it typically forms a stable heterodimer with other EGFR family members to allow ligand binding and signal transduction. However, HER2 has been shown to homodimerize at high concentrations to activate intracellular signaling pathways independent of ligand binding [28]. Signal transduction causes transphosphorylation of the intracellular domains, leading to the activation of downstream second messengers [29, 30]. This results in the activation of the mitogen-activated protein kinase (MAPK)/extracellular signal-related kinase (ERK) signaling pathway, which increases angiogenesis, cell proliferation, differentiation, and survival [31]. HER2 can also activate the phosphoinositide 3-kinase (PI3K)/protein kinase B (Akt) signaling pathway, which is known to promote tumorigenesis and resistance to apoptosis [32]. PI3K/Akt pathway activation is also associated with increased infiltration of cancer-associated fibroblasts (CAF) and tumor-associated

macrophages (TAM) within the tumor microenvironment [32, 33]. CAF and TAM play an important role in breast cancer progression by establishing an immunosuppressive environment via cytokines and promoting metastasis by extracellular matrix (ECM) remodeling [34]. HER2 status is evaluated by IHC and *in situ* hybridization methods such as fluorescence *in situ* hybridization, which detects gene amplification. A positive result is defined as *HER2* amplification in greater than 10% of tumor cells [35]. The standard of care for HER2-positive breast cancer is treatment with anti-HER2 therapeutics, such as the monoclonal antibody trastuzumab (Herceptin). Trastuzumab binds the extracellular domain of HER2 and inhibits signal transduction through several proposed mechanisms. However, resistance to trastuzumab therapy is common, and the recurrence risk of lymph-node negative HER2+ breast cancer is estimated at 5-30% [12, 36, 37].

Finally, breast tumors can be further classified into distinct molecular subtypes by gene expression profiling. Two studies used cDNA microarrays to analyze the gene expression patterns of over 100 combined human breast tumor samples [38, 39]. Since then, multigene panels have been developed and incorporated into the regular clinical evaluation of breast tumors. The most widely adapted multigene panel is The Oncotype DX Breast Recurrence Score, which evaluates the potential response of ER/PR-positive tumors to different types of therapies [18]. Other multigene panels exist, such as MammaPrint, EndoPredict, and Prosigna/PAM50; however, evidence for their clinical use is lacking [17, 18]. The subtypes are based on differences in the activation, mutation, and amplification of genes such as *PI3KCA*, *GRB7*, *ERBB3*, *TP53*, and *BRCA*, which have well-defined roles in the growth and progression of breast tumors. The breast tumors

can be classified as having a low-risk gene expression signature (GES), or high-risk GES [12]. The expression of the nuclear proliferation marker Ki-67 is also assessed by IHC to further differentiate the breast tumor subtypes. High Ki-67 expression was initially defined as greater than 14% positive cell staining. That number has since been adjusted to approximately 20-30% positive cell staining, but there is not a clear consensus [12]. High Ki-67 expression indicates high tumor cell proliferation and is correlated with worse overall prognosis. However, Ki-67 assessment is not included as a necessary measurement in the latest AJCC Staging Manual because of uncertainty surrounding its clinical implications. Nevertheless, Ki-67 is still regularly measured to get a full picture of the tumor biology [40, 41].

#### **1.1.4 Breast cancer subtype classification and prognosis**

The breast cancer subtype is assigned by compiling the anatomic and prognostic characteristics of the tumor. Determining the subtype is essential for standardized patient care and provides an accurate estimate of prognosis. The luminal A subtype is the most frequent type of invasive breast cancer, accounting for 30-40% of all cases. Luminal A tumors are ER-positive, highly PR-positive (>20%), HER2-negative, and Ki-67 low (<14%). They are typically low-grade (1 or 2) ductal carcinomas with a low-risk GES. Luminal A tumors have the best prognosis out of all the subtypes with a 4-year survival rate of 92.5% based on SEER data [40, 42]. The luminal B subtype is the second most common, accounting for 20-30% of invasive breast cancer cases. Luminal B tumors are ER-positive, PR-positive (<20%), HER2-positive or negative, and Ki-67 high (>14%). The Ki-67 expression level is one of the distinguishing features between luminal A and

luminal B breast cancers [40]. Luminal B type breast tumors are often grade 2 or 3 invasive ductal carcinomas with a high-risk GES. Mutations of the *PI3KCA* gene are present in 40% of luminal B breast tumors resulting in the constitutive activation of the PI3K/Akt pathway [43]. Due to advances in targeted therapy, the prognosis of luminal B breast cancer is positive, with a 4-year survival rate of 90.3% [42].

HER2 is positively detected in 12-20% of invasive breast tumors and can be subdivided into the HER2-enriched (HER2-E) subtype and the luminal-like HER2 subtype. It is notable that HER2 is detected in other forms of breast cancer, but these are less common. Some studies do not distinguish specific HER2-positive subtypes, while many believe there is substantial precedent for distinguishing the groups [44, 45]. The HER2-E subtype accounts for over 50% of HER2-positive cases and is characterized by high expression of HER2, HER2 amplicon genes (*GRB7*), negative ER/PR expression, and high Ki-67 levels [40]. Because of the significant activation of survival pathways by HER2-E breast tumors, the HER2-E subtype benefits the most from targeted anti-HER2 therapies [44]. HER2-E tumors are generally high-grade and aggressive but have a 4-year survival rate of 82.7% due to the development of effective neoadjuvant and adjuvant anti-HER2 therapies [42]. Luminal-like HER2-positive breast tumors are HER2-positive, ER/PR-positive, and have high Ki-67 expression. However, HER2 and ER/PR expression are lower than in the HER2-E and luminal A/B subtypes, respectively. HER2 in ER/PR-positive breast cancer is known to reduce the effectiveness of endocrine therapy and promote resistance to chemotherapeutics [46, 47]. A proposed mechanism of resistance is the activation of HER2, and subsequently, the PI3K/Akt pathway to downregulate ER and

PR expression. The downregulation of ER and PR causes the tumor to become more aggressive [48]. However, the combination of targeted HER2 and ER/PR therapies improves the overall prognosis to a 4-year survival of approximately 90% [40].

Triple-negative breast cancer (TNBC) accounts for 15-20% of breast cancer cases and is considered particularly aggressive. The TNBC subtype is immunohistochemically identified by its lack of ER, PR, and HER2 receptors. However, TNBC represents a heterogeneous group of breast cancers which are further categorized by several different methods. One of the most common is Lehmann's classification, which analyzed the gene expression profiles of 587 TNBC tumors [49]. This analysis identified six distinct molecular subtypes of TNBC [50, 40]. The subtypes are basal-like 1 (BL1), basal-like 2 (BL2), mesenchymal, mesenchymal stem-like (MSL), luminal androgen receptor (LAR), and immunomodulatory (IM). IHC analysis of cytokeratin 5/6, androgen receptor, and p53 expression can help identify the subtype and serve as prognostic indicators in TNBC [51]. However, it has been shown that this classification does not accurately estimate survival over a 20-year period. There is now evidence that each TNBC subtype is heterogeneous and can be subclassified by the severity of the genetic profile [52]. TNBC tumors are often classified as IDC, but other less frequent tumor types can also be triple-negative. Common features are that the tumors are usually diagnosed late, with a high-grade, large size, lymph node metastases, and young age of diagnosis [53]. TNBC has been associated with numerous risk factors such as African ancestry, obesity, higher waist-to-hip ratio, and lack of breastfeeding. Certain genetic mutations also predispose women to TNBC. Approximately 10% of all breast cancer cases are considered familial;

2-6 % of these are attributed to mutations in the *BRCA1* and *BRCA2* genes. *BRCA* mutations carry a 30-70% increased risk of developing breast cancer. When breast cancer does develop, TNBC is diagnosed in 70-90% of *BRCA1* and 16-23% of *BRCA2* mutation carriers. However, *BRCA1/BRCA2* mutations account for only 15.4% of all TNBC cases [53, 54]. TNBC has the worst prognosis of all the breast cancer subtypes, with a 4-year survival of 77% [42]. This is due to the lack of targeted therapies for TNBC and the aggressiveness of the disease phenotype. The presence of tumor-infiltrating lymphocytes (TIL) and programmed death-ligand 1 (PD-L1) expression in the tumor microenvironment are positive prognostic indicators in TNBC [55]. Novel therapeutics such as atezolizumab, an anti-PD-L1 antibody, are proving to be effective in increasing the overall survival of patients with TNBC when combined with chemotherapy [55]. There is now evidence that the molecular subtype of TNBC is a good predictor of the effectiveness of certain treatments [56]. Figure 1.2 shows a summary of the molecular markers expressed by different subtypes of breast cancer.

### **1.1.5 Overview of the tumor microenvironment**

It is now understood that interactions between the tumor and its microenvironment are essential for cancer growth and progression. The tumor microenvironment is comprised of the ECM, blood vessels, non-malignant cells, and signaling molecules [57]. TIL, TAM, CAF, and adipocytes are some of the cells that have been identified as components of the breast tumor microenvironment. The function of these cells in the

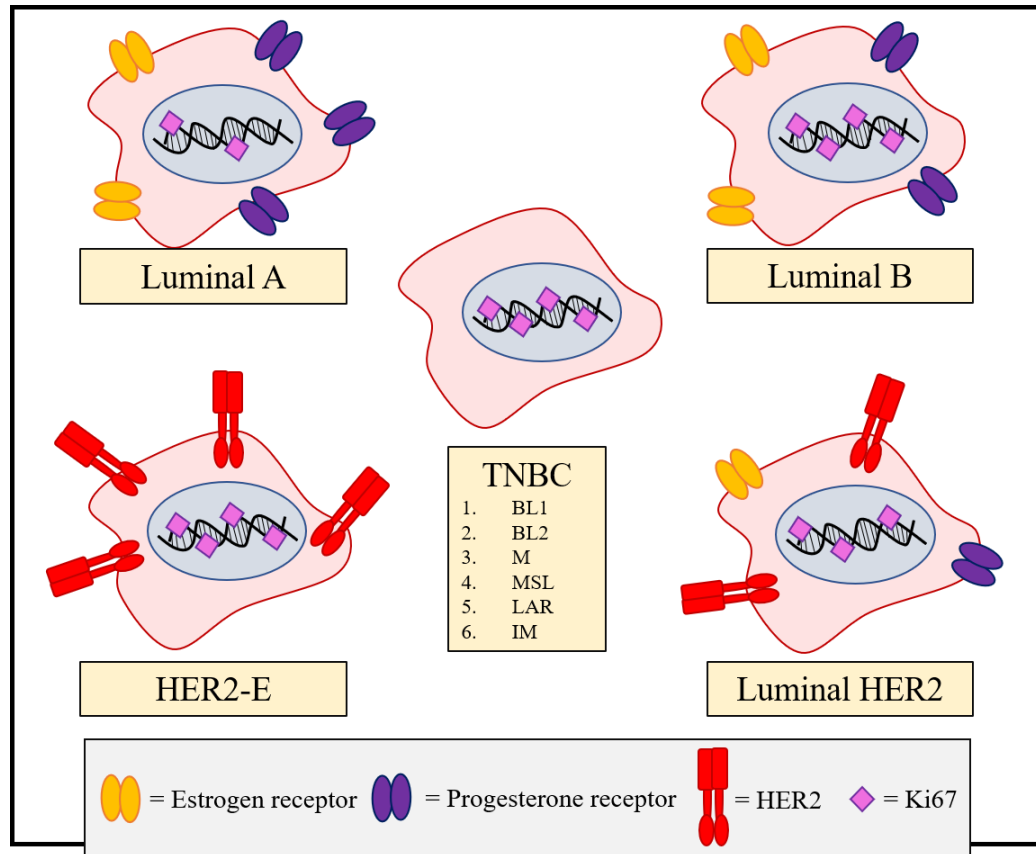


**Figure 1.2:** Overview of breast cancer subtypes by IHC markers

Breast tumors are evaluated by IHC to determine the ER/PR, HER2, and Ki67 expression levels. Breast cancer can be divided into five subtypes based on the expression profile: luminal A (ER-positive, PR-positive (>20%), HER2-negative, Ki-67 low), luminal B (ER-positive, PR-positive (<20%), HER2-positive or negative, Ki-67 high), HER2-E (ER/PR-negative, high HER2, high Ki-67), luminal-HER2 (ER/PR-positive, HER2 positive, high Ki-67), and TNBC (ER/PR-negative, HER2-negative, Ki-67 high). The six TNBC subtypes are basal-like 1 (BL1), basal-like 2 (BL2), mesenchymal (M), mesenchymal stem-like (MSL), luminal androgen receptor (LAR), and immunomodulatory (IM). Figure created in Microsoft PowerPoint 2016.

microenvironment evolves as the tumor grows. The cancer immunoediting hypothesis describes three phases of tumor progression: elimination, equilibrium, and escape. As cancer progresses, tumor cells acquire modifications, such as reduced antigen expression, that prevent detection and elimination by immune cells. The escape stage occurs when the immune system has exhausted its ability to restrict tumor growth [58, 59]. Depending on the extent of progression, immune cells can enhance or inhibit cancer progression by the secretion of pro- and anti-inflammatory biomolecules. TIL include T cells and B cells, which can have pro- and anti-tumorigenic functions. CD8<sup>+</sup> and CD4<sup>+</sup> T helper 1 (Th1) cells secrete the cytokine interferon-gamma (IFN- $\gamma$ ), among other anti-tumorigenic factors, which has been shown to slow the progression of cancer [60]. In breast cancer, IFN- $\gamma$  has been shown to enhance the expression of the cell cycle inhibitor proteins p27, p16, and p21, causing decreased proliferation of tumor cells [61]. However, there is also evidence that excess IFN- $\gamma$  can increase the aggressiveness of tumor cells [62]. B cells secrete interleukin (IL)-10, which has dual effects in the tumor microenvironment. In T cells and macrophages, IL-10 is known to block the production of the pro-inflammatory cytokines tumor necrosis factor (TNF)- $\alpha$ , IL-6, IL-8, and vascular endothelial growth factor (VEGF) by inhibiting the nuclear factor (NF)- $\kappa$ B pathway [63]. The NF- $\kappa$ B pathway is a central mediator in the inflammatory response. Upon activation by pro-inflammatory molecules, the NF- $\kappa$ B transcription factor enters the nucleus and induces cell proliferation, angiogenesis, immune evasion, and metastasis. Certain pro-inflammatory cytokines, such as TNF- $\alpha$ , are produced by and activate the NF- $\kappa$ B pathway in an autocrine feedback loop [64, 65]. Because of its ability to inhibit pro-inflammatory

cytokine synthesis, IL-10 is considered a potent inhibitor of tumorigenesis. However, IL-10 also activates the Janus kinase (JAK)/signal transducer of activation (STAT) pathway. Upon ligand binding and receptor dimerization, JAK becomes activated and phosphorylates STAT transcription factors. The activated STAT can then enter the nucleus to regulate gene expression. Four JAK (Jak1-3, Tyk2) and seven STAT (STAT1-4, STAT5a, STAT5b, STAT6) family members have been identified, where different JAK and STAT combinations are activated in response to different ligand/receptor pairs [66]. IL-10, via the IL-10 receptor, has been shown to activate STAT1, STAT3, and STAT5. The role of STAT1 and STAT5 activation in response to IL-10 is not well characterized. However, IL-10 induced STAT3 activation is known to cause the transcription of proliferative and anti-apoptotic genes [67, 68]. Additionally, excess IL-10 contributes to tumor escape by inhibiting the production of pro-inflammatory cytokines that are essential for immune surveillance. In breast cancer, IL-10 is often elevated in the serum and is correlated with increased metastasis and poor prognosis [64, 69].

TAMs are highly abundant within breast tumors and can comprise over 50% of the tumor mass. Breast cancer cells attract monocytes from the blood vessels by secreting colony-stimulating factor 1 (CSF1) and chemokine ligand 2 (CCL2). Once at the tumor site, monocytes are differentiated into subsets of TAM that perform distinct roles. Differentiation occurs in response to signals from the tumor microenvironment [70]. M1-like TAMs are activated by IFN- $\gamma$  and TNF- $\alpha$  secreted by Th1 cells. M1-like TAMs secrete pro-inflammatory cytokines and reactive oxygen species (ROS) and are associated with a good prognosis in early-stage cancer. Alternatively, M2-like TAMs are activated

by cytokines released from CD4<sup>+</sup> T helper 2 (Th2) cells, such as IL-10, IL-4, and transforming growth factor beta (TGF- $\beta$ ). M2-like TAMs express factors that support tumor growth (TGF- $\beta$ ), angiogenesis (VEGF), immunosuppression (IL-10, PD-L1), and ECM remodeling (matrix metalloproteinases, MMP) [71, 72]. M2-like TAMs play a key role in ECM remodeling because they express the highest level of protease activity in the tumor microenvironment. M2-like TAMs actively degrade the ECM to allow invasion of tumor cells into the surrounding tissues. Additionally, ECM degradation releases growth factors such as TGF- $\beta$  and VEGF, which further promotes angiogenesis and growth of the tumor cells [71]. Because of this, high levels of M2-like TAMs in the breast tumor microenvironment are associated with a poor prognosis. The ratio of M1/M2-like TAMs is used as a prognostic indicator where a high ratio suggests a good response to chemotherapy [70, 72].

Like TAMs, CAFs originate from cells that are recruited and differentiated by signals in the tumor microenvironment. CAFs can arise from many different cell types and thus have a variety of functions and expression levels. However, identifying different subtypes within the tumor microenvironment is difficult due to the lack of specific CAF markers. The main source of CAFs in breast cancer are resident fibroblasts and mesenchymal stem cells (MSC) [73]. Conditioned media from MDA-MB-231 (TNBC) and MCF-7 (luminal A) breast cancer cells were shown to induce the differentiation of human adipose tissue-derived stem cells (hASC) into CAFs [74]. The conditioned media were found to have a high concentration of TGF- $\beta$ . Blocking TGF- $\beta$  using a neutralizing antibody and receptor inhibitor prevented the differentiation of hASCs into CAFs [74].

This is significant because breast tumors are surrounded by adipose tissue, which is highly enriched with hASCs, thus generating a major proportion of CAFs.

Upon differentiation, CAFs begin to produce their own TGF- $\beta$ , which maintains their differentiation via an autocrine loop [73]. Like many signaling molecules in the tumor microenvironment, TGF- $\beta$  has dual roles depending on the extent of progression. In early-stage breast cancer, TGF- $\beta$  inhibits tumorigenesis by upregulating the cell cycle inhibitor proteins p21 and p15, and by activating apoptotic signaling pathways [75]. In well-established tumors, TGF- $\beta$  has potent pro-tumorigenic properties such as inducing angiogenesis, immune suppression, ECM remodeling, and epithelial-mesenchymal transition (EMT) [76]. EMT is the process through which epithelial cells lose their polarity and cell-cell adhesion and move towards an invasive and migratory mesenchymal phenotype. TGF- $\beta$  induces the expression of MMP and mesenchymal cell markers, such as vimentin, to degrade the ECM and facilitate tumor escape. Additionally, TGF- $\beta$  is known to activate the PI3K/Akt, NF- $\kappa$  $\beta$ , and STAT3 signaling pathways and is, therefore, a central regulator of tumorigenesis [77]. CAFs have also been linked to increasing lymph node metastasis and TAM presence in the tumor microenvironment. Because of their significant pro-tumorigenic functions, CAFs are associated with a poor prognosis in breast cancer [78].

Due to the large proportion of adipose tissue in the breast, adipocytes are a major component of the breast tumor microenvironment. Using *in vitro* and *in vivo* models of breast cancer, adipocytes in the tumor microenvironment were shown to have decreased adipocyte markers, low lipid content, and increased protease and pro-inflammatory

cytokine secretion. These adipocytes were subsequently named cancer-associated adipocytes (CAA). Co-culture experiments show that the mechanism by which adipocytes transition to CAAs is a tumor cell-mediated process; however, this process is not well-defined [79]. The microRNA (miRNA) mmu-miR-5112 has been identified as a potential driving force behind CAA development; mmu-miR-5112 was found to be significantly upregulated in adipocytes upon co-culture with breast cancer cells [80]. Studies have shown that exosomes released from tumor cells carry cargo, such as miRNAs, which can exert pro-tumorigenic effects in the microenvironment [81]. Therefore, it is possible that mmu-miR-5112 is carried in exosomes released from tumor cells to drive CAA development. This miRNA is thought to function as a cytoplasmic polyadenylation element-binding protein 1 (*Cpeb1*) gene suppressor, which is an inhibitor of IL-6 synthesis [80]. Adipocytes co-cultured with breast cancer cells showed increased IL-6 expression and migration of tumor cells. IL-6 is a pleiotropic cytokine that promotes invasion, metastasis, angiogenesis, and resistance to therapy. This is due to its ability to activate multiple signaling pathways involved in tumorigenesis, such as NF- $\kappa$ B and JAK/STAT3 signaling. CAAs also secrete TGF- $\beta$ , CCL2, MMPs, and multiple other pro-tumorigenic factors that support tumor development and the recruitment of other microenvironment cells, such as TAMs [82].

Adipocytes also function to provide lipids to breast cancer cells to use as a source of energy. A hallmark of cancer is disrupted metabolism. Cancer cells often obtain energy via glycolysis rather than oxidative phosphorylation, causing an increase in lactate production, a phenomenon known as the Warburg effect [83]. Tumors also have altered

lipid metabolism to meet the energy demands of the highly proliferative cells. Cancer cells can increase the endogenous synthesis of lipids, or lipogenesis, by upregulating the expression of lipogenic enzymes such as fatty acid synthase (FASN) and acetyl-coenzyme A (CoA) carboxylase. High levels of FASN expression are correlated with poor prognosis in breast cancer [84]. However, the bulk of lipids acquired by cancer cells are obtained from exogenous sources. Tumor cells induce lipolysis in CAAs, causing the release of free fatty acids (FFA), which are then taken up by the cancer cells by the scavenger receptor cluster of differentiation 36 (CD36). The co-culture of breast cancer cells and adipocytes was shown to increase the rate of FFA uptake by upregulating CD36 expression [83]. Aggressive subtypes of breast cancer, such as TNBC, have highly proliferative cells that allow the tumor to progress rapidly. Fast growing tumors require more energy than slower growing tumors. Because of this, the TNBC cell line MDA-MB-231 take up FFA from CAAs faster than slower-proliferating cells, such as the luminal MCF-7 cell line. The tumor secreted factors that induce lipolysis include IL-6 and TNF- $\alpha$ , which cause adipose atrophy, but this process is not well-characterized [85]. Excess tumor-driven lipolysis results in a common condition called cachexia or wasting syndrome, which is often considered life-threatening in cancer patients. The accumulated lipids can be stored in lipid droplets within the cancer cells, which provides an immediate source of energy that can be accessed when necessary. Lipid droplets are thought to play a role in promoting metastasis due to their ability to supply energy to cancer cells traveling to secondary sites [86]. A high lipid droplet content in cancer cells is now considered a marker of aggressiveness [84]. Cancer cells acquire metabolites from lipids

via mitochondrial fatty acid  $\beta$ -oxidation (FAO), which then feed into the tricarboxylic acid (TCA) cycle to provide energy. In addition to providing a source of energy, exogenous lipids are also used by cancer cells to synthesize bioactive lipids, impact membrane fluidity, and promote resistance to therapy. Blocking endogenous lipid metabolism by cancer cells has long been a therapeutic target of interest with little success. Attempts to inhibit enzymes such as FASN and ACC have not been feasible due to their significant involvement in normal physiological processes [86]. Until recently, exogenous lipid uptake by tumor cells was not considered to have a critical role in cancer progression. Now, therapeutic agents that target exogenous lipid uptake are being developed to downregulate CD36, inhibit intracellular CAA lipolysis, and block tumor-induced adipocyte to CAA transition [83, 84]. For example, in breast cancer the lipolytic enzyme adipose triglyceride (TG) lipase (ATGL) was shown to liberate FFA from lipid droplets within the tumor cells. The FFA released by ATGL are transported into the mitochondria by carnitine palmitoyltransferase 1A (CPT1A) and used for FAO and mitochondrial biogenesis. This interaction was shown to be dependent on CPT1A expression in breast cancer. ATGL expression level was also correlated with breast cancer aggressiveness. Because of this, ATGL is under investigation for use as a potential therapeutic target in breast cancer [87]. However, these targets are also involved in many normal physiological processes which could reduce their effectiveness as anti-cancer agents. Figure 1.3 summarizes the interaction between a breast tumor and the microenvironment.

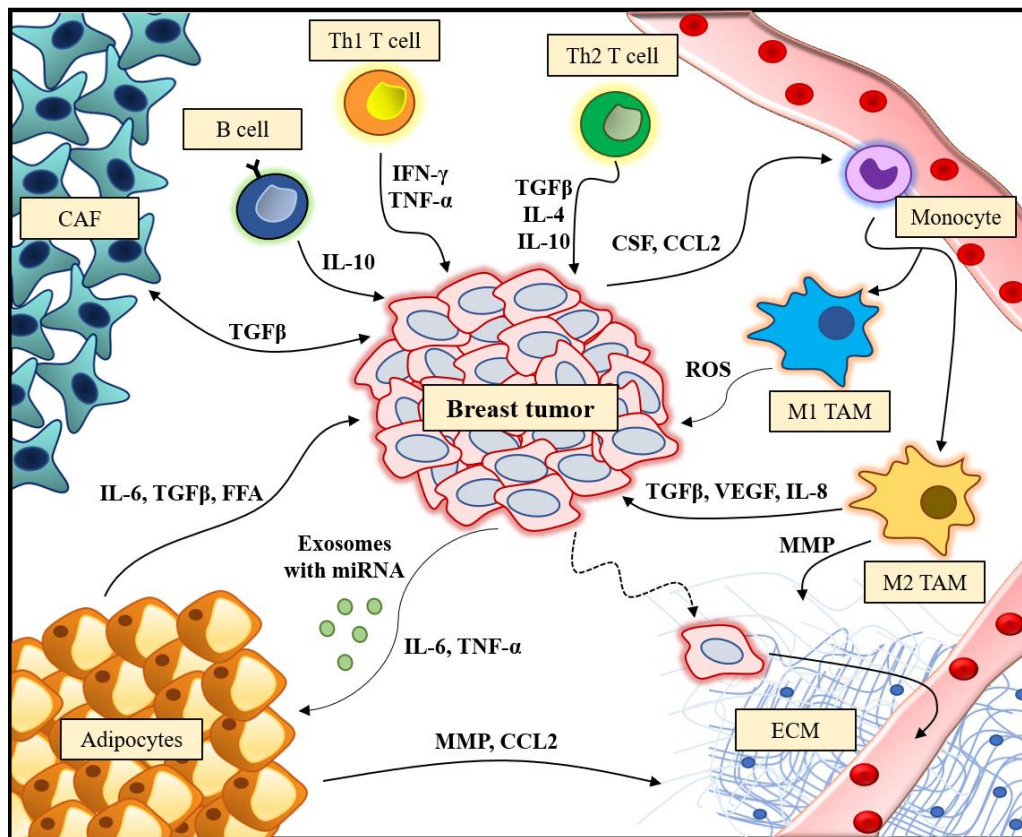


**Figure 1.3:** Interactions in the breast tumor microenvironment

Cells within the tumor microenvironment significantly influence the progression of breast cancer. Tumor cells secrete pro-inflammatory cytokines and chemokines, which can induce pro-tumorigenic changes in the surrounding cells. Monocytes are attracted from the circulation (CSF, CCL2) and differentiate into M1-like and M2-like tumor-associated macrophages (TAM), which support tumor growth (TGF- $\beta$ ), angiogenesis (VEGF, ROS), immunosuppression (IL-10), and ECM remodeling (MMP). Th1, Th2, and B cells also secrete cytokines (IFN- $\gamma$ , TNF- $\alpha$ , IL-10, IL-4, TGF- $\beta$ ), which promote tumorigenesis and activate other cells in the microenvironment. Cancer-associated fibroblasts (CAF) are activated by TGF- $\beta$  secreted from breast cancer cells, which then produce their own supply of TGF- $\beta$ . Breast cancer cells also release exosomes containing mRNA to develop cancer-associated adipocytes (CAA). CAA release many pro-tumorigenic factors (IL-6, TGF- $\beta$ , CCL2, MMPs) and supply a source of energy via FFA stored in lipid droplets. Multiple other cell-cell interactions are not shown. Together, the cells of the microenvironment can facilitate tumor progression. Figure created in Microsoft PowerPoint 2016.

## 1.2 Overview of lipoproteins

Before exogenous lipids can be used by cells as an energy source, they must first travel through the circulation. Due to the hydrophobic nature of lipids, they are unable to travel freely in the plasma and are instead transported in lipoproteins. Lipoproteins are large complexes with a hydrophobic core of TG and cholesteryl esters, and a hydrophilic monolayer made up of phospholipids (PL), free cholesterol, and one or more apolipoprotein [88]. Apolipoproteins can help maintain the structure of lipoproteins, act as cofactors for enzymes involved in lipid hydrolysis, and allow the detection of specific lipoprotein subtypes by cell surface receptors. Lipoproteins were initially divided into six classes based on their density measured by ultracentrifugation [89]. Now, lipoproteins can be further categorized based on size, lipid composition, and function, to represent the heterogeneity of lipoproteins within each class [90].

Apolipoprotein B (apoB) is a large protein produced by the liver and intestine and is secreted only upon association with lipids. The liver synthesizes the full-length apoB protein, called apoB100. The intestinal apoB undergoes mRNA editing, where a cytidine is deaminated to uridine, causing the introduction of a stop codon. The truncated protein is called apoB48 and is identical to the N-terminal 48% of apoB100. ApoB-type apolipoproteins are non-exchangeable, which is a characteristic that allows the measurement of specific subtypes of lipoproteins [91]. Chylomicrons are large, TG-rich, apoB48-associated lipoproteins that are formed by the enterocytes of the small intestine. Their primary function is to transport lipids obtained from the diet to cells throughout the body. Lipoprotein lipase (LPL) is attached to the surface of endothelial cells lining blood

vessels and hydrolyzes the TG from circulating chylomicrons. Chylomicrons are also associated with apoC-II, which is a cofactor for LPL activation. As discussed previously, the FFA released from TG hydrolysis can be used immediately as cell metabolic fuel or can be stored as TG in adipocyte lipid droplets for future access [89, 92]. Once depleted of their TG stores, the resulting cholesteryl ester-rich chylomicron remnants are removed from the circulation by hepatic low-density lipoprotein (LDL) receptor-related protein 1 (LRP1) This interaction requires association with apoE, an LRP1 ligand [93, 94].

Endogenously synthesized hepatic TG are packaged into very low-density lipoproteins (VLDL), which are associated with apoB100. During translation, apoB100 is simultaneously translocated and is initially lipidated by microsomal TG transfer protein within the endoplasmic reticulum (ER) to form primordial or pre-VLDL; this VLDL becomes increasingly TG-rich by fusing with lipid droplets in the cytosol [95]. Mature VLDL is eventually released from hepatocytes to deliver lipids to cells. Like chylomicrons, apoC-II is associated with VLDL, to facilitate TG hydrolysis by LPL. VLDL TG are hydrolyzed by LPL to form intermediate-density lipoproteins (IDL). Approximately 50-70% of IDL is further hydrolyzed by LPL and hepatic lipase (HL) to produce LDL. LDL function as the major carriers of cholesterol in the circulation [96]. The LDL receptor interacts with apoB100 to facilitate LDL uptake via receptor-mediated endocytosis. The cholesterol is used by cells as components of the cell membrane and for the formation of steroid hormones and bile acids [97]. The process of lipid delivery to cells via apoB-containing lipoproteins is called forward lipid transport [96].

High-density lipoproteins (HDL) are a heterogeneous group of small, dense lipoproteins that can be categorized based on apolipoprotein expression; the major apolipoprotein associated with HDL is apoA-I (LpA-I). However, to achieve certain functions, HDL can associate with apoA-II in addition to apoA-I (LpA-I:A-II). HDL is further classified by other physical properties such as density (HDL<sub>2</sub>, HDL<sub>3</sub>), shape, and size [98]. The major function of HDL is to deliver excess cholesterol from peripheral tissues to the liver for biliary excretion. This process, called reverse cholesterol transport, is vital to the maintenance of cholesterol levels within cells [99]. Most cell types are unable to clear cholesterol themselves and rely on HDL to prevent cholesterol accumulation. Excess cholesterol is detrimental and can cause membrane rigidity, apoptosis, and contribute to atherosclerotic vascular disease [100]. Reverse cholesterol transport occurs in two stages, with the first being cholesterol efflux from peripheral cells to apoA-I or HDL. Adenosine triphosphate (ATP)-binding cassette transporter 1 (ABCA1) transfers free cholesterol to lipid-free apoA-I, forming nascent HDL. The transporters ATP-binding cassette subfamily G member 1 (ABCG1) and scavenger receptor class-B type I (SR-BI) efflux cholesterol to mature HDL particles [99]. In the second stage, HDL can be hydrolyzed by HL and endothelial lipase (EL) to form HDL remnants, which can be removed by the liver. HDL can transfer lipids to apoB-containing lipoproteins via cholesteryl ester transfer protein, which are then removed by the LDL receptor. Alternatively, SR-BI expressed on the liver can interact with apoA-I to remove cholesteryl esters from HDL for excretion. HDL cholesterol levels were first reported to

have an inverse relationship with cardiovascular risk in the 1960s. Since then, the protective effects of HDL in lipid homeostasis have been extensively documented [98].

### **1.3 Lipoprotein lipase**

#### **1.3.1 Overview of the *sn*-1 lipases**

As previously highlighted, the delivery of lipids to cells from lipoproteins in the circulation is essential for a variety of cellular functions. Lipases are the enzymes that mediate this process by the hydrolysis of ester bonds in TG, PL, and cholesteryl esters [101]. HL, EL, and LPL have phospholipase A<sub>1</sub> (PLA<sub>1</sub>) and TG lipase activities, which can generate FFA, di- and monoacylglycerols by the hydrolysis of TG at the *sn*-1 position, and lysophospholipids by the hydrolysis of PL at the *sn*-1 position, as per Figure 1.4 [102]. In addition to providing energy to cells via FFA, hydrolysis products generated by *sn*-1 family lipases have important implications in cell signaling. For example, lysophospholipids such as lysophosphatidic acid (LPA) can interact with certain G protein-coupled receptors (GPCR) to activate signaling through MAPK/ERK, PI3K/Akt, and cell-cycle control pathways [103]. Of note, LPA has been shown to induce pro-tumorigenic cytokine secretion (IL-6, IL-8, VEGF, MMP) and promote cancer cell proliferation, survival, and metastasis [104].

Alignment of the amino acid sequences revealed the high sequence homology between the *sn*-1 lipases. Because of this, it is thought that they share a common ancestral origin [105]. Site-directed mutagenesis studies showed that the active site motif (Gly-Xaa-Ser-Xaa-Gly) is conserved across all lipases. Other highly conserved sequence areas

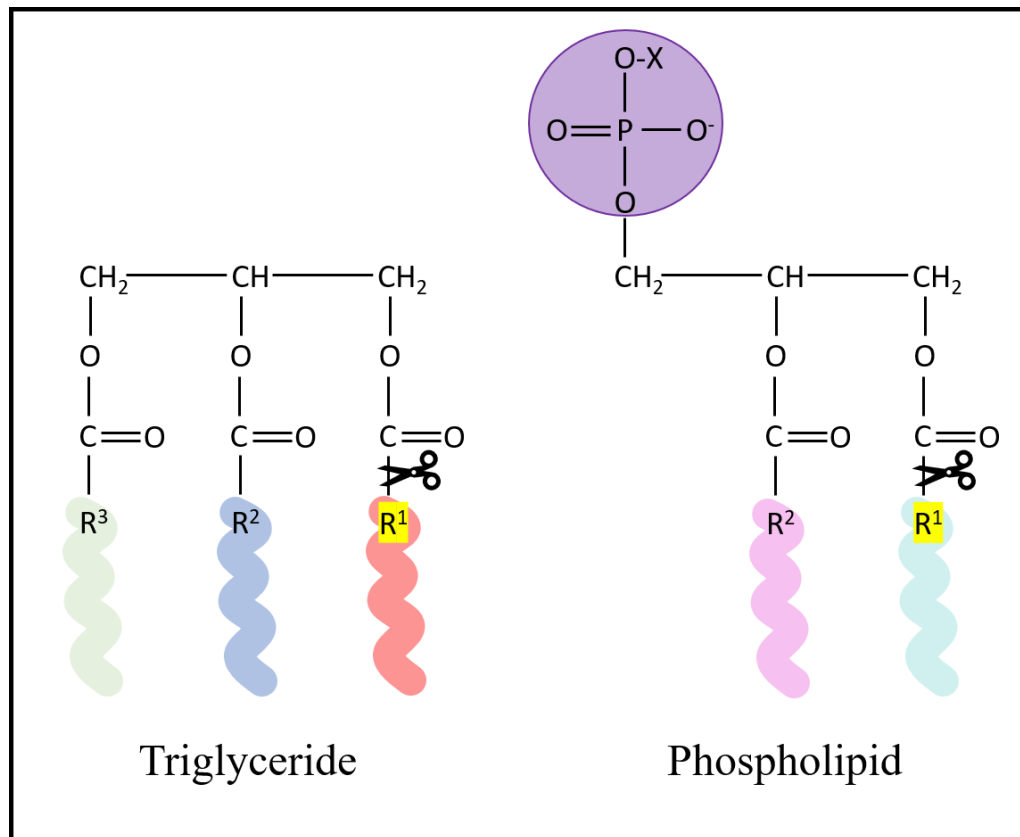


**Figure 1.4:** The *sn*-1 cleavage point of a general phospholipid and triglyceride

HL, EL, and LPL can generate free fatty acids (FFA), di- and monoacylglycerols from TG, and lysophospholipids from PL. These lipases act at the *sn*-1 position, as shown (scissors), to remove acyl chains for use by the surrounding cells. Figure created in Microsoft PowerPoint 2016.

include glycosylation sites, lipid-binding domains, and disulfide bridges [106]. A molecular model of LPL was originally designed using x-ray crystal structures of pancreatic lipase (PL), which provided information on the structure-function relationship of LPL [106]. The N-terminal domain and C-terminal domain are connected by a flexible linker region that allows substrate access to the catalytic site. Structural features of HL and EL can be inferred based on their sequence similarities to LPL. For example, the presence of an  $\alpha/\beta$ -fold in the catalytic region forms a 'lid' that can control substrate access to the active site in *sn*-1 lipases [105, 106]. The C-terminal domain contains heparin-binding sites that allow *sn*-1 lipases to attach to the surface of capillary endothelial cells via heparan sulfate proteoglycans (HSPG) [101]. In addition, *sn*-1 lipases have a non-catalytic bridging function that promotes lipid uptake by cells [105]. However, differences in tissue expression and substrate preference emphasize the distinct roles of HL, EL, and LPL.

HL is predominantly expressed by hepatocytes but is also detected in macrophages, and ovarian and adrenal tissues [107, 108]. HL does not have substrate specificity and hydrolyzes TG and PL from all circulating lipoproteins. HL is also involved in facilitating lipoprotein-receptor interactions in liver lipid metabolism. Because of its multifunctional role, the impact of HL on disease progression is unclear [109]. EL has been detected in the lungs, liver, testis, ovary, and placenta, where it is anchored to vascular endothelial cells. EL is also expressed in macrophages [110]. EL has strong PLA<sub>1</sub> activity and low TG lipase activity, and it preferentially hydrolyzes lipids from HDL. LPL is highly expressed in the adipose tissue, skeletal muscle, and cardiac

muscle, but is also present in the mammary tissue, brain, spleen, lungs, and macrophages. Except in macrophages, LPL is produced by parenchymal cells and then transferred to capillary endothelial cells to access lipoproteins in the circulation. LPL primarily hydrolyzes TG from chylomicrons and VLDL [111, 112].

### **1.3.2 LPL synthesis and processing**

LPL must be synthesized by parenchymal cells, assembled into the correct structure, then transported to the surface of endothelial cells to exert its effects. The LPL gene is located on chromosome 8p22 and encodes 475 amino acids; a 27 amino acid signal peptide is cleaved to produce the mature 448 amino acid protein [113]. LPL is synthesized in the rough ER and becomes increasingly glycosylated as it moves through the *cis*- and *trans*- Golgi network. The significant glycosylation of LPL accounts for 8-12% of the protein and increases the mass from 51 kDa, the approximate subunit mass, to 55 kDa. Studies using ultracentrifugation determined that functional LPL exists as a homodimer [114]. However, in 2019 the crystal structure of LPL bound to an accessory protein was determined and the results suggest that LPL may also be active as a monomer [115].

LPL homodimers are arranged in a head to tail configuration, with a hole in the middle of the interface that is suspected to have a biological function, such as FFA transfer. LPL must interact with lipase maturation factor 1 (LMF1) to form the correct tertiary structure and dimerize [116]. LMF1 is a transmembrane chaperone located in the ER that binds partially folded LPL monomers, forms fully folded monomers, and releases

functional homodimers. If LPL is misfolded, it remains in the ER and is targeted for degradation. In disorders affecting LMF1 expression, LPL secretion decreases, and misfolded protein accumulates in the ER [117]. The mechanism of LPL transport to the vascular endothelial cells is poorly understood. However, following secretion from the parenchymal cells, LPL is shuttled by glycosylphosphatidylinositol-anchored high-density lipoprotein-binding protein 1 (GPIHBP1) to the endothelial surface [118, 101]. A significant reduction in LPL activity was shown to result from loss of GPIHBP1 expression due to LPL being trapped in the interstitial space. Recently, a crystal structure of the LPL-GPIHBP1 complex showed that the C-terminal domain of LPL and GPIHBP1 interact at a 1:1 ratio [119]. From studies investigating LPL-GPIHBP1 interactions, a new model of LPL attachment in the vascular endothelium has been developed (Figure 1.5). Upon secretion from parenchymal cells, LPL is picked up by HSPG in the interstitial space and then transferred to GPIHBP1 on endothelial cells, which has a higher binding affinity. In GPIHBP1 knockout models, LPL remains attached to HSPG in the interstitial space, which lowers the plasma LPL activity. Additionally, using *in vivo* and *in vitro* models, it was revealed that LPL bound to HSPG preferentially moves to GPIHBP1 in the medium, on the surface of cells, and on agarose beads. In this model, HSPG functions to prevent LPL from leaving the local environment, facilitating transfer to GPIHBP1. This ensures that LPL is expressed near the cells that produced, it, so that lipoprotein hydrolysis products reach the tissues that require them [120].

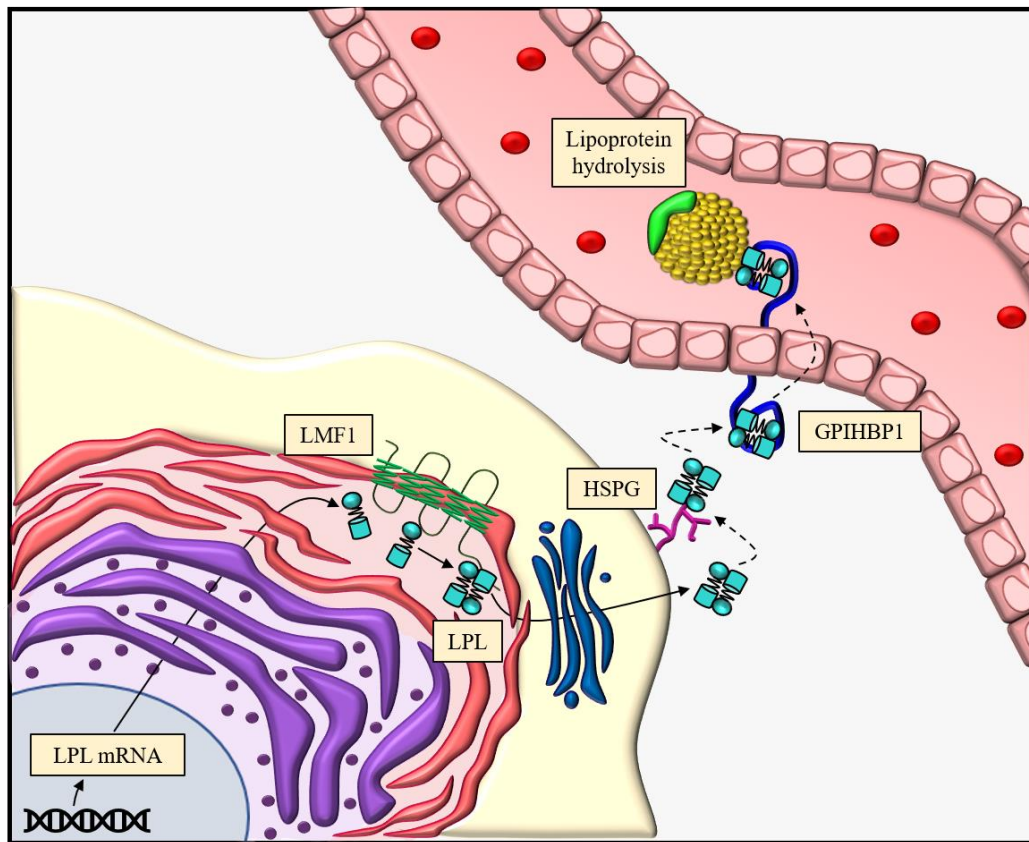


**Figure 1.5:** Transport of LPL from parenchymal cells to the vascular endothelial surface

Tissue parenchymal cells produce lipoprotein lipase (LPL) mRNA, which is translated into LPL monomers in the endoplasmic reticulum (ER). LPL monomers are bound by lipase maturation factor 1 (LMF1), an ER transmembrane chaperone, which assists in the folding and dimerization of mature LPL. LPL dimers then move through the *cis*- and *trans*- Golgi network to become glycosylated and are then secreted into the interstitial space. LPL is bound by heparan sulfate proteoglycan (HSPG) near the site of secretion and then transferred to endothelial-bound glycosylphosphatidylinositol-anchored high-density lipoprotein-binding protein 1 (GPIHBP1). LPL is then able to hydrolyze circulating lipoproteins to transfer FFA to cells. Figure created in Microsoft PowerPoint 2016.

### 1.3.3 Regulation of LPL activity

Once at the endothelial surface, LPL hydrolyzes TG from apoB-containing TG-rich lipoproteins, as discussed previously. ApoC-II is an essential cofactor for LPL activation that is associated with chylomicrons, VLDL, and HDL. Disruptions in the structure or production of apoC-II results in high plasma TG levels and produces the same phenotype as LPL deficiency. Other apoC proteins also play a role in LPL regulation. ApoC-I and apoC-III have been shown to noncompetitively inhibit LPL activity by affecting its ability to bind to lipoproteins [121, 122].

Specific cytokines are also known to affect LPL activity. In mice, the combination of IFN- $\gamma$  and TNF- $\alpha$  synergistically reduce LPL activity, mRNA, and protein levels. Cytokine-regulated gene transcription elements have been identified in the 5' flanking region of the LPL gene. Some positively regulate LPL expression, such as IFN- $\gamma$ -responsive element and the nuclear factor-1-like motif [123]. TNF- $\alpha$  was determined to inhibit LPL gene transcription by interfering with nuclear factors involved in transcription [124]. Other cytokines had no effect on their own but caused significant effects while in combination. For example, IL-6 and leukemia inhibitory factor only caused a decrease in LPL activity when combined. This is a crucial observation and is more representative of physiological conditions. At any given time, many different cytokines circulate within the same tissue environment in both normal and diseased states. In cancer, the combination of IFN- $\gamma$  and TNF- $\alpha$  has been implicated in the development of wasting syndrome [123, 125]. CSF, which can be secreted from breast cancer cells, has been shown to increase

LPL expression in macrophages [126]. Finally, TGF- $\beta$  has been shown to inhibit LPL gene transcription, but the mechanism is not well understood [127].

#### **1.4 LPL hydrolysis products and their relevance to breast cancer**

Our laboratory has previously determined the species and abundance of the lipids released by the LPL hydrolysis of total lipoproteins [128]. Treatment of human macrophages with total LPL hydrolysis products resulted in the activation of several signaling nodes that are also involved in cancer. For example, the hydrolysis products caused an increase in the phosphorylation of macrophage-CSF receptor (M-CSFR), platelet-derived growth factor receptor (PDGFR), VEGF receptor 2, and STAT1. Activation of these factors are known to cause immune cell recruitment, angiogenesis, pro-inflammatory cytokine secretion, and resistance to apoptosis. The strongest effect of LPL hydrolysis products was on PDGFR, which had a 4-fold increase in phosphorylation, as determined by antibody array, and results in a 2-fold increase in platelet-derived growth factor (PDGF) induced cell migration [128, 130]. Like many other growth factors, PDGF is dysregulated in cancer and has been shown to promote migration, angiogenesis, growth, and survival. In breast cancer, increased PDGFR expression is correlated with aggressive subtypes with high grade, node metastasis, and early recurrence. PDGFR was found to be upregulated in 20% of primary TNBC tumors; as discussed previously, TNBC has the worst prognosis of all breast cancer subtypes [129]. CAFs in the tumor microenvironment are known to secrete significant amounts of PDGF. In luminal (MCF-7) and TNBC (MDA-MB-231) cell lines, PDGF released from CAFs was shown to stimulate tumor cell proliferation via PDGFR. In addition, TNBC cells were shown to

induce upregulated PDGFR expression in TAMs. There was also a significant increase in phosphorylated Akt levels in TAMs, which was discussed earlier in terms of promoting tumorigenesis and resistance to apoptosis [130, 131]. Interestingly, our laboratory also reported a significant increase in Akt phosphorylation in macrophages following incubation with LPL hydrolysis products. This effect was due to the FFA component of the hydrolysis products [128].

Our laboratory has also analyzed the gene expression changes in human macrophages in response to LPL hydrolysis products. Hydrolysis products were found to cause significant changes in genes involved in cell cycle control, response to IFN and ER stress, and various other functions [132]. In addition, LPL hydrolysis products were shown to increase pro-inflammatory TNF- $\alpha$  secretion from endothelial cells. Hydrolysis products also increased the expression of intracellular adhesion molecule (ICAM) by endothelial cells [133]. In early cancer, ICAM is associated with increased T cell response. However, once cancer escapes immune surveillance, ICAM is known to have pro-tumorigenic effects. In breast cancer, ICAM is upregulated by TNF- $\alpha$  and IFN- $\gamma$  and has been shown to be positively correlated with more aggressive subtypes. It is thought that ICAM is involved in tumor cell invasion and metastasis by promoting intravasation [134]. Also, our laboratory showed that LPL hydrolysis products significantly increase the gene expression of TNF- $\alpha$ , IL-1 $\beta$ , and IL-6 in MCF-7 breast cancer cells [Noel, Pickett & Brown, unpublished].

There is substantial evidence that suggests a link between the hydrolysis products generated by LPL from total lipoproteins and the progression of breast cancer. As

discussed, LPL is highly expressed by adipose tissue which surrounds breast tumors. Additionally, mRNA and protein expression of LPL has been detected in select breast cancer cell lines [135, 112]. Therefore, it is possible that LPL expressed by breast cancer cells and adipocytes can hydrolyze lipoproteins to support the energy requirements of the highly proliferative tumor cells [84]. The effect of hydrolysis products on signaling pathways and pro-inflammatory cytokine secretion from breast cancer cells may further connect lipoprotein metabolism and breast cancer progression (Figure 1.6). However, this concept has not been investigated. Determining the novel role of LPL in breast cancer will provide the basis of future studies that could reveal new targets for disease treatment.

### **1.5 Hypothesis**

I hypothesize that the hydrolysis products generated by LPL from total lipoproteins will lead to increased cell metabolic activity and pro-inflammatory cytokine secretion in breast cancer cells.

### **1.6 Objectives**

The specific objectives of this research were 1) to assess breast cancer cell metabolic activity in response to total lipoprotein hydrolysis products generated by LPL, and 2) to assess cytokine expression and secretion by breast cancer cells in response to total lipoprotein hydrolysis products generated by LPL.

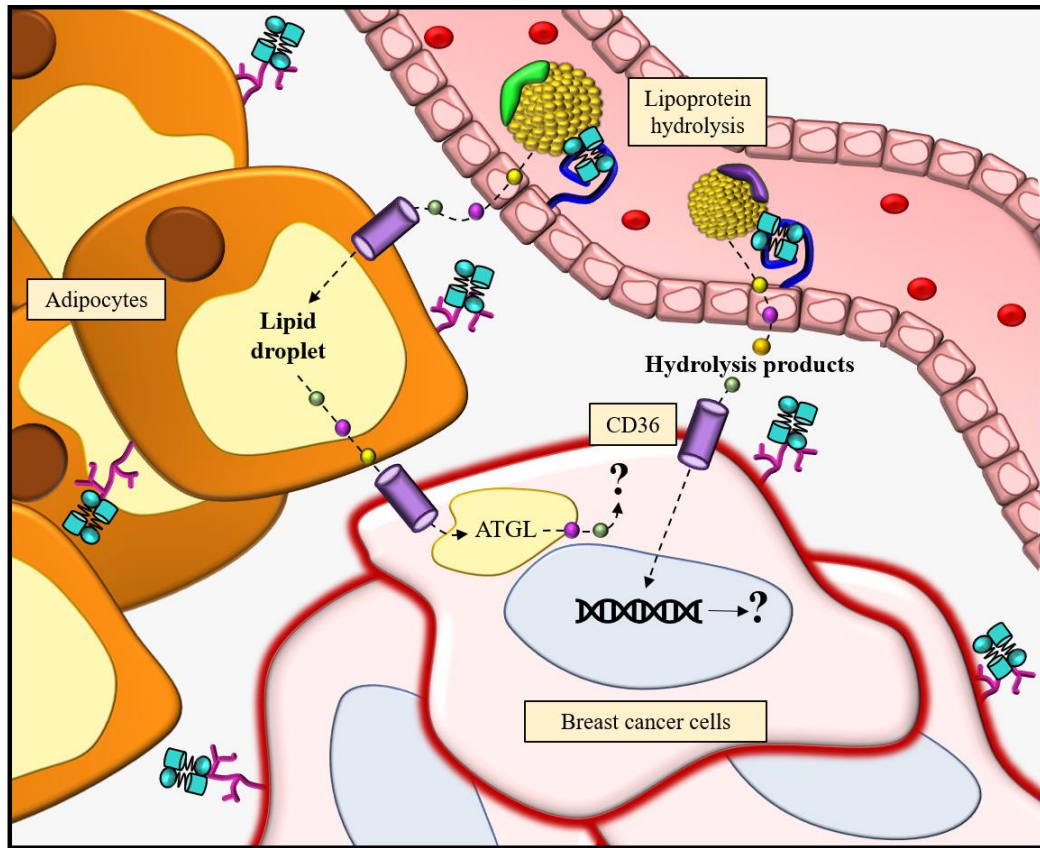


**Figure 1.6:** Schematic of how total lipoprotein hydrolysis products generated by LPL could influence breast cancer progression

LPL is expressed by adipocytes and breast cancer cells within the tumor microenvironment. Hydrolysis products may contribute to breast cancer progression by inducing gene transcription and activating pro-tumorigenic signaling pathways. Excess lipids are stored in lipid droplets. ATGL can liberate stored lipids within breast cancer cells. Breast cancer cells can induce lipolysis in adipocytes to further support tumor progression. Determining the impact of hydrolysis products on breast cancer is the focus of this research. Figure created in Microsoft PowerPoint 2016.

## **Chapter 2    Materials and Methods**

### **2.1 Mammalian cell culture**

#### **2.1.1 HEK-293 cell culture and maintenance**

Human embryonic kidney (HEK-293) cells obtained from the American Type Culture Collection, (ATCC) were grown in T75 culture flasks (#C353136, Corning Life Sciences) with growth medium consisting of Dulbecco's Modified Eagle Medium (DMEM) containing 584 mg/L L-glutamine, 4.5 g/L glucose, 3.7 g/L sodium bicarbonate and 110 mg/L sodium pyruvate (#SH30243FS, Fisher Scientific), supplemented with 10% v/v fetal bovine serum (FBS) (#A7906-100G, Sigma-Aldrich-Aldrich) and 1% v/v antibiotic/antimycotic (A/A) (#15240062, Invitrogen), with a pH of 7.2-7.4. The cells were maintained at 37°C with 5% CO<sub>2(g)</sub>. At 80-90% confluency, the spent medium was discarded, and the cells were washed with 5 mL of non-supplemented DMEM medium. Following this, the cells were incubated for 2 minutes at 37°C with 2.5 mL of 0.25% (w/v) trypsin-ethylenediaminetetraacetic acid (EDTA) (#25200056, Fisher Scientific) to allow the cells to detach from the flask surface. After incubation, the flask was washed with 10 mL of supplemented growth medium, and the cell suspension was mixed by pipette. Lastly, 1 mL of cell-containing medium was added to a new flask containing 14 mL of growth medium and incubated at 37°C with 5% CO<sub>2(g)</sub>.

#### **2.1.2 MCF-7 and T47D cell culture and maintenance**

MCF-7 and T47D human breast cancer cells (ATCC) were cultured in 100-mm dishes (#150466, Fisher Scientific) with growth medium consisting of Roswell Park

Memorial Institute (RPMI)-1640 medium containing 25 mM HEPES, 2.0 g/L sodium bicarbonate, and 0.3 mg/L L-glutamine (#SH30255.01, Fisher Scientific), supplemented with 10% v/v FBS and 1% v/v A/A, with a pH of 7.2-7.4. The cells were incubated at 37°C with 5% CO<sub>2(g)</sub>. At 80-90% confluency, the spent medium was discarded, and the cells were washed with 5 mL of non-supplemented RPMI medium. The cells were then incubated for 2-4 minutes at 37°C with 3.0 mL of 0.25% (w/v) trypsin-EDTA. After incubation, 7 mL of growth medium was added to the culture dish, and the cells were mixed. The cell-containing medium was transferred to a 15 mL tube and centrifuged at 200 ×g for 5 minutes to form a pellet; the supernatant was discarded, and the cell pellet was resuspended in supplemented RPMI growth medium. Following resuspension, 300-500 µL of cell-containing medium was added to a new culture dish containing 10 mL of growth medium and incubated at 37°C with 5% CO<sub>2(g)</sub>.

### **2.1.3 MDA-MB-231, MDA-MB-468, and SKBR3 cell culture and maintenance**

MDA-MB-231, MDA-MB-468, and SKBR3 human breast cancer cells (ATCC) were cultured following the protocol in section 2.1.2, using DMEM growth medium (prepared as per section 2.1.1) instead of RPMI growth medium.

### **2.1.4 MCF-10a cell culture and maintenance**

MCF-10a non-tumorigenic human breast cells (ATCC) were cultured in 100-mm dishes with DMEM/F-12 medium containing 365 mg/L L-glutamine, 3.2 g/L glucose, 2.438 g/L sodium bicarbonate and 55 mg/L sodium pyruvate (#11320033, Fisher Scientific), supplemented with 5% v/v horse serum (#26050088, Fisher Scientific), 20

ng/mL epidermal growth factor (EGF) (#CB-40052, Fisher Scientific), 10 µg/mL insulin (#12585014, Fisher Scientific), 0.5 µg hydrocortisone (#AC352450010, Fisher Scientific), and 1% v/v A/A, with a pH of 7.2-7.4. The cells were incubated at 37°C with 5% CO<sub>2(g)</sub>. At 80-90% confluency, the spent medium was discarded, and the cells were washed with 5 mL of non-supplemented DMEM/F-12 medium. The cells were then incubated for 2-4 minutes at 37°C with 3.0 mL of 0.25% (w/v) trypsin-EDTA. After incubation, 7 mL of growth medium was added to the culture dish, and the cells were mixed. The cell-containing medium was transferred to a 15 mL tube and centrifuged at 200 ×g for 5 minutes to form a pellet; the supernatant was discarded, and the cell pellet was resuspended in supplemented DMEM/F-12 growth medium. Following resuspension, 300 µL of cell-containing medium was added to a new culture dish containing 10 mL of growth medium and incubated at 37°C with 5% CO<sub>2(g)</sub>.

## **2.2 HEK-293 transfection with recombinant LPL plasmid**

### **2.2.1 HEK-293 cell transfection**

At 70-80% confluency, HEK-293 cells were detached from the culture flask following incubation at 37°C with 0.25% (w/v) trypsin-EDTA as per section 2.1.1. The cells were mixed thoroughly with 21 mL of DMEM growth medium, and 10 mL of cells were seeded in two 100-mm culture dishes. The cells were incubated at 37°C with 5% CO<sub>2(g)</sub> for 24 hours. After 24 hours, Lipofectamine<sup>TM</sup> transfection reagent (#11668027, Fisher Scientific) containing 5.85 µg of pcDNA3.LPL plasmid (#V79020, Fisher Scientific) or without LPL plasmid (mock control) was added to the cells [128]. Our

laboratory has previously reported no difference in lipase activity between control cells transfected with an empty pcDNA3 vector and cells transfected with no vector [132]. Following 5 hours of incubation, 5 mL DMEM growth medium supplemented with 20% v/v FBS and 2% v/v A/A was also added to the cells. After 19 hours of incubation, the cells were washed with 5 mL of DMEM and then treated with 5 mL of heparinized DMEM medium containing 1% v/v A/A and 10 U/mL heparin (Organon); heparin displaces LPL from the cell surface allowing it to be collected in the medium. After 23.5 hours of incubation, 1 mL of heparinized DMEM containing 100 U/mL heparin and 1% v/v A/A was added, and the cells were incubated for 30 minutes at 37°C with 5% CO<sub>2(g)</sub>. The media from both plates were collected in 15 mL tubes and centrifuged to remove cell debris. LPL-containing media and mock media were aliquoted in 1.5 mL tubes and stored at -80°C until use.

### **2.2.2 Lysis and collection of LPL-transfected and mock HEK-293 cells**

The plates of cells were washed three times with 2 mL of 0.01 M ice-cold phosphate-buffered saline (PBS) at pH 7.0. Cell lysis buffer (#9803S, Cell Signaling Technology) supplemented with 0.1% v/v protease/phosphatase inhibitor (#5872S, Cell Signaling Technology) was added to each plate of cells and placed on ice for 15 minutes. The cells were scraped into the lysis buffer, collected into 1.5 mL tubes, and stored at -80°C until use.

To determine the protein concentration of the cell lysates, a bicinchonic acid (BCA) Protein Assay kit (#PI23235, Fisher Scientific) was used according to the

manufacturer's instructions. A 96-well plate was prepared containing a standard curve of albumin (from 0 mg/mL to 2,000 mg/mL) and cell lysates in BCA assay buffer, which was incubated at 37°C for 30 minutes. The absorbance at 562 nm was measured using a PowerWave XS microplate reader (BioTek), which was used to calculate the protein concentration of the samples. The protein concentration of the cell lysates was used to calculate how much sample to load in subsequent protein gels.

## **2.3 Qualitative and quantitative analysis of LPL**

### **2.3.1 SDS-PAGE and western blot**

Heparinized media and cell lysates were analyzed by sodium dodecyl sulfide polyacrylamide gel electrophoresis (SDS-PAGE). A stock solution of 29:1 acrylamide:bis-acrylamide (#A3574, Sigma-Aldrich) was used to prepare a 10% (w/v) resolving gel and a 4% (w/v) stacking gel. For media samples, 15  $\mu$ L heparinized medium was mixed with 5  $\mu$ L of 4x sample solution (50% v/v glycerol, 6% v/v  $\beta$ -mercaptoethanol, 10% w/v SDS, and 0.01% w/v bromophenol blue) in a 1.5 mL tube. Cell lysate samples were first analyzed by a BCA assay to determine the protein concentration as per section 2.2.2, following which a 20  $\mu$ L solution consisting of 5  $\mu$ g of protein, 5  $\mu$ L of 4x sample solution, and deionized water was prepared in a 1.5 mL tube. Media and lysate samples were boiled for 6 minutes before loading 20  $\mu$ L of the sample into the wells of the gel. Gels ran at 200V for approximately 45 minutes, a 1x Tris-glycine-SDS (TGS) solution with a pH of 7.4 diluted from 10x TGS containing 25 mM Tris, 192 mM glycine, and 0.1% SDS (#1610772, Bio-Rad) was used as running buffer.

Separated proteins were transferred onto nitrocellulose membranes (#1620115, Bio-Rad) at 70V at 4°C for 75 minutes using ice-cold transfer buffer (TGS supplemented with 20% v/v methanol). After transfer, the membranes were blocked on a rocker at 4°C overnight in blocking solution consisting of 1x Tris-buffered saline (TBS) at pH 7.4, 5% w/v bovine serum albumin (BSA) (#A7906, Sigma-Aldrich), and 0.05% v/v Tween-20 (#P9416, Sigma-Aldrich). Following blocking, the membranes were incubated with the primary antibody of choice diluted in blocking solution at 4°C overnight. The primary antibodies used were a polyclonal anti-human LPL antibody (#sc-32885, Santa Cruz Biotechnology) at a 1:2,000 dilution, and an anti-mouse  $\beta$ -actin antibody at a 1:5,000 dilution (#NB600-501, Novus Biologicals). After the primary antibody incubation, the membranes were washed four times with 15 mL of TBS containing 0.05% v/v Tween-20 by rocking at room temperature for 10 minutes between each wash. Next, the appropriate secondary antibody was diluted in blocking solution and incubated with the membranes for 2 hours at room temperature with rocking. The secondary antibodies used were a 1:2,000 dilution of donkey anti-rabbit antibody conjugated to horseradish peroxidase (HRP) (#SA1-200, Fisher Scientific), or a 1:2,000 dilution of a donkey anti-mouse antibody conjugated to HRP (#SA1-100, Fisher Scientific). After 2 hours, the membranes were again washed four times with TBS containing 0.05% v/v Tween-20. Finally, the membranes were developed with the ECL<sup>TM</sup> Prime Western Blotting Detection Kit (#RPN2232, GE Healthcare) according to the manufacturer's instructions. Chemiluminescence was detected using an ImageQuant LAS detection system (GE

Healthcare) upon cooling to -25°C. ImageJ software was used to analyze bands on the resulting images [136].

### **2.3.2 Lipase activity assay**

The chromogenic lipase substrate 1,2-*O*-dilauryl-*rac*-3-glutaric-resorufin ester (#D7816-10MG, Sigma-Aldrich) was used to measure the enzymatic activity of LPL as previously described [137]. A 2 mg/mL resorufin ester stock solution was prepared using dioxane (#360481, Sigma-Aldrich) and stored protected from light at 4°C until use. In triplicate, 15 µL of LPL or mock heparinized media (see section 2.2) were added to a 96-well plate (#12565383, Fisher Scientific) containing 165 µL of lipase assay buffer (20 mM Tris, 1 mM EDTA, pH 8.0). The resorufin ester stock was diluted to 0.3 mg/mL in lipase assay buffer, and 20 µL was added to each sample well immediately before taking measurements. The absorbance was measured continuously over 60 minutes at 572 nm using a Synergy fluorescent plate reader (BioTek) set to 25°C. The amount of resorufin produced, proportional to the activity of the sample, was determined using a standard curve (0, 0.2, 0.4, 0.6, 0.8, 1.2, 2.0, 3.0, 4.0, 6.0, 8.0 µM) prepared from a 400 µM resorufin ester stock solution.

## **2.4 Lipoprotein isolation and quantification**

### **2.4.1 Total lipoprotein isolation**

Overnight-fasted plasma of normolipidemic anonymous donors was collected to isolate total lipoproteins ( $\rho < 1.21$  g/mL). Blood was provided in 50 mL tubes containing 2 mL of 0.2 M EDTA solution and then centrifuged at 2,800 rpm (1471 x *g*) using a

Heraeus™ Multifuge™ X1R centrifuge (Fisher Scientific) for 15 minutes at 4°C. Following centrifugation, the plasma in the supernatant was pooled, the total volume was measured, and the density of the plasma was determined using an analytical balance. A high-density gradient solution consisting of 38.25 g of NaCl, 88.5 g of KBr, 2.5 mL of 0.2 M EDTA, and 250 mL deionized water was used to adjust the density of the plasma to 1.21 g/mL. Equal volumes of the adjusted plasma were transferred to four ultracentrifuge tubes and placed in a 70.1Ti rotor (#342184, Beckman) to undergo ultracentrifugation. Ultracentrifugation was performed using a Beckman L90K centrifuge set to 50,000 rpm (256,631 x g) for 44 hours at 4°C. 44 hours later, the total lipoproteins were collected from the top layer of the gradient and pooled in another tube and placed on ice. Approximately 10 cm of cellulose dialysis tubing (#S25645B, Fisher Scientific) was boiled for 30 minutes in a solution consisting of 500 mL of deionized water, 2% w/v NaHCO<sub>3</sub>, and 1 mM EDTA. The total lipoproteins were transferred into the cooled tubing and dialyzed in 4 L PBS for 48 hours at 4°C, changing the PBS every 12 hours. The lipoproteins were stored under N<sub>2(g)</sub> at 4°C after dialysis to prevent oxidation.

#### **2.4.2 Phospholipid quantification in total lipoproteins**

The phospholipid content of the total lipoproteins was quantified using the Wako Phospholipid C assay kit (#997-01801, Wako Diagnostics), according to manufacturer's instructions. In a 96-well plate, 5 µL of total lipoproteins were added in triplicate to wells containing 15 µL of PBS. A 54 mg/dL choline chloride solution (equivalent to 300 mg/dL phospholipids) was diluted in PBS to generate a standard curve (0, 75, 150, 225, 300 mg/dL). Two hundred µL of color reagent was added to the lipoprotein samples and

standard solutions, which were then mixed and incubated for 5 minutes at 37°C. The phospholipid concentration of the total lipoproteins was determined from the absorbance of the samples at 600 nm using a Synergy fluorescent plate reader.

## **2.5 Lipoprotein hydrolysis product generation, quantification, and treatment of breast cancer and MCF-10a cells**

### **2.5.1 Hydrolysis of total lipoproteins by LPL**

Lipoprotein hydrolysis products were generated by incubating a 1:1 ratio of total lipoproteins with either heparinized medium containing LPL, or heparinized medium containing no LPL (mock) (see section 2.2.2), at 37°C for 4 hours in 1.5 mL tubes. Following incubation, the samples were placed on ice, and the amount of FFA produced was quantified (see section 2.5.2), and subsequently used to treat breast cancer cells (see section 2.5.3).

### **2.5.2 Quantification of the FFA content of lipoprotein hydrolysis products**

The FFA content of the lipoprotein hydrolysis products produced by LPL was measured using the NEFA-HR(2) commercial kit (#999-34691, Wako Diagnostics), according to manufacturer's instructions. A 1 mM oleic acid stock solution (#276-76491, Wako Diagnostics) was diluted in deionized water to generate a standard curve (0, 0.5, 0.75, 1.0, 1.5, 2.0, 4.0 nmol/well). To a 96-well plate, 4 µL of the standard curve solutions and 4 µL of LPL hydrolysis products or mock products were added in triplicate. Solvent A (225 µL of 50 mmol/L phosphate buffer, pH 7.0, 0.05% sodium azide) was added to each well and incubated for 10 minutes at 37°C. Ten minutes later, 75 µL of

Solvent B (2.4 mmol/L 3-methyl-N-ethyl-N-( $\beta$ -hydroxyethyl)-aniline) was added to each well and incubated at 37°C for 10 minutes. Sample absorbance was measured at 550 nm at 37°C using a Synergy fluorescent plate reader. The FFA content of each sample was determined from the standard curve.

### **2.5.3 Treatment of breast cancer and MCF-10a cells with lipoprotein hydrolysis products**

To prepare for treatment, breast cancer and MCF-10a cells at 80-90% confluency were pelleted and resuspended as described in section 2.1. The cell concentration was determined by mixing a 1:1 ratio of cell suspension and Trypan Blue (#15250061, Fisher Scientific), and counting the live cells using a hemocytometer (#02-671-54, Fisher Scientific). Cells were diluted to  $1.5 \times 10^3$  cells per mL in the appropriate growth medium for the cell line being treated (see section 2.1), and 150  $\mu$ L per well was seeded for control and treatment groups in a 96-well plate. For the collection of cell lysates, cells were instead diluted to  $3.86 \times 10^5$  cells per mL in the appropriate growth medium, and 2.5 mL was seeded into each well of a 6-well plate. Cells were incubated for 24 hours at 37°C with 5% CO<sub>2(g)</sub> before treatment.

After 24 hours, the cells were pre-treated for 1 hour with a fatty acid-free medium solution consisting of 0.2% w/v fatty acid-free bovine serum albumin (FAF-BSA) (#A7030, Sigma-Aldrich), 25  $\mu$ g/ mL of the lipase inhibitor tetrahydrolipstatin (THL) (#O4139, Sigma-Aldrich) dissolved in dimethyl sulfoxide (DMSO) (#276855, Sigma-Aldrich), 1% v/v A/A, and the appropriate plain culture medium for the cell line being

treated (see section 2.1). During this time, the hydrolysis products generated by LPL were diluted to 0.68 mM, a concentration within the normal range in the blood, with the fatty acid-free medium solution described above. An equal volume of mock products were also mixed with the same fatty acid-free medium solution. After the pre-treatment period, 150  $\mu$ L of diluted LPL hydrolysis products or mock products were added to the breast cancer or MCF-10a cells in triplicate and the cells were incubated at 37°C for 24 hours. Blank wells, untreated cells, and cells treated with DMSO as a vehicle control were also included in the 96-well plate. Following incubation, 50  $\mu$ L of cell supernatant was collected from each well and stored at -80°C for future analysis. The metabolic activity of the cells in the 96-well plate was assessed by MTT (3-(4, 5-dimethylthiazolyl-2)-2,5-diphenyltetrazolium bromide) assay (see section 2.6.1).

## **2.6 Analyses of breast cancer and MCF-10a cell metabolic activity and cytokine secretion**

### **2.6.1 Measurement of cell metabolic activity by MTT assay**

The metabolic activity of cells treated with either lipoprotein or mock hydrolysis products was determined with an MTT assay. The yellow tetrazolium compound MTT (#M6494, Fisher Scientific) was dissolved in PBS to make a 5 mg/mL solution.

Following treatment and collection of 50  $\mu$ L of cell supernatant as per section 2.5.3, 10  $\mu$ L of MTT solution was added to each well used in the 96-well plate, and then incubated for 4 hours at 37°C. After 4 hours, purple formazan crystals formed from the reduction of MTT were visible in the wells. The formazan crystals were dissolved by adding 100  $\mu$ L

of 0.1 N HCl in isopropanol (#AC167880025, Fisher Scientific) to each well and mixing thoroughly. The absorbance of the samples was read at 570 nm and 630 nm using a PowerWave XS microplate reader. The 630 nm reference wavelength was subtracted from the sample absorbance at 570 nm to account for background noise. From this, the sample blank was subtracted to give the corrected absorbance for each sample. The absorbance is proportional to the metabolic activity of the cell.

## **2.6.2 Analysis of cytokine expression by cytokine array**

The presence and relative levels of cytokines in the supernatant of MDA-MB-231 and MCF-7 cells, treated with either lipoprotein or mock hydrolysis products, were measured using the Proteome Profiler<sup>TM</sup> Human Cytokine Array (#ARY005B, R&D Systems) according to the manufacturer's instructions. While the supernatants were thawed on ice, the cytokine array membranes were blocked using Array Buffer 4 for 1 hour on a rocking platform shaker. Samples were prepared by incubating 1 mL of cell supernatant, 0.5 mL Array Buffer 4, and 15  $\mu$ L of human cytokine array detection antibody cocktail for 1 hour at room temperature. The samples were added to the membranes and incubated overnight at 2°C on a rocking platform shaker. The next day, membranes were washed three times with wash buffer before being incubated with a streptavidin-HRP solution for 30 minutes at room temperature. The membranes were washed again and then transferred to a glass plate using tweezers. One mL of Chemi Reagent Mix (a 1:1 mixture of stabilized hydrogen peroxide and luminol) was pipetted evenly over each membrane and incubated for 1 minute. Immediately after, excess Chemi Reagent Mix was blotted from the membranes using an absorbent wipe, the glass plate

was wrapped tightly with plastic wrap, and the membranes were visualized (with exposure times from 30 seconds to 10 minutes) using an ImageQuant LAS detection system set to chemiluminescence. ImageJ software was used to obtain pixel density values of each spot of the array; the identity of the cytokines was determined by matching the spots to the coordinates on a transparency overlay provided by the manufacturer. Duplicate spots were averaged to get the average pixel density for each cytokine of the array, which was proportional to the relative amount of cytokine in the sample. Pixel density data were normalized to the reference spots and presented as a percent of mock for each array to account for measurement variability.

### **2.6.3 ELISA to measure the concentration of TNF- $\alpha$ , IL-4, and IL-6 cytokines**

The concentrations of TNF- $\alpha$ , IL-6, and IL-4 in the supernatant of breast cancer and MCF-10a cells, treated with either lipoprotein or mock hydrolysis products, were measured using the Human TNF- $\alpha$ , Human IL-6, or Human IL-4 DuoSet<sup>®</sup> ELISA development system, respectively (#DY210, #DY206, #DY204 - R&D Systems). Minor adjustments were made to the manufacturer's protocol for both cytokines. The plates were prepared by adding 100  $\mu$ L of capture antibody, diluted as per manufacturer's instructions, to each well and incubating overnight at room temperature. Following incubation, the wells were emptied and washed three times with wash buffer (0.05% Tween 20 in PBS, pH 7.2-7.4) using a squirt bottle. After the last wash, the plates were blotted against absorbent wipes to remove any remaining wash buffer. The wells were blocked for 2 hours at room temperature with 300  $\mu$ L of reagent diluent (1% FAF-BSA in PBS, pH 7.2-7.4, 0.2  $\mu$ m filtered). During this time, the cell supernatants were thawed on

ice, and a standard curve was generated by serial dilution of recombinant human TNF- $\alpha$  (15.6, 31.3, 62.5, 125, 250, 500, 1,000 pg/mL), recombinant human IL-6 (9.38, 18.8, 37.5, 75, 150, 300, 600 pg/mL), or recombinant human IL-4 (31.3, 62.5, 125, 250, 500, 1000, 2,000 pg/mL). Upon thawing, the samples were prepared by diluting each stock supernatant in reagent diluent at a 1:10, 1:100, and 1:1,000 ratio. Undiluted supernatant was also included in the assay for each set of samples. Following the blocking period, the wells were washed and emptied as described above and 200  $\mu$ L of each sample was added in duplicate to the plate, which was sealed and incubated at room temperature for two hours. The wells were washed and emptied, then 100  $\mu$ L diluted detection antibody was added to each well and incubated at room temperature for two hours. Following this, the wells were washed and emptied and 100  $\mu$ L of a streptavidin-HRP solution was added to each well and incubated at room temperature for 20 minutes out of direct light. During this time, the 1-Step<sup>TM</sup> Ultra TMB-ELISA substrate solution (#34028, Fisher Scientific) was equilibrated to room temperature. After the plates were washed and emptied, 100  $\mu$ L of substrate solution was added to each well and incubated at room temperature for 20 minutes out of direct light. To stop the colour development, 50  $\mu$ L of 2 M H<sub>2</sub>SO<sub>4</sub> was added to each well and mixed thoroughly. The absorbance was immediately read at 450 nm and 540 nm using a PowerWave XS microplate reader. The 540 nm reference wavelength was subtracted from the sample absorbance at 450 nm to account for background noise. The concentration of TNF- $\alpha$ , IL-6, and IL-4 in the samples was calculated from the standard curve.

#### **2.6.4 Western blot of breast cancer cell lysates**

LPL expression in breast cancer cell lysates was assessed by western blot. Lysates were collected as described in sections 2.2.2 and 2.5.3 and stored at -80°C until use. The lysates were thawed on ice and a BCA assay was used to determine the amount of protein in the sample. SDS-PAGE and western blotting were performed as described in section 2.3.1, using a polyclonal anti-human LPL primary antibody (#sc-32885, Santa Cruz Biotechnology) at a 1:2,000 dilution and a HRP-conjugated donkey anti-rabbit secondary antibody (#SA1-200, Fisher Scientific) at a 1:2,000 dilution. Simultaneously,  $\beta$ -actin was assessed as a loading control in the same cell lysate samples on a separate membrane using an anti-mouse  $\beta$ -actin antibody (#NB600-501, Novus Biologicals) at a 1:5,000 dilution, and an HRP-conjugated donkey anti-mouse secondary antibody (#SA1-100, Fisher Scientific) at a 1:2,000 dilution. The membranes were developed with the ECL™ Prime Western Blotting Detection Kit according to manufacturer's instructions. Images were captured on the chemiluminescence setting using an ImageQuant LAS detection system. ImageJ software was used to analyze bands on the resulting images.

#### **2.6.5 Analysis of endogenous LPL activity in heparinized media from breast cancer and MCF-10a cells**

To determine if breast cancer cells have endogenous LPL activity, two 6-well plates of each breast cancer cell line used were prepared, as described in section 2.5.3. Following 24 hours of incubation, one 6-well plate from each cell line was treated with 100 U/mL of heparin for 30 minutes at 37°C. The supernatant from the heparinized cells

and the control cells were collected and tested for enzymatic activity using a resorufin ester lipase substrate, as described in section 2.3.2. LPL produced by HEK-293 transfection (see section 2.2.1) was included as a positive control. The absorbance was measured continuously over 60 minutes at 572 nm using a Synergy fluorescent plate reader (BioTek) set to 25°C.

## **2.7 Bioinformatics gene expression analysis of LMF1 in breast cancer and normal breast tissue**

Gene expression data from 20 breast cancer cell lines, 31 breast cancer patient samples, and six normal breast tissue samples were obtained from the Gene Expression Omnibus (GEO) database (GPL570-Affymetrix Human Genome U133 Plus 2.0 Array platform). The data were robust multi-chip average (RMA) normalized by Pitts *et al.* as described [138]. The NetAffx Analysis Center by Affymetrix was used to identify the LMF1 probe IDs, which were then used to filter and average the gene expression data. Gene expression data were analyzed and grouped by breast cancer subtype using Genesis 1.8.1.

## **2.8 Statistical analysis**

Statistical analyses were performed using unpaired Student's t-test or one-way ANOVA, unless otherwise stated. All data are shown as mean  $\pm$  SD, with significance assigned to differences with a  $p < 0.05$ .

## Chapter 3 Results

### 3.1 Assessment of recombinant human LPL following HEK-293 transfection

#### 3.1.1 Western blot and activity assay

From the western blot of LPL and mock-transfected HEK-293 heparinized media, it is evident that the full-length LPL protein was produced and collected (Figure 3.1A). A resorufin ester substrate was used as described to measure the catalytic activity of the recombinant LPL. As expected, heparinized media from LPL-transfected cells showed significantly more lipase activity compared to mock-transfected heparinized media. The rate of resorufin production, which is proportional to the lipase activity, was  $2.97 \pm 0.36$   $\mu\text{mol}/\text{mL}/\text{min}$  versus  $0.195 \pm 0.01$   $\mu\text{mol}/\text{mL}/\text{min}$ , respectively (Figure 3.1B). These results confirm that LPL was successfully transfected and could be used to generate lipoprotein hydrolysis products for subsequent experiments.

#### 3.1.2 Hydrolysis of total lipoproteins

After confirming that LPL was active, total lipoproteins were incubated with either heparinized media containing LPL, or heparinized media containing no LPL (mock) at  $37^{\circ}\text{C}$  for 4 hours. As anticipated, the amount of FFA generated by LPL was significantly higher than the FFA generated from mock media containing no LPL ( $1.3 \pm 0.007$   $\text{nmol}/\mu\text{L}/4\text{h}$  FFA versus  $0.070 \pm 0.005$   $\text{nmol}/\mu\text{L}/4\text{h}$  FFA, respectively) (Figure 3.2). The hydrolysis products were diluted to 0.68 mM by FFA content in fatty acid-free media before being used to treat breast cells. Mock products were diluted by the same factor before being used to treat control cells.

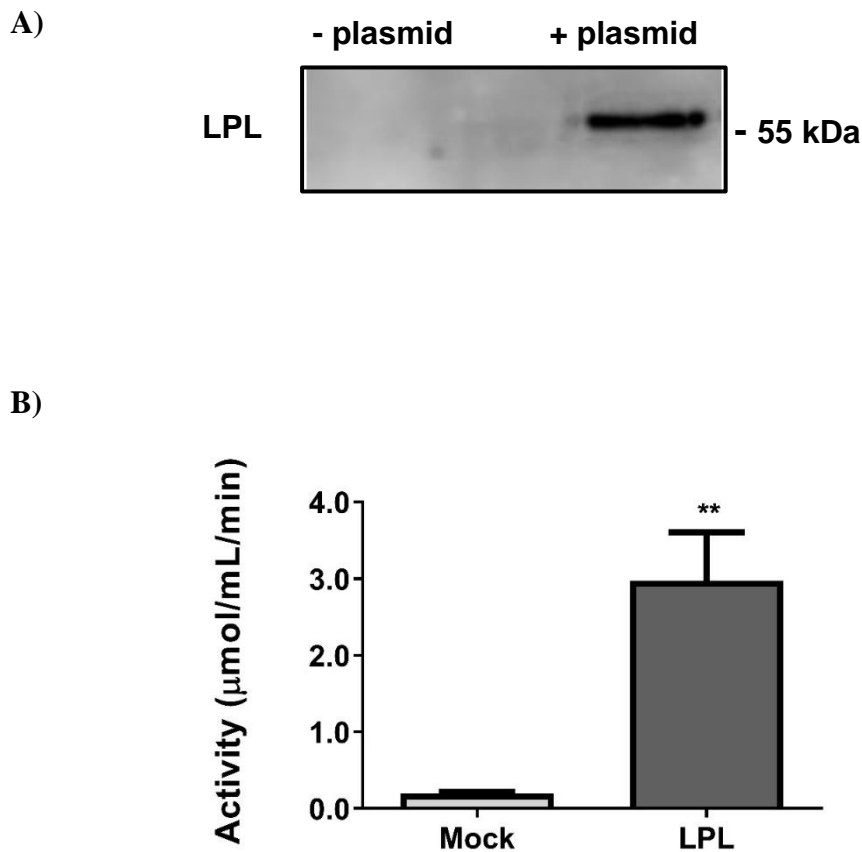


**Figure 3.1:** Analysis of LPL protein expression and enzymatic activity following HEK-293 cell transfection with LPL plasmid

HEK-293 cells were transfected with or without LPL plasmid. Heparinized media and cell lysates were collected from both groups. **(A)** Western blot of heparinized media from transfected cells to detect LPL. **(B)** The enzymatic activity of heparinized media from mock and LPL-transfected cells was determined using a resorufin ester substrate. Data are presented as mean ( $n=3$ )  $\pm$  SD, with  $p= 0.012$  (\*\*) calculated using unpaired t-test.

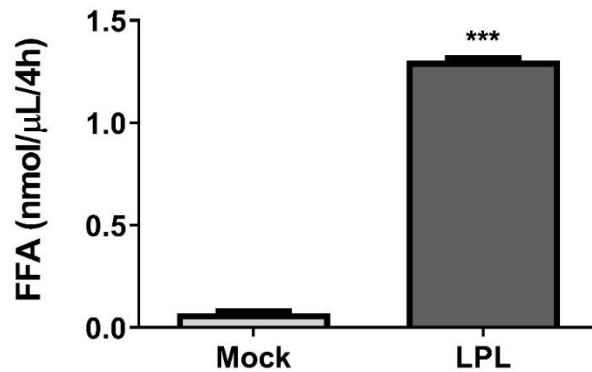


**Figure 3.2:** FFA quantification of total lipoprotein hydrolysis products after incubation with LPL or mock-transfected heparinized media

Heparinized media and cell lysates from LPL or mock-transfected HEK-293 cells were incubated at a 1:1 ratio with total lipoproteins ( $p < 1.21$  g/mL) for 4 hours at 37°C to generate hydrolysis products. The FFA content of the hydrolysis products was quantified using the NEFA-HR(2) commercial kit according to manufacturer's instructions. Data are presented as mean ( $n=3$ )  $\pm$  SD, with  $p < 0.001$  (\*\*\*) calculated using unpaired t-test.

### **3.2 The effect of total lipoprotein hydrolysis products on the metabolic activity of breast cancer and MCF-10a cells**

One of the objectives of this study was to determine the effect of total lipoprotein hydrolysis products on the metabolic activity of breast cancer cells. To determine if the breast cancer subtype affects the metabolic response to hydrolysis products, five breast cancer cell lines representing different subtypes of breast cancer were examined. It is well established that cancer cells have altered lipid metabolism, therefore, the non-tumorigenic mammary epithelial cell line MCF-10a was included as a control. MCF-7 (ER/PR-positive, HER2-negative), T47D (ER/PR-positive, HER2-negative), SKBR3 (ER/PR-negative, HER2-positive), MDA-MB-231 (TNBC), MDA-MB-468 (TNBC) and MCF-10a cells were cultured and treated for 24 hours with total lipoprotein hydrolysis products generated by LPL or mock heparinized media, as per section 2.5. The metabolic activity of the cells post-treatment was measured by MTT assay. Interestingly, the metabolic activity of all cell lines treated with LPL-generated hydrolysis products was significantly increased by approximately 20% compared to the mock-transfected control, as shown in Figure 3.3. Because LPL-generated hydrolysis products affected all of the cell lines similarly, regardless of basal metabolic level, it suggests that the increase is not a subtype-specific effect. However, due to the high expression of LPL in the adipose tissue surrounding breast tumors, breast cancer cells have access to a rich source of FFA in their microenvironment. Because of this, we hypothesize that breast cancer cells *in vivo* may upregulate their metabolic activity upon access to LPL-generated hydrolysis products. Therefore, LPL-generated hydrolysis products within the tumor microenvironment may

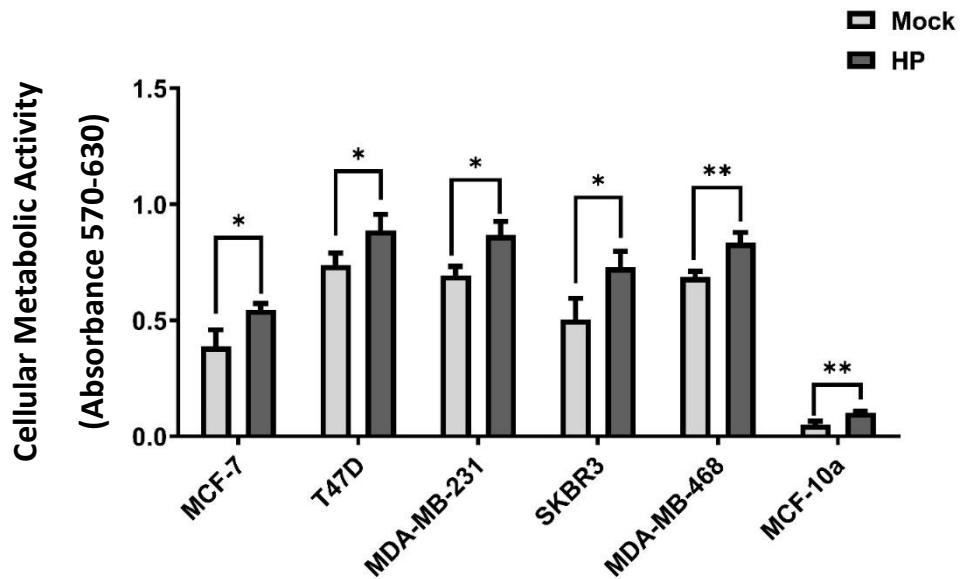


**Figure 3.3:** MTT assay of breast cancer and MCF-10a cells following 24 hours of treatment with LPL hydrolysis products or mock hydrolysis products generated from total lipoproteins

MCF-7, T47D, SKBR3, MDA-MB-231, MDA-MB-468 breast cancer cells and MCF-10a cells were treated with total lipoprotein hydrolysis products generated by LPL or mock heparinized media for 24 hours. Four hours after the addition of MTT reagent, the absorbance of the samples was read at 570 nm and 630 nm using a PowerWave XS microplate reader. Sample absorbance was calculated by subtracting the 630 nm reference wavelength and sample blank from the absorbance at 570 nm. The absorbance is proportional to the metabolic activity of the cell. Data are presented as mean ( $n=3$ )  $\pm$  SD, with  $p < 0.05$  (\*) and  $p < 0.01$  (\*\*) calculated using an unpaired t-test. A one-way ANOVA was performed to compare the mock-treated breast cancer and non-tumorigenic cells and a statistically significant difference was found.

cause breast cancer to grow and progress more quickly. However, MCF-10a cells also showed an increase in cell metabolic activity in response to the LPL-generated hydrolysis products, indicating that this effect is not cancer-specific.

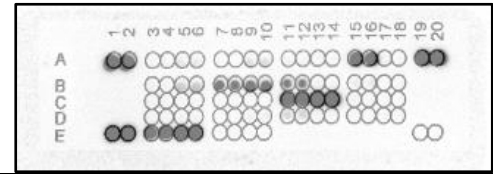
### **3.3 The effect of total lipoprotein hydrolysis products on the cytokine secretion profile of MDA-MB-231 and MCF-7 breast cancer cells**

Our laboratory previously showed that hydrolysis products generated by LPL increase the gene expression of the pro-inflammatory cytokines TNF- $\alpha$ , IL-1 $\beta$ , and IL-6 in macrophages [Noel, Pickett, & Brown, unpublished]. It is also known that pro-inflammatory cytokines create a favorable microenvironment that promotes breast cancer progression. Therefore, the next objective of this study was to determine if there is an effect of total lipoprotein hydrolysis products on cytokine secretion in breast cancer cells. The presence and relative levels of 36 different cytokines (Table 1) in the supernatant of MDA-MB-231 and MCF-7 cells treated with either lipoprotein or mock hydrolysis products were measured via cytokine array as described in section 2.6.2.

#### **3.3.1 The effect of total lipoprotein hydrolysis products on MDA-MB-231 cell cytokine secretion**

Following incubation of the cytokine arrays with MDA-MB-231 cell supernatants, differences between the mock and hydrolysis products treated arrays were visible (Figure 3.4A). The average pixel density for each cytokine was determined using ImageJ software, and data were normalized to the reference spots on the array. Compared to

**Table 1: Cytokines detected by the Proteome Profiler™ Human Cytokine Array**



<b>A1, A2</b>	Reference	<b>B11, B12</b>	ICAM-1/CD54	<b>D7, D8</b>	IL-17A
<b>A3, A4</b>	CCL1/I-309	<b>B13, B14</b>	IFN- $\gamma$	<b>D9, D10</b>	IL-17E
<b>A5, A6</b>	CCL2	<b>B15, B16</b>	IL-1 $\alpha$ /IL-1F1	<b>D11, D12</b>	IL-18
<b>A7, A8</b>	MIP-1 $\alpha$ / $\beta$	<b>B17, B18</b>	IL-1 $\beta$	<b>D13, D14</b>	IL-21
<b>A9, A10</b>	CCL5	<b>C3, C4</b>	IL-1ra	<b>D15, D16</b>	IL-27
<b>A11, A12</b>	CD40 Ligand	<b>C5, C6</b>	IL-2	<b>D17, D18</b>	IL-32 $\alpha$
<b>A13, A14</b>	C5/C5a	<b>C7, C8</b>	IL-4	<b>E1, E2</b>	Reference
<b>A15, A16</b>	CXCL1/GRO $\alpha$	<b>C9, C10</b>	IL-5	<b>E3, E4</b>	MIF
<b>A17, A18</b>	CXCL10	<b>C11, C12</b>	IL-6	<b>E5, E6</b>	Serpin E1
<b>A19, A20</b>	Reference	<b>C13, C14</b>	IL-8	<b>E7, E8</b>	TNF- $\alpha$
<b>B3, B4</b>	CXCL11	<b>C15, C16</b>	IL-10	<b>E9, E10</b>	TREM-1
<b>B5, B6</b>	CXCL12	<b>C17, C18</b>	IL-12 p70	<b>E19, E20</b>	Negative control
<b>B7, B8</b>	G-CSF	<b>D3, D4</b>	IL-13		
<b>B9, B10</b>	GM-CSF	<b>D5, D6</b>	IL-16		

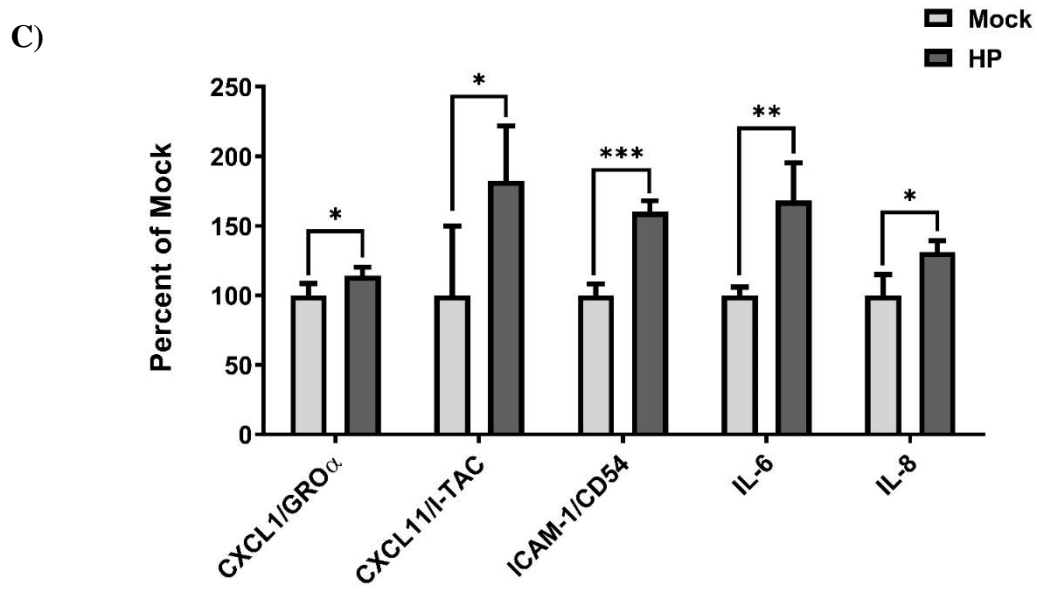
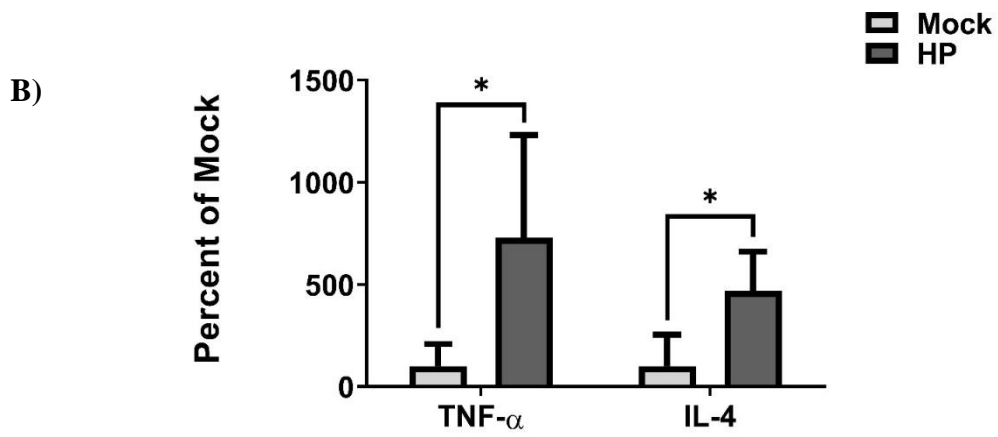
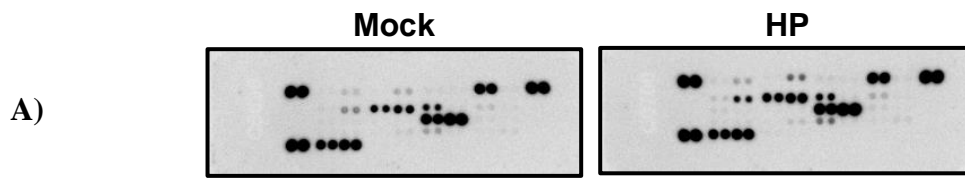


**Figure 3.4** Cytokine array analysis of MDA-MB-231 breast cancer cell supernatant from cells treated with total lipoprotein hydrolysis products generated by LPL or mock heparinized media for 24 hours

MDA-MB-231 breast cancer cells were treated with total lipoprotein hydrolysis products generated by LPL or mock heparinized media for 24 hours. The cell supernatants were collected and stored at -80 °C until use. **(A)** A representative image of cytokine array development following incubation with supernatant from MDA-MB-231 cells treated with mock or LPL hydrolysis products. **(B & C)** Cytokine arrays were visualized using an ImageQuant LAS detection system set to detect chemiluminescence. ImageJ software was used to obtain pixel density values of each spot of the array, and duplicate spots were averaged to determine the relative amount of each cytokine in the sample. **(B)** Highly-expressed and **(C)** low-expressed cytokines were separated for clarity. Data are presented as a percent of mock with mean ( $n=3$ )  $\pm$  SD,  $p<0.05$  (\*),  $p<0.01$  (\*\*), and  $p<0.001$  (\*\*\*) calculated using unpaired t-test.

the mock-transfected control, the hydrolysis products-treated MDA-MB-231 cells had a significant increase in the secretion of multiple cytokines. The data were split into high (Figure 3.4B) and low regulated (Figure 3.4C) cytokines for clarity, with values of greater than 250% of mock considered to be highly-regulated.

### **3.3.2 The effect of total lipoprotein hydrolysis products on MCF-7 cell cytokine secretion**

Differences between the mock and hydrolysis products treated arrays were also visible with supernatant from MCF-7 cells (Figure 3.5A). However, unlike the MDA-MB-231 cells, there was a statistically significant decrease in IL-1 $\alpha$  and IL-27 in the hydrolysis product- treated MCF-7 cells compared to control (mock) (Figure 3.5B). There were no statistically significant increases in cytokine secretion.

### **3.4 The effect of total lipoprotein hydrolysis products on TNF- $\alpha$ , IL-4, and IL-6 cytokine secretion in breast cancer and MCF-10a cells**

Based on the results of the cytokine arrays, I decided to measure the concentration of TNF- $\alpha$ , IL-4, and IL-6 in the supernatants by ELISA, of MCF-7, T47D, SKBR3, MDA-MB-231, MDA-MB-468 breast cancer and MCF-10a cells treated with lipoprotein or mock hydrolysis products.

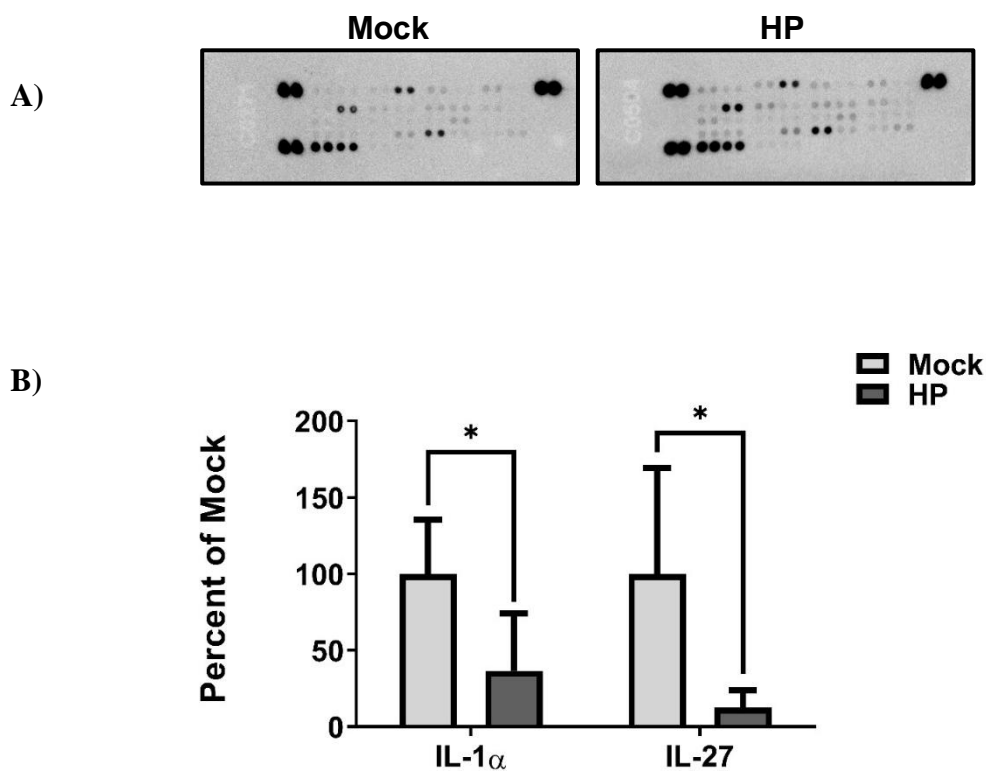


**Figure 3.5:** Cytokine array analysis of MCF-7 breast cancer cell supernatant from cells treated with total lipoprotein hydrolysis products generated by LPL or mock heparinized media for 24 hours

(A) A representative image of cytokine array development following incubation with supernatant from MCF-7 cells treated with mock or LPL hydrolysis products. (B) Cytokine arrays were visualized using an ImageQuant LAS detection system set to detect chemiluminescence. ImageJ software was used to obtain pixel density values of each spot of the array, and duplicate spots were averaged to determine the relative amount of each cytokine in the sample. Data are presented as a percent of mock with mean ( $n=3$ )  $\pm$  SD,  $p<0.05$  (\*),  $p<0.01$  (\*\*), and  $p<0.001$  (\*\*\*) calculated using unpaired t-test.

### **3.4.1 TNF- $\alpha$ cytokine secretion in breast cancer and MCF-10a cells following hydrolysis products treatment**

Across all the cell lines tested, TNF- $\alpha$  was only detected in the undiluted hydrolysis product-treated MDA-MB-231 and MDA-MB-468 cell supernatants (Figure 3.6). These results are generally consistent with the expression pattern of the TNF- $\alpha$  data obtained for MDA-MB-231 and MCF-7 cells by the cytokine arrays.

### **3.4.2 IL-4 cytokine secretion in breast cancer and MCF-10a cells following hydrolysis products treatment**

For MDA-MB-231 undiluted samples, IL-4 secretion was significantly increased in the hydrolysis products treated cells compared to control (mock) (Figure 3.7). Also, IL-4 secretion from undiluted MDA-MB-468 cell supernatant was detected in hydrolysis product-treated cells, but not mock-treated cells. The MCF-7, T47D, SKBR3, and MCF-10a cells did not secrete detectable levels of IL-4 in treated or control cells. These results also similar to the IL-4 data obtained from the cytokine arrays.

### **3.4.3 IL-6 cytokine secretion in breast cancer and MCF-10a cells following hydrolysis products treatment**

For both the MDA-MB-231 and MDA-MB-468 undiluted supernatants, IL-6 secretion was significantly increased in the hydrolysis products treated cells compared to control (Figure 3.8). There were no significant differences between the diluted samples for both cell lines. Significant IL-6 secretion from undiluted SKBR3 cell supernatant was

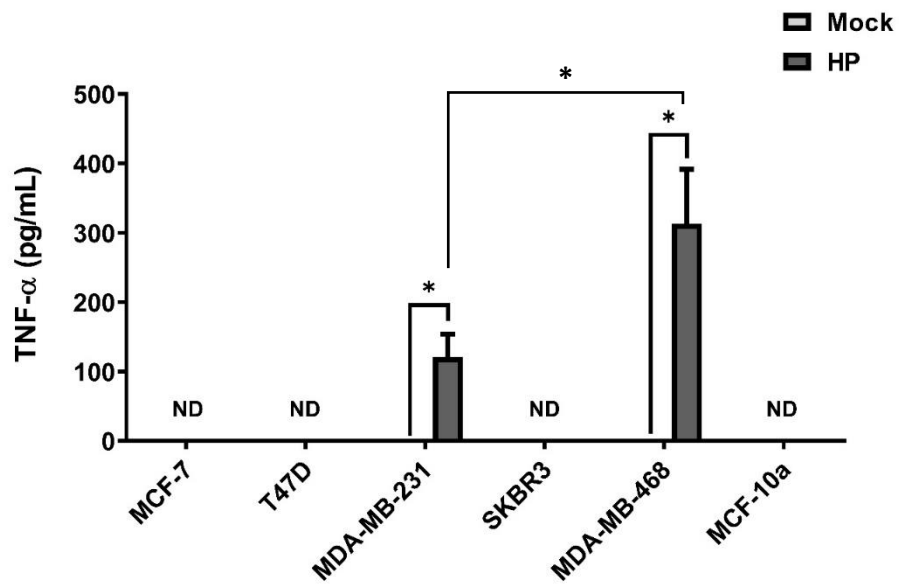


**Figure 3.6:** Quantification of TNF- $\alpha$  cytokine expression in supernatant collected from breast cancer and MCF-10a cells, treated with hydrolysis products generated from total lipoproteins by LPL or mock heparinized media

MCF-7, T47D, MDA-MB-231, MDA-MB-468 breast cancer cells and MCF-10a cells were treated with total lipoprotein hydrolysis products generated by LPL or mock heparinized media for 24 hours. The expression of TNF- $\alpha$  is significantly greater from MDA-MB-468 cells than MDA-MB-231 cells treated with LPL hydrolysis products.

ND= not detected. Data are presented as mean ( $n=3$ )  $\pm$  SD, with  $p<0.05$  (\*) calculated using unpaired t-test.

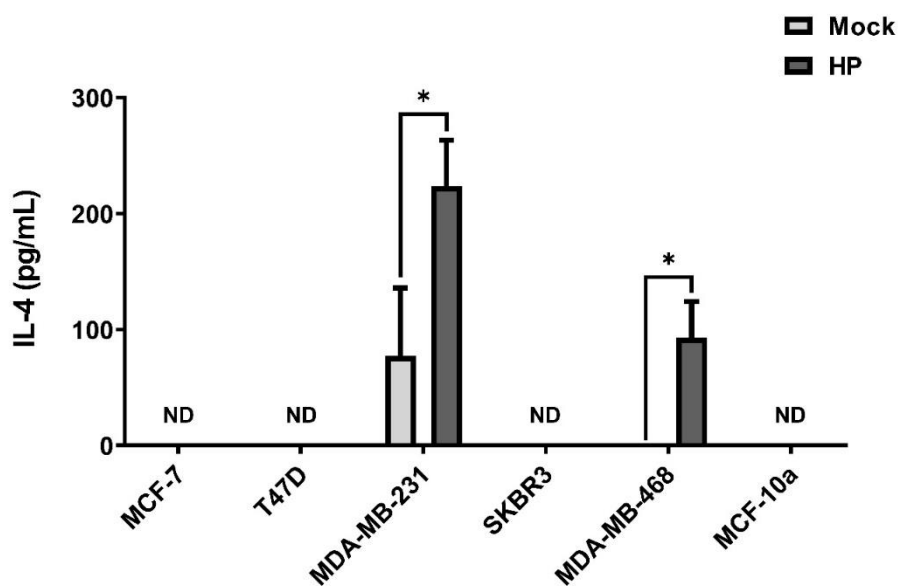


**Figure 3.7:** Quantification of IL-4 cytokine expression in supernatant collected from breast cancer and MCF-10a cells, treated with hydrolysis products generated from total lipoproteins by LPL or mock heparinized media

MCF-7, T47D, MDA-MB-231, MDA-MB-468 breast cancer cells and MCF-10a cells were treated with total lipoprotein hydrolysis products generated by LPL or mock heparinized media for 24 hours. ND=not detected. Data are presented as mean ( $n=3$ )  $\pm$  SD, with  $p < 0.05$  (\*) calculated using unpaired t-test.

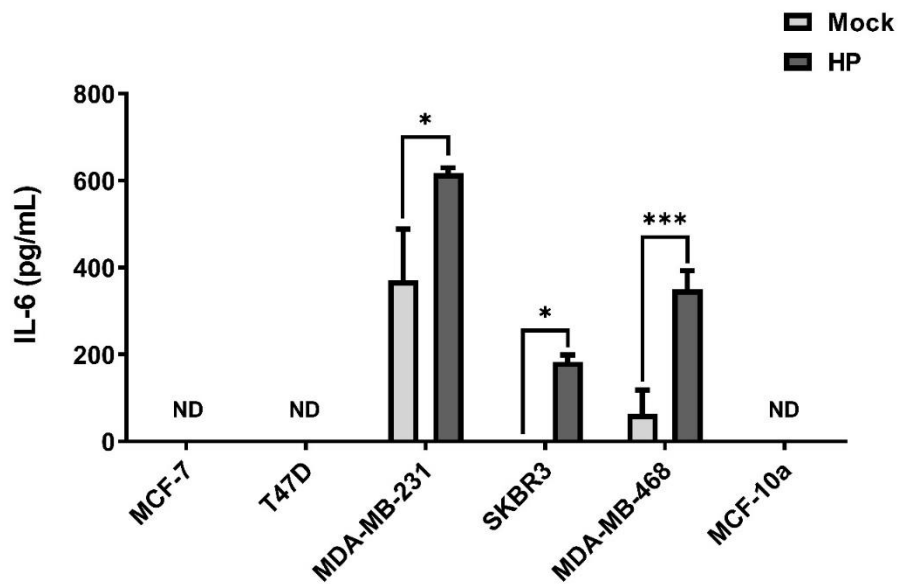


**Figure 3.8:** Quantification of IL-6 cytokine expression in supernatant collected from breast cancer and MCF-10a cells, treated with hydrolysis products generated from total lipoproteins by LPL or mock heparinized media

MCF-7, T47D, MDA-MB-231, MDA-MB-468 breast cancer cells and MCF-10a cells were treated with total lipoprotein hydrolysis products generated by LPL or mock heparinized media for 24 hours. ND=not detected. Data are presented as mean ( $n=3$ )  $\pm$  SD, with  $p < 0.05$  (\*) calculated using unpaired t-test.

detected in hydrolysis product-treated cells, but not mock-treated cells. The MCF-7, T47D, and MCF-10a cells did not secrete detectable levels of IL-6 in treated or control cells. These results also agree with the IL-6 data obtained for MDA-MB-231 and MCF-7 cells by the cytokine arrays.

### **3.5 Assessment of LPL expression in breast cancer cells**

Immunoblot analyses were performed to determine if the breast cancer cell lines chosen for this study express LPL. Mock-transfected and LPL-transfected HEK-293 cell lysates were included as negative and positive controls, respectively. Distinct bands were detected in the MCF-7 and T47D cell lysates, and a faint band was detected in SKBR3 cell lysate (Figure 3.9). While LPL was found to be expressed, the apparent molecular weight of the detected LPL band does not match the position of the positive control. This could indicate issues with the specificity of the chosen antibody. However, the LPL band detected in the MCF-7, T47D, and SKBR3 cell lysates is at the same position as each other, which suggests that the breast cancer cells may express abnormal LPL. LPL was not detected in the MDA-MB-231 cell lysate.

### **3.6 Assessment of endogenous LPL activity in breast cancer cells**

A resorufin ester lipase was used to determine if the endogenous LPL expressed by breast cancer cells is enzymatically active. As mentioned previously, heparin displaces LPL from the cell surface, allowing it to be collected in the medium. The supernatant from the heparinized cells and the control cells were collected for analysis. LPL produced by HEK-293 transfection was included as a positive control, and mock-transfected media

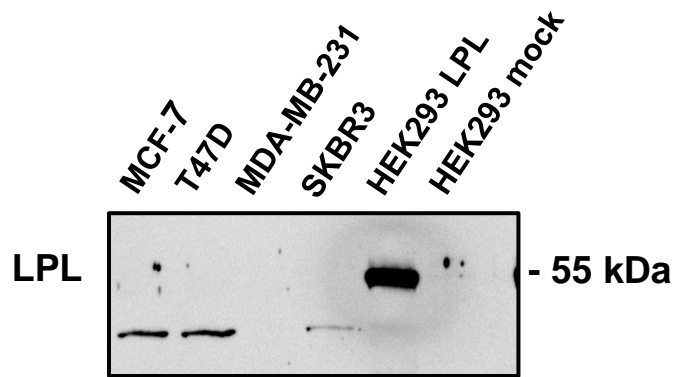


**Figure 3.9:** Representative image of a western blot for detection of LPL in breast cancer cell lysates

Recombinant human LPL from HEK-293 cell transfection was used as a positive control. Aberrantly expressed LPL was detected in the cell lysates of MCF-7, T47D, and SKBR3 cells. LPL was not detected in the MDA-MB-231 cell lysate. One representative image from three replicates is shown.

was included as a negative control. As seen in Figure 3.10, no significant difference in activity between the heparinized and non-heparinized breast cancer cell supernatants was detected, indicating that the even if LPL is expressed by the breast cancer cell lines, it is not enzymatically active. Additionally, there was no significant difference between the breast cancer samples and the negative control.

### **3.7 LMF1 expression in breast cancer cell lines, breast cancer patient samples, and normal breast tissue**

LMF1 expression was assessed through bioinformatics to determine if a defect in LPL processing could account for the inactive LPL expressed by the breast cancer cells. The gene expression of LMF1 in 20 breast cancer cell lines, 31 breast cancer patient samples, and six normal breast tissue samples was measured using data obtained from the Gene Expression Omnibus (GEO) database. The results show that across the majority of samples tested, *LMF1* mRNA expression is lower than in normal breast tissue (Figure 3.11). Some of the primary patient samples have moderate to high LMF1 expression compared to breast cancer cell lines. This could be due to the heterogeneity of the cells in the primary tumor samples and patient-specific effects. Likewise, one of the six normal breast tissue samples had lower LMF1 expression than the others. Overall, the data indicate that LMF1 expression may become dysregulated in breast cancer; however, this likely differs between patients and requires further investigation.

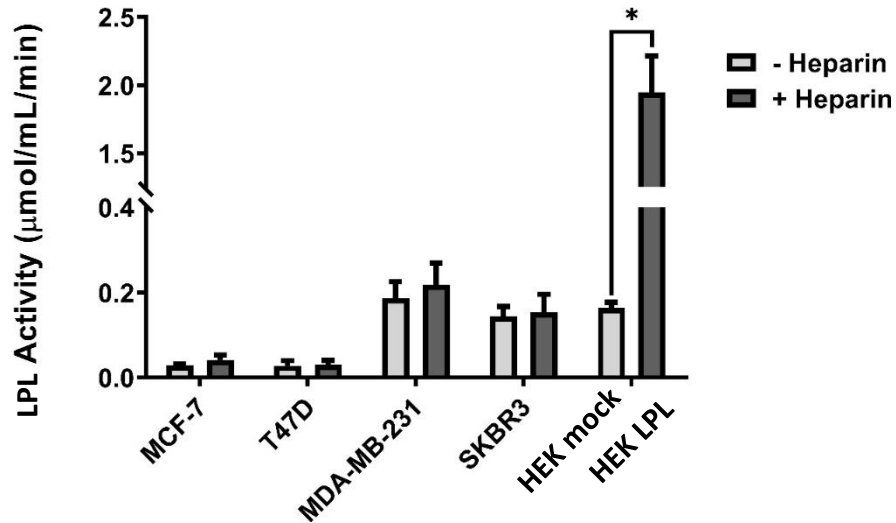


**Figure 3.10:** Analysis of endogenous LPL activity in heparinized and non-heparinized supernatant collected from breast cancer cells

Recombinant human LPL from HEK-293 cell transfection was used as a positive control (and mock as negative control). Pairs of heparinized and non-heparinized samples with no significant difference were considered enzymatically inactive. Data are presented as mean ( $n=3$ )  $\pm$  SD, with  $p<0.05$  (\*) calculated using unpaired t-test.

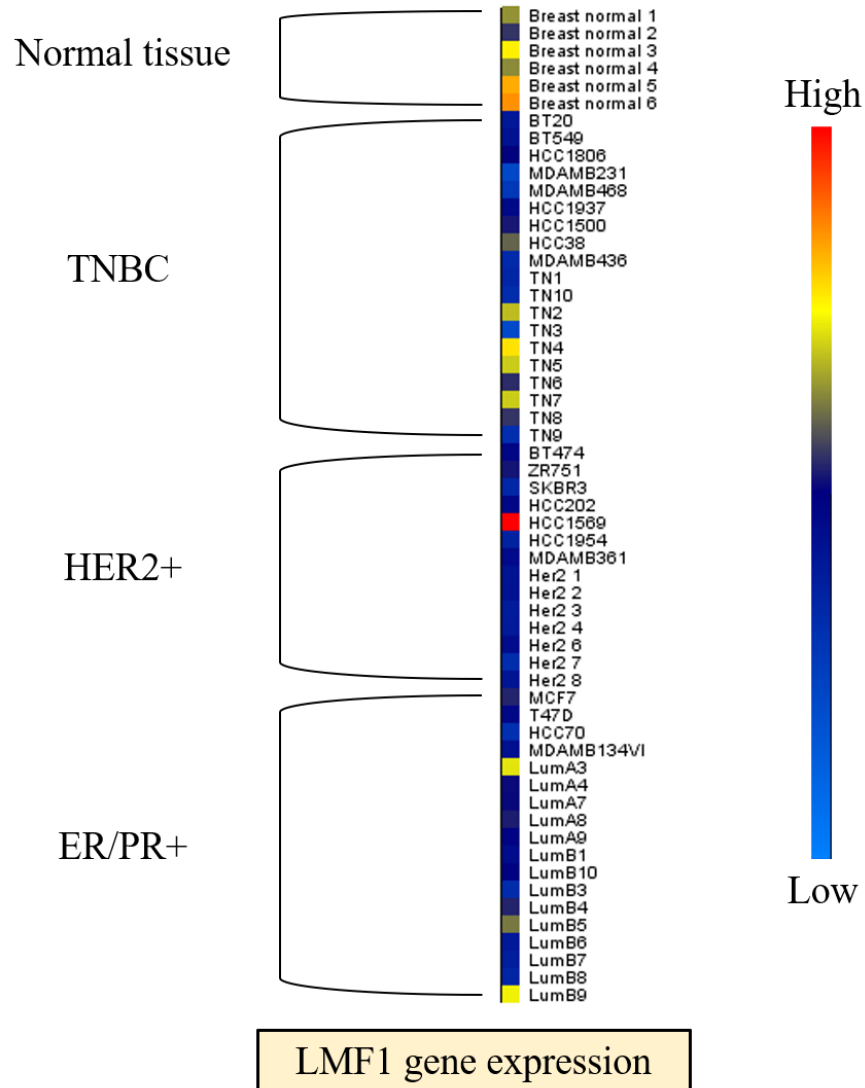


**Figure 3.11:** Analysis of *LMF1* mRNA expression in breast cancer cell lines, primary breast tumor samples, and normal breast tissue

Gene expression data from 20 breast cancer cell lines, 31 breast cancer patient samples, and six normal breast tissue samples were obtained from the Gene Expression Omnibus (GEO) database. *LMF1* probe IDs were obtained used to filter and average the gene expression data. Gene expression data were analyzed and grouped by subtype using Genesis 1.8.1.

## Chapter 4 Discussion

### 4.1 Total lipoprotein hydrolysis products generated by LPL modulate breast cell metabolic activity

One of the hallmarks of cancer is altered tumor cell metabolism. As discussed, breast cancer cells increase the rate of *de novo* lipogenesis by upregulating the expression of lipogenic enzymes such as FASN and ACC [84]. Additionally, cancer cells induce lipolysis in CAAs to increase the uptake of FFA via CD36, which breast cancer cells are known to express and upregulate [83, 132]. Previous studies have shown that many breast cancer cell lines express varying levels of LPL mRNA. Further, active LPL provided to breast cancer cells in culture increases the rate of cell growth [112]. This study determined that total lipoprotein hydrolysis products generated by LPL increase the cell metabolic activity of breast cancer cells, regardless of subtype. Additionally, the metabolic activity of the non-tumorigenic MCF-10a breast cell line was also increased. However, the basal metabolic activity of the breast cancer cells is greater than the non-tumorigenic breast cells, and subsequently increases in response to LPL hydrolysis products. This is critical because even though the effect of LPL hydrolysis products is not breast cancer cell-specific, an increase in breast cancer cell metabolic activity within the tumor microenvironment could cause significant effects on breast cancer growth *in vivo*. While an increase in metabolic activity does not necessarily indicate an increase in cell growth, it is tempting to say that these results are related.

There are multiple ways to explain the increase in breast cell metabolic activity shown in this study. Our laboratory has previously reported an increase in the gene expression of *CD36*, perilipin 2 (*PLIN2*), and carnitine palmitoyltransferase 1A (*CPT1A*) in THP-1 macrophages in response to total lipoprotein hydrolysis products. From these data, it was proposed that THP-1 macrophages respond to excess lipid by upregulating genes involved in intracellular lipid trafficking and the transfer of FFA into the mitochondria for FAO [132]. It is likely that a similar scenario occurs in breast cells. However, in cancer cells, this process could become pathological if the excess FFA are used to fuel breast cancer progression. It is already known that breast cancer cells increase their CD36 expression when in the presence of lipid-rich adipocytes [83]. This allows cancer cells to increase their uptake of exogenous lipids, which can then be stored in lipid droplets or immediately used as a source of energy. Further work is required to determine if a similar scenario occurs in non-tumorigenic breast cells. PLIN2 is a lipid droplet protein that is expressed in many tissues, including the mammary gland, that is directly correlated with intracellular lipid content. An increase in PLIN2 expression results in an increase in lipid droplet formation. High PLIN2 levels are detected in many types of cancer, and its expression has been shown to promote tumorigenesis and tumor cell maintenance [139]. In breast cancer, the overexpression of PLIN2 is associated with a significantly worse prognosis [140]. To reach the mitochondrial matrix for FAO, FFA are first converted into acyl-CoA esters by acyl-CoA synthetase, which are substrates for CPT1. CPT1 is embedded in the outer mitochondrial membrane and catalyzes a transesterification reaction to convert acyl-CoA to acyl-carnitine, which are then brought

across the inner mitochondrial membrane by carnitine acylcarnitine translocase. Once inside the mitochondria, CPT2 converts the acyl-carnitine back into acyl-CoA, which can be sequentially degraded by FAO [141]. FAO also produces substrates for the TCA cycle, which further provides energy for cancer progression. As discussed previously, CPT1A is the rate-limiting step of FAO. Therefore, increasing the expression of CPT1A significantly increases the rate at which cells can perform FAO. Overexpression of CPT1A is strongly correlated with breast cancer progression; CRISPR-mediated CPT1A knockdown enhanced breast cancer cell apoptosis and is being investigated as a therapeutic target [142, 143]. Clearly, the ability of LPL hydrolysis products to increase the gene expression of *CD36*, *PLIN2*, and *CPT1A* has important implications in breast cancer. While gene expression does not necessarily reflect protein expression, the overexpression of *CD36*, *PLIN2*, and *CPT1A* that is seen in breast cancer could be due to the upregulation of *CD36*, *PLIN2*, and *CPT1A* in response to LPL hydrolysis products, as shown in THP-1 cells. Further studies will need to be done to clearly establish this link, as our laboratory demonstrated in THP-1 cells [132]. However, if a similar gene expression profile is found, this would provide a connection between the uptake of hydrolysis products generated by LPL and the progression of breast cancer.

Additional work in our laboratory has shown that the FFA component of lipoprotein hydrolysis products can activate Akt in a dose-dependent manner in THP-1 macrophages [144]. PI3K becomes activated by the binding of growth factors to RTK or GPCR. Following activation, PI3K phosphorylates phosphatidylinositol (4,5) bisphosphate (PIP<sub>2</sub>) to form phosphatidylinositol (3,4,5) trisphosphate (PIP<sub>3</sub>). PIP<sub>3</sub>

recruits Akt to the cell membrane, where it is activated upon phosphorylation by phosphatidylinositol-dependent kinase 1 (PDK1) and mechanistic target of rapamycin (mTOR) complex 2 (mTORC2), at the T308 and S473 sites, respectively [145]. Of note, our laboratory has shown that the FFA component of LPL hydrolysis products results in the phosphorylation of both Akt sites [144]. PI3K/Akt signaling is terminated by phosphatase and tensin homolog (PTEN), which dephosphorylates PIP<sub>3</sub> to PIP<sub>2</sub>. It is well established that the PI3K/Akt signaling pathway is dysregulated in breast cancer [146]. Active Akt phosphorylates many different substrates, such as FOXO transcription factors, mTORC1, and glycogen synthase kinase 3. Phosphorylating these substrates causes an increase in breast cancer cell growth, glucose metabolism, proliferation, resistance to apoptosis, lipogenesis, and lipid accumulation, among other effects [147, 148]. In addition to this, breast tumors often have mutations in different components of the PI3K/Akt pathway. As discussed, HER2 is overexpressed in 15-20% of breast cancer cases and can activate PI3K/Akt signaling [32, 33]. Mutations in the *PI3KCA* gene are present in over 25% of all breast cancer cases (40% of luminal B type), resulting in the constitutive activation of PI3K/Akt signaling [43, 149]. Similarly, PTEN mutations are present in approximately 25% of breast cancer cases and result in the loss of inhibition and, thus, the continuous activation of PI3K/Akt [146, 149]. Therefore, Akt activation via the FFA component of LPL hydrolysis products could contribute to the increase in breast cell metabolic activity seen in this study (Figure 3.3). An interesting observation is the ability of LPL hydrolysis products to significantly increase the activation of PDGFR in THP-1 cells [126]. Additionally, LPL hydrolysis products significantly increase the

activation of Akt [144]. It is known that stimulation of cells with PDGF activates PI3K/Akt signaling through a PDGFR [145]. This suggests that in cancer cells, the hydrolysis products generated by LPL may upregulate PDGFR phosphorylation and Akt activation to sustain PI3K/Akt signaling, and thus, tumorigenesis. It is interesting to note that PDGF is also known to upregulate LPL expression [150]. Studies to confirm the presence of this positive-feedback loop in breast cancer cells will be necessary (Figure 4.1). If validated, this interaction could establish a central role of LPL hydrolysis products in promoting and maintaining tumorigenesis.

A limitation of this study was the use of the MTT assay to measure cell metabolic activity. The MTT solution is reduced by oxidoreductase enzymes to purple formazan crystals within metabolically active cells. The formazan crystals are then dissolved in a dilute acid and the absorbance of the samples can be measured. An increase in absorbance compared to control cells could be the result of increased mitochondrial metabolism, cell division, or decreased cell death [151]. However, while the assay did provide accurate measurements of breast cancer cell metabolic activity as intended, the MTT assay does not measure cell proliferation. Further studies will be required to confirm whether there is an increase in cell number in addition to an increase in metabolic activity. Also, measuring the expression of targets upregulated by hydrolysis products in THP-1 macrophages, such as *PLIN2*, *CPT1A*, and PDGFR, and additional lipid metabolism genes, will help to decipher how breast cancer metabolic activity is increased. Regardless, these data justify a more in-depth investigation of breast cancer cell metabolic activity in response to LPL hydrolysis products.

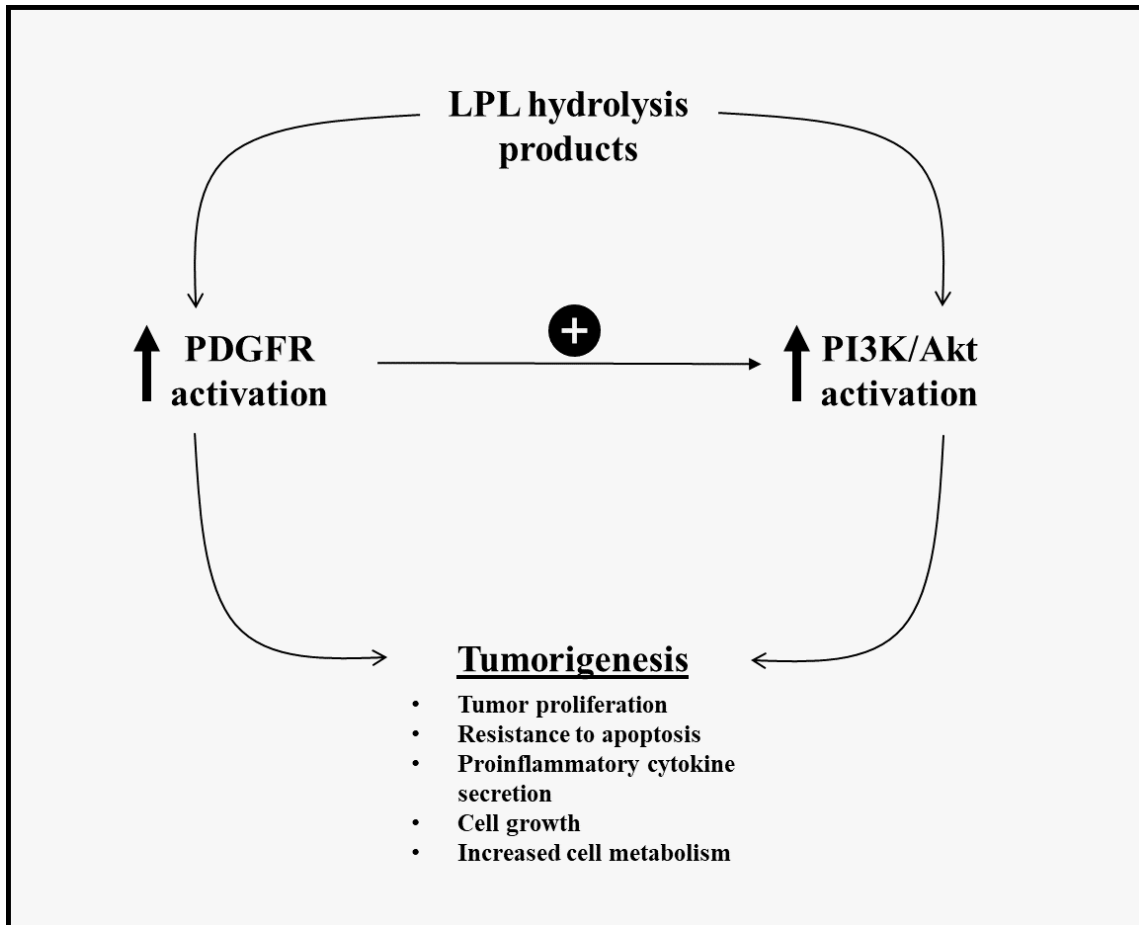


**Figure 4.1:** Proposed positive-feedback loop in breast cancer cells to sustain tumorigenesis

LPL hydrolysis products have been shown to significantly increase both PDGFR and PI3K/Akt activation. Additionally, PI3K/Akt signaling is known to become activated through a PDGFR. Both PDGFR and PI3K/Akt activation are known to promote tumorigenesis through multiple mechanisms. Therefore, the hydrolysis products generated by LPL may upregulate PDGFR phosphorylation and Akt activation to sustain PI3K/Akt signaling, and thus, tumorigenesis.

## **4.2 Total lipoprotein hydrolysis products generated by LPL cause subtype-specific cytokine secretion from breast cancer cells**

The tumor microenvironment is a critical influence on breast cancer growth and progression. Breast cancer cells can secrete cytokines to induce changes in the surrounding cells, and similarly, cells of the microenvironment can secrete cytokines to support or reduce cancer survival. Therefore, I sought to determine the effect of LPL hydrolysis products on cytokine secretion in breast cancer cells. To get a broad understanding of the cytokine secretion profile, cytokine arrays were used to analyze the response of MDA-MB-231 (TNBC) and MCF-7 (luminal A) cells to hydrolysis products. These cell lines were chosen as they represent the most and least aggressive breast cancer subtypes, respectively. Interestingly, the analysis revealed that hydrolysis products resulted in a significant difference in the secretion of several pro-tumorigenic cytokines. However, I found that the secretion profiles were different between the MDA-MB-231 and the MCF-7 cells (Figures 3.4 & 3.5).

The secretion profile of the TNBC cells is undoubtedly pro-tumorigenic. The most significant upregulation was seen in TNF- $\alpha$  and IL-4. As discussed, breast cancer cells can produce and utilize TNF- $\alpha$  to activate NF- $\kappa$ B signaling. NF- $\kappa$ B activation is clearly favorable for tumor progression, as it induces cell proliferation, angiogenesis, immune evasion, and metastasis [64, 65]. A result of NF- $\kappa$ B activation is increased expression of IL-8, which was also found to be significantly increased in this study. IL-8 promotes angiogenesis, tumor cell migration, and immune cell infiltration in breast cancer [152]. Similarly, activation of NF- $\kappa$ B by TNF- $\alpha$  increases the expression of ICAM in breast

cancer, which is upregulated to promote metastasis and is associated with more aggressive subtypes [134]. Unsurprisingly, the cytokine array data revealed a significant increase in ICAM-1 secretion, which suggests that LPL hydrolysis products may promote the development of a more aggressive tumor cell phenotype. The chemokine CXCL1, which promotes immune cell invasion and angiogenesis, was also found to be upregulated. Interestingly, CXCL1 is also induced by TNF- $\alpha$ . My data suggests that TNF- $\alpha$  has a major impact on the cytokine secretion profile of MDA-MB-231 cells. On the other hand, IL-4 has long been described as an anti-inflammatory cytokine that induces apoptosis in breast cancer cells [153]. However, IL-4 secretion activates M2-like TAM, which are strongly pro-tumorigenic [70]. Though not relevant in the cell culture, increased IL-4 secretion from breast cancer cells could contribute to a pro-tumorigenic microenvironment *in vivo*. The pleiotropic cytokine IL-6 was also found to be increased in response to LPL hydrolysis products. IL-6 is involved in multiple aspects of tumor progression, including invasion, metastasis, angiogenesis, and resistance to therapy. The broad impact of IL-6 is due to its ability to activate many different signaling pathways that have pro-tumorigenic functions, such as NF- $\kappa$ B and JAK/STAT3 [82, 63]. The final cytokine that was found to be upregulated in MDA-MB-231 cells, being CXCL11, was slightly unexpected. CXCL11 is a chemokine that attracts mononuclear immune cells to the tumor microenvironment. Once in the tumor microenvironment, the immune cells may have a pro- or anti-tumorigenic effect depending on the context. CXCL11 is primarily induced by IFN- $\gamma$ , yet there was no IFN- $\gamma$  secretion detected in this study [154]. An explanation for this could be that the IFN- $\gamma$  secretion was below the detectable level

of the cytokine array. A level of detection is not assigned to the cytokine arrays, however, most analytes are detectable in the pg/mL range. Taken together, these data suggest that hydrolysis products promote tumorigenesis by upregulating pro-tumorigenic cytokine secretion in TNBC.

The results from the MCF-7 cell cytokine array analysis are more difficult to interpret. Unlike the MDA-MB-231 cells, which saw an increase in many different cytokines involved in tumorigenesis, MCF-7 cells only showed a significant decrease in IL-1 $\alpha$  and IL-27. IL-1 $\alpha$  is a pro-inflammatory cytokine that can promote cancer progression by activating NF- $\kappa$ B and JAK/STAT3 signaling. Because of its pro-tumorigenic effects, it could be expected that IL-1 $\alpha$  would be upregulated in breast cancer cells following LPL hydrolysis products treatment [155]. However, IL-1 $\alpha$  has been shown to inhibit MCF-7 cell proliferation by causing cell cycle arrest [156]. This is an interesting and counterintuitive observation because it indicates that the downregulation of IL-1 $\alpha$  by LPL hydrolysis products may actually function to sustain tumorigenesis in MCF-7 cells. However, this effect is clearly subtype-specific. Similarly, IL-27 is known to have both pro- and anti-tumorigenic effects. IL-27 can induce the activation of T cells in the tumor microenvironment, which have different effects depending on the degree of progression. IL-27 can also activate STAT1, which has potent anti-proliferative effects, induce apoptosis, and enhance immune cell elimination of cancer cells [157]. Like IL-1 $\alpha$ , the downregulation of IL-27 by LPL hydrolysis products may be pro-tumorigenic in our model. Because of their multi-functional roles, IL-1 $\alpha$  and IL-27 likely have both pro- and

anti-inflammatory effects *in vivo*. However, these data suggest that LPL hydrolysis products may also promote tumorigenesis in luminal A breast cancer.

The data acquired from the cytokine arrays highlight the importance of the breast cancer subtype on the response to stimuli in the tumor microenvironment. The LPL hydrolysis products appear to induce a pro-tumorigenic cytokine secretion profile in different subtypes of breast cancer through distinct mechanisms. To further understand the effect of subtype on LPL hydrolysis products-induced cytokine secretion, I measured TNF- $\alpha$ , IL-6, and IL-4 expression by ELISA in four additional breast cell lines (Figures 3.6-3.8). The dynamic range of each ELISA was 15.6-1000 pg/mL, 9.38-600 pg/mL, and 31.3-2000 pg/mL respectively. In agreement with the cytokine array data, TNF- $\alpha$  was significantly increased in MDA-MB-231 cells, as well as the other TNBC cell line tested, the MDA-MB-468 cells. TNF- $\alpha$  expression was significantly higher in the MDA-MB-468 cells, which may indicate that they have a more pronounced response to LPL hydrolysis products. Similarly, IL-6 expression was significantly increased in both TNBC cell lines following incubation with hydrolysis products. HER2-positive SKBR3 cells also secreted detectable levels of IL-6 following LPL hydrolysis products treatment. Finally, IL-4 secretion was significantly upregulated in both TNBC cell lines. Thus, these data suggest that the impact of LPL hydrolysis products on breast cancer progression is subtype-specific. TNF- $\alpha$ , IL-6, and IL-4 were all upregulated in both TNBC cell lines; likewise, TNF- $\alpha$ , IL-6, and IL-4 were not secreted at detectable levels by either MCF-7 or T47D cells, the luminal A cell lines of this study, or by the non-tumorigenic MCF-10a cells. SKBR3 cells treated with LPL hydrolysis products secreted detectable levels of IL-6, but

not TNF- $\alpha$  or IL-4. A potential issue is that the cytokines are secreted but are below the detection limit of the assay. However, the MDA-MB-231 cytokine array and ELISA data agree, which suggests that the luminal cell lines simply do not express the measured cytokines. Previously, our laboratory showed that LPL hydrolysis products significantly increase the gene expression of TNF- $\alpha$ , IL-1 $\beta$ , and IL-6 in MCF-7 breast cancer cells [Noel, Pickett, & Brown, unpublished]. My results contradict these gene expression data. It is possible that the gene expression analysis had a lower level of detection than the cytokine array and ELISA which could account for the differences in the results. However, gene expression does not necessarily equate to protein expression or secretion, so this discrepancy will have to be further investigated to fully understand [158].

#### **4.3 Endogenous LPL expressed by breast cancer cells is not enzymatically active and may be a result of dysregulated LMF1 expression**

Breast tumors have two potential sources of LPL hydrolysis products: adipose tissue that surrounds breast tumors highly expresses LPL, and certain breast cancer cell lines express LPL mRNA and protein [112, 135]. Because all the cell lines chosen for this study had not been previously assessed for LPL protein expression, I performed immunoblotting to detect its presence in breast cancer cell lysates (Figure 3.9). The resulting data were surprising for a few reasons. The LPL expressed by MCF-7, T47D, and SKBR3 breast cancer cells in my study was detected at a lower molecular mass than control HEK-293 transfected LPL. However, the mass of the detected LPL was consistent among the breast cancer cell lysates. MDA-MB-231 cells were not shown to express LPL, despite previous reports that TNBC has the highest level of LPL mRNA expression

across breast cancer subtypes [159]. In addition, the previous study that measured LPL protein expression did not detect LPL in T47D cells; however, my data suggest that LPL may be present, but aberrantly expressed. The discrepancy could be due to the use of different antibodies to detect LPL. Our laboratory uses a commercial polyclonal anti-human LPL antibody (#sc-32885, Santa Cruz Biotechnology) with an epitope corresponding to residues 28-80 of human LPL, whereas the previous report produced its own anti-human LPL antibody corresponding to residues 21-36 of human LPL. The mass of the LPL protein detected in the previous study was 85 kDa, which is considerably greater than the 56-58 kDa mass that is expected [112, 105]. This could account for the differences reported. Following this, I assessed the enzymatic activity of the abnormal breast cancer LPL using a resorufin ester substrate, as described (section 2.6.5). No activity was detected in any of the breast cancer cell lines that expressed LPL protein (Figure 3.10). Therefore, even if the breast cancer cell lines express LPL it is not active.

To attempt to explain the presence of the inactive LPL, I investigated the expression of *LMF1*, as it is required for proper LPL folding, dimerization, and transport to the golgi [117]. LPL is heavily glycosylated in the golgi, therefore, interruption of this process could result in the lower LPL mass detected in this study [114]. Additionally, glycosylation of certain conserved sites in the N-terminal domain of LPL is required to produce a functional enzyme [160]. The results show that across the majority of samples analyzed, *LMF1* mRNA expression is lower than in normal breast tissue (Figure 3.11). Dysregulation of *LMF1* in breast cancer could cause issues with LPL folding, which could produce the inactive LPL protein detected in this study. Under normal conditions,

LPL production is tightly regulated, and misfolded proteins are retained in the ER for degradation [118]. However, cancerous cells do not behave like normal cells, and thus it is possible that ER degradation is not as tightly regulated, allowing misfolded LPL to escape detection [161]. This is speculative and will require further investigation.

However, LMF1 dysregulation may have a role in the abnormal expression of LPL by breast cancer cells. An extensive analysis of LPL expression across multiple breast cancer cell lines should be performed to verify the presence of LPL, due to the disagreement between the data reported here and in other studies [112]. Dysregulation of LPL glycosylation in the golgi could result in a lower protein mass, therefore, proteins involved in this process should also be investigated [114].

#### **4.4 Future perspectives**

The present study has identified a number of potential targets to investigate in future studies. Previous work in our laboratory has identified a number of targets in THP-1 macrophages that are affected by LPL hydrolysis products treatment. My data indicates that many of these targets are also worth measuring in breast cancer cells treated with LPL hydrolysis products. As discussed, the expression of *CD36*, *PLIN2*, and *CPT1A* at the gene and protein levels should be investigated due to their role in intracellular lipid trafficking and the transfer of FFA into the mitochondria for FAO [132]. *CD36*, *PLIN2*, and *CPT1A* are already known to be overexpressed in breast cancer, thus, showing that LPL hydrolysis products upregulate *CD36*, *PLIN2*, and *CPT1A* may provide a better understanding of the mechanism [132, 139, 143]. Other targets that should be assessed include Akt phosphorylation and PDGFR upregulation to sustain PI3K/Akt signaling and

tumorigenesis in breast cancer. If performed, these analyses would help to explain the increased breast cancer cell metabolic activity seen in response to LPL hydrolysis products. Further, it could directly link LPL hydrolysis products to breast cancer tumorigenesis.

Cytokine array analysis of additional breast cancer cell lines would help to elucidate the effect of subtype on the cytokine secretion induced by LPL hydrolysis products. Additionally, analysis of signaling pathways involved in cytokine regulation, such as NF- $\kappa$ B and JAK/STAT, would help to determine how LPL hydrolysis products differentially affect cytokine secretion in different breast cancer subtypes. The co-culture of breast cancer cells exposed to hydrolysis products and varying tumor microenvironment cells would be useful to assess cytokine secretion in a more physiologically-relevant model.

Finally, the expression of LPL by breast cancer cells should be thoroughly investigated to determine which cell lines definitively express LPL. Different antibodies to detect LPL could be tested. The protein expression of LMF1 in breast cancer should be assessed to validate the decrease in LMF1 mRNA expression indicated by my bioinformatics analysis. LMF1 could also be overexpressed in breast cancer cells to determine if the loss of LMF1 protein is the cause of the abnormal LPL detected in this study. Another possible area worth investigating is the dysregulation of LPL glycosylation in the golgi, which could result in a lower protein mass [114].

#### **4.5 Overall conclusion**

This study has shown that LPL hydrolysis products may directly promote breast cancer growth and progression by increasing cell metabolic activity and inducing a pro-tumorigenic cytokine secretion profile from tumor cells. The increase in cell metabolic activity may be through the upregulation of genes previously identified by our laboratory in a THP-1 model of atherosclerosis. An interesting finding of this study is the ability of LPL hydrolysis products to induce different pro-tumorigenic cytokine expression profiles in different breast cancer subtypes. This strongly suggests that LPL hydrolysis products have distinct effects between subtypes, that could result in promoting breast cancer progression. Unexpectedly, endogenous LPL expressed by breast cancer cells was determined to be enzymatically inactive, which disproves the idea that breast cancer cells can generate their own LPL hydrolysis products. Regardless, the high expression of LPL by adipose tissue in the tumor microenvironment provides an abundant source of LPL hydrolysis products. Therefore, the data presented in this study are still physiologically relevant. Overall, the results of this study highlight the potential for a central role of LPL hydrolysis products in the growth and progression of breast cancer.

## References

- [1] Canadian Cancer Statistics Advisory Committee, "Canadian cancer statistics," Canadian Cancer Society , Toronto, 2019.
- [2] D. R. Brenner, H. K. Weir, A. A. Demers, L. F. Ellison, C. Louzado, A. Shaw, D. Turner, R. R. Woods and L. M. Smith, "Projected estimates of cancer in Canada in 2020," *Canadian Medical Association Journal*, vol. 192, no. 9, 2020.
- [3] American Society of Clinical Oncology (ASCO), "Breast cancer: symptoms and signs," Cancer.Net, 2019.
- [4] National Breast Cancer Foundation, "Breast cancer anatomy and how cancer starts," National Breast Cancer Foundation, Sydney, 2020.
- [5] P. A. Thomas, *Breast cancer and its precursor lesions: making sense and making it early*, Kansas City: Humana Press, 2011.
- [6] M. Mullooly, Z. G. Khodr, C. M. Dallal, S. J. Nyante, M. E. Sherman, R. Falk, L. M. Liao, J. Love, L. A. Brinton and G. L. Gierach, "Epidemiologic risk factors for in situ and invasive breast cancers among postmenopausal women in the National Institutes of Health-AARP diet and health study," *American Journal of Epidemiology*, vol. 12, no. 186, pp. 1329-1340, 2017.
- [7] E. Wong, S. Chaudhry and M. Rossi, "Breast cancer," *McMaster Pathophysiology Review*, Hamilton, 2018.
- [8] L. Zelek, M. Spielmann and A. Le Cesne, "Primary breast sarcomas," in *Management of Rare Adult Tumours*, Paris, Springer, 2010, pp. 373-378.
- [9] L. Da Silva, P. T. Simpson and S. R. Lakhani, "Lobular carcinoma in situ," in *Management of Breast Diseases*, Berlin, Springer Berlin Heidelberg, 2010, pp. 181-199.
- [10] H. Y. Wen and E. Brogi, "Lobular carcinoma in situ," *Surgical Pathology Clinics*, vol. 11, no. 1, pp. 123-145, 2018.
- [11] M. V. Seijen, E. H. Lips, A. M. Thompson, S. Nik-Zainal, A. Futreal, S. E. Hwang, E. Verschuur, J. Lane and J. Jonkers, "Ductal carcinoma in situ: to treat or not to treat, that is the question," *British Journal of Cancer*, vol. 121, no. 4, pp. 285-292, 2019.

- [12] N. Harbeck, F. Penault-Liorca, J. Cortes, M. Gnant, N. Houssami, P. Poortmans, K. Ruddy, J. Tsang and F. Cardoso, "Breast cancer," *Nature Reviews Disease Primers*, vol. 5, no. 66, 2019.
- [13] S. R. Lakhani, International Agency for Research on Cancer, World Health Organization, *Who Classification of Tumours of the Breast, Fourth Edition*, Lyon: International Agency for Research on Cancer (IRAC), 2012.
- [14] J. W. Sozzi and R. O. Mirimanoff, "Primary breast lymphoma," in *Management of Rare Adult Tumours*, Paris, Springer, 2010, pp. 357-366.
- [15] M. Yin, H. B. Mackley, J. J. Drabick and H. A. Harvey, "Primary female breast sarcoma: clinicopathological features, treatment, and prognosis," *Scientific Reports*, vol. 6, no. 31497, 2016.
- [16] J. A. Lyons, J. Myles, B. Pohlman, R. M. Macklis, J. Crowe and L. Richard, "Treatment and prognosis of primary breast lymphoma," *American Journal of Clinical Oncology*, vol. 23, no. 4, pp. 334-336, 2000.
- [17] S. Kalli, A. Semine, S. Cohen, S. P. Naber, S. S. Makim and M. Bahl, "American Joint Committee on Cancer's staging system for breast cancer, eighth edition: what the radiologist needs to know," *Radiographics: A Review Publication of the Radiological Society of North America*, vol. 38, no. 7, pp. 1921-1933, 2018.
- [18] A. Mahul, F. L. Greene, S. B. Edge, C. C. Compton, G. J. E, R. K. Brookland, L. Meyer, D. M. Gress, D. R. Byrd and D. P. Winchester, "The eighth edition AJCC cancer staging manual: continuing to build a bridge from a population-based to a more "personalized" approach to cancer staging," *CA: A Cancer Journal for Clinicians*, vol. 67, no. 2, pp. 93-99, 2017.
- [19] E. A. Rakha, J. S. Reis-Filho and F. Baehner, "Breast cancer prognostic classification in the molecular era: the role of histological grade," *Breast Cancer Research*, vol. 12, no. 207, 2010.
- [20] C. W. Elston and I. O. Ellis, "Pathological prognostic factors in breast cancer. I. The value of histological grade in breast cancer: experience from a large study with long-term follow-up," *Histopathology*, vol. 19, no. 5, pp. 403-410, 1991.
- [21] A. M. Schwartz, D. E. Henson, C. Dechang and S. Rajamarthandan, "Histologic grade remains a prognostic factor for breast cancer regardless of the number of positive lymph nodes and tumor size: a study of 161 708 cases of breast cancer

- from the SEER program," *Archives of Pathology and Laboratory Medicine*, vol. 138, no. 8, pp. 1048-1052, 2014.
- [22] J. M. Higa and R. G. Fell, "Sex hormone receptor repertoire in breast cancer," *International Journal of Breast Cancer*, vol. 2013, no. 284036, 2013.
- [23] M. Sui, Y. Huang, B. H. Park, N. E. Davidson and W. Fan, "Estrogen receptor  $\alpha$  mediates breast cancer cell resistance to paclitaxel through inhibition of apoptotic cell death," *Cancer Research*, vol. 67, no. 11, pp. 5337-5344, 2007.
- [24] Y. Li, D. Yang, X. Yin, X. Zhang, J. Huang, Y. Wu, M. Wang, Z. Yi, H. Li and G. Ren, "Clinicopathological characteristics of breast cancer-specific survival of patients with single hormone receptor-positive breast cancer," *JAMA Network Open (Oncology)*, vol. 3, no. 1, 2020.
- [25] H. Pan, R. Gray, J. Braybrooke, C. Davies, C. Taylor, P. McGale and R. Peto, "20-year risks of breast-cancer recurrence after stopping endocrine therapy at 5 years," *The New England Journal of Medicine*, vol. 377, no. 19, pp. 1836-1846, 2017.
- [26] C. R. King, M. H. Kraus and S. A. Aaronson, "Amplification of a novel v-erbB-related gene in a human mammary carcinoma," *Science*, vol. 229, no. 4717, pp. 974-976, 1985.
- [27] A. Nasrazadani, R. A. Thomas, S. Oesterreich and A. V. Lee, "Precision medicine in hormone receptor-positive breast cancer," *Frontiers in Oncology*, vol. 8, 2018.
- [28] A. Dittrich, H. Gautrey, D. Browell and A. Tyson-Capper, "The HER2 signaling network in breast cancer—like a spider in its web," *Journal of Mammary gland Biology and Neoplasia*, vol. 19, pp. 253-270, 2014.
- [29] U. Krishnamurti and J. F. Silverman, "HER2 in breast cancer: a review and update," *Advances in Anatomical Pathology*, vol. 21, no. 2, pp. 100-107, 2014.
- [30] D. B. Peckys, D. Hirsch, T. Gaiser and N. de Jonge, " Visualisation of HER2 homodimers in single cells from HER2 overexpressing primary formalin fixed paraffin embedded tumour tissue," *Molecular Medicine*, vol. 25, no. 42, 2019.
- [31] C. Bartholomeusz, A. M. Gonzalez-Angulo, P. Liu, N. Hayashi, A. Lluch, F.-L. J and G. N. Hortobagyi, "High ERK protein expression levels correlate with shorter survival in triple-negative breast cancer patients," *The Oncologist*, vol. 17, no. 6, pp. 766-774, 2012.

- [32] A. Ruiz-Saenz, C. Dreyer, M. R. Campbell, V. Steri, N. Gullizia and M. M. Moasser, "HER2 amplification in tumors activates PI3K/Akt signaling independent of HER3," *Cancer Research*, vol. 78, no. 13, 2018.
- [33] H. Qin, L. Liu, S. Sun, D. Zhang, J. Sheng, B. Li and W. Yang, "The impact of PI3K inhibitors on breast cancer cell and its tumor microenvironment," *PeerJ*, vol. 6, no. 5092, 2018.
- [34] Y. Lin, J. Zu and H. Lan, "Tumor-associated macrophages in tumor metastasis: biological roles and clinical therapeutic applications," *Journal of Hematology and Oncology*, vol. 12, no. 76, 2019.
- [35] F. Zakrzewski, W. de Back, M. Weigert, T. Wenke, S. Zeugner, R. Mantey, C. Sperling, K. Freidrich, I. Roeder, D. Aust, G. Baretton and P. Honscied, "Automated detecton of the HER2 gene amplification status in Fluoresence in situ hybridization images for the diagnostics of cancer tissues," *Scientific Reports*, vol. 9, no. 8231, 2019.
- [36] L. Dean, "Trastuzumab (Herceptin) Therapy and ERBB2 (HER2) Genotype," in *Medical Genetics Summaries*, Bethesda: National Center for Biotechnology Information, 2012.
- [37] S. M. Tolaney, H. Guo, S. Pernas, W. T. Barry, D. A. Dillion and L. Ritterhouse, "Seven-year follow-up analysis of adjuvant paclitaxel and trastuzumab trial for node-negative, human epidermal growth factor receptor 2-positive breast cancer," *Journal of Clinical Oncology*, vol. 37, no. 22, pp. 1868-1875, 2019.
- [38] C. M. Perou, T. Sorlie, M. B. Eisen, M. van de Rijn, S. S. Jeffery, C. A. Rees, J. R. Pollack, D. T. Ross, L. A. Johnsen, L. A. Aklsen, O. Fluge, A. Pergamenschikov, C. Williams, S. X. Zhu, P. E. Lonning, A.-L. Borrensens-Dale, P. O. Brown and D. Botstein, "Molecular portraits of human breast tumours," *Nature*, vol. 406, pp. 747-752, 2000.
- [39] T. Sorlie, C. M. Perou, R. Tibshirani, T. Aas, S. Geisler, H. Johnsen, T. Hastie, M. B. Eisen, M. va de Rijn, S. S. Jeffery, T. Thorsen, H. Quist, J. C. Matese, P. O. Brown, D. Botstein, P. E. Lonning and A.-L. Borrensens-Dale, "Gene expression patterns of breast carcinomas distiguish tumor subclasses with clinical implications," *Proceedings of the National Academy of Sciences*, vol. 98, no. 19, pp. 10869-10874, 2001.

- [40] S. M. Fragomeni, A. Sciallils and J. S. Jeruss, "Molecular subtypes and local-regional control of breast cancer," *Surgical Oncology Clinics of North America*, vol. 27, no. 1, pp. 95-120, 2018.
- [41] M. Dowsett, T. O. Nielsen, R. A'Hern, J. Bartlett, R. C. Coombes, J. Cuzick, M. Ellis, N. L. Henry, J. C. Hugh, T. Lively, L. McShane, S. Paik, F. Penault-Llorca, L. Prudkin, M. Regan, J. Salter, C. Sotiriou, I. E. Smith, G. Viale, J. A. Zujewski and D. F. Hayes, "Assessment of Ki67 in breast cancer: recommendations from the International Ki67 in Breast Cancer working group," *Journal of the National Cancer Institute*, vol. 103, no. 22, pp. 1656-1664, 2011.
- [42] N. Howlader, K. A. Cronin, A. W. Kurian and R. Andridge, "Differences in breast cancer survival by molecular subtypes in the united states," *Cancer Epidemiology, Biomarkers, and Prevention*, vol. 27, no. 6, pp. 619-626, 2018.
- [43] T. Davoli, K. E. Mengwasser, J. Duan, T. Chen, C. Christensen, E. C. Wooten, A. N. Anselmo, M. Z. Li, K.-K. Wong, K. T. Khale and S. J. Elledge, "Funcational genomics reveals that tumors with activating phosphoinositide 3-kinase mutations are dependent on accelerated protein turnover," *Genes & Development*, vol. 30, no. 24, pp. 2684-2695, 2016.
- [44] A. Prat, T. Pascual, C. De Angelis, C. Gutterrez, A. Llombart-Cussac, W. T. J. Cortes, B. Rexer, L. Pare, F. A. A. C. Wolff, S. Morales, B. Adamo, F. Braso-Maristany, M. Vidal, J. Veeraghavan, I. Krop, P. Galvan, A. C. Pavlick and B. E. A. Bermejo, "HER2-enriched subtype adn erbb2 expression in her2-positive breast cancer treated with dual her2 blockade," *Journal of the National Cancer Institute*, vol. 112, no. 1, pp. 46-54, 2020.
- [45] B. Martin-Castillo, C. Oliveras-Ferraros, A. Vazquez-Martin, S. Cufí, J. M. Moreno, B. Corominas-Faja, A. Urruticoechea, Á. G. Martín, E. López-Bonet and J. A. Menendez, "Basal/HER2 breast carcinomas: integrating molecular taxonomy with cancer stem cell dynamics to predict primary resistance to trastuzumab (herceptin)," *Cell Cycle*, vol. 12, no. 2, pp. 225-245, 2013.
- [46] P. Vici, L. Pizztuli, C. Natoli, M. Maugeri-Sacca, M. Mottolese and P. Marchetti, "Triple positive breast cancer: a distinct subtype?," *Cancer Treatment Reviews*, vol. 41, no. 2, pp. 69-76, 2015.
- [47] A. Prat, L. A. Carey, B. Adamo, M. Vidal, J. Tabernero, J. Cortes, J. S. Parker and C. M. Perou, "Molecular features and survival outcomes of the intristic subtypes within HER2-positive breast cancer," *Journal of the National Cancer Institute*, vol. 106, no. 8, 2014.

- [48] C. K. Osborne and R. Schiff, "Mechanisms of Endocrine Resistance in Breast Cancer," *Annual Review of Medicine*, vol. 62, pp. 233-247, 2011.
- [49] B. D. Lehmann, J. A. Bauer, X. Chen, M. E. Sanders, A. B. Chakravarthy, Y. Shyr and J. A. Pietenpol, "Identification of human triple-negative breast cancer subtypes and preclinical models for selection of targeted therapies," *The Journal of Clinical Investigation*, vol. 121, no. 7, pp. 2750-2767, 2011.
- [50] A. C. Garrido-Castro, N. U. Lin and K. Polyak, "Insights into molecular classifications of triple-negative breast cancer: improving patient selection for treatment," *Cancer Discovery*, vol. 9, no. 2, pp. 176-198, 2019.
- [51] P. Tang and G. Tse, "Immunohistochemical surrogates for molecular classification of breast carcinoma: a 2015 update," *Archives of Pathology & Laboratory Medicine*, vol. 140, pp. 806-814, 2016.
- [52] D.-Y. Wang, Z. Jiang, Y. Ben-David, J. R. Woodgett and E. Zacksenhaus, "Molecular stratification within triple-negative breast cancer subtypes," *Scientific Reports*, vol. 9, no. 19, 2019.
- [53] D. L. Ellsworth, C. E. Turner and R. E. Ellsworth, "A review of the hereditary component of triple negative breast cancer: high- and moderate-penetrance breast cancer genes, low-penetrance loci, and the role of nontraditional genetic elements," *Journal of Oncology*, p. 10, 2019.
- [54] A. R. Venkitaraman, "Functions of BRCA1 and BRCA2 in the biological response to DNA damage," *Journal of Cell Science*, vol. 114, pp. 3591-3598, 2001.
- [55] A. Marra, G. Viale and G. Curigliano, "Recent advances in triple negative breast cancer: the immunotherapy era," *BMC Medicine*, vol. 17, no. 90, 2019.
- [56] E. Montagna, P. Maisonneuve, N. Rotmensz, G. Canello, M. Iorfida, A. Balduzzi, V. Galimberti, P. Veronesi, A. Luini, G. Pruneri, L. Bottiglieri, M. G. Mastropasqua, A. Goldhirsch, G. Viale and M. Colleoni, "Heterogeneity of triple-negative breast cancer: histologic subtyping to inform the outcome," *Clinical Breast Cancer*, vol. 13, no. 1, pp. 31-39, 2013.
- [57] D. Hanahan and L. M. Coussens, "Accessories to the crime: functions of cells recruited to the tumor microenvironment," *Cancer Cell*, vol. 21, no. 3, pp. 309-322, 2012.

- [58] G. P. Dunn, L. J. Old and R. D. Schreiber, "The immunobiology of cancer immunosurveillance and immunoediting," *Immunity*, vol. 21, no. 2, pp. 137-148, 2004.
- [59] H. Tower, M. Ruppert and K. Britt, "The immune microenvironment of breast cancer progression," *Cancers*, vol. 11, no. 9, 2019.
- [60] L. Hui and Y. Chen, "Tumor microenvironment: Sanctuary of the devil," *Cancer Letters*, vol. 368, pp. 7-13, 2015.
- [61] B. S. Kochupurakkal, Z. C. Wang, T. Hua, A. C. Culhane, S. J. Rodig, K. Rojkovic-Molek, J.-B. Lazaro, A. L. Richardson, D. K. Biswas and J. D. Iglehart, "RelA-induced interferon response negatively regulates proliferation," *PLoS One*, vol. 10, no. 10, 2015.
- [62] M. Mojic, K. Takeda and Y. Hayakawa, "The dark side of IFN- $\gamma$ : its role in promoting cancer immunoevasion," *International Journal of Molecular Sciences*, vol. 19, no. 1, 2018.
- [63] A. J. G. Schottelius, M. W. Mayo, R. B. Sartor and A. S. Baldwin, "Interleukin-10 signaling blocks inhibitor of kappaB kinase activity and nuclear factor kappaB DNA binding," *Journal of Biological Chemistry*, vol. 274, no. 45, pp. 31868-31864, 1999.
- [64] G. Landskron, M. De la Fuente, C. Thuwajit and M. A. Hermoso, "Chronic inflammation and cytokines in the tumor microenvironment," *Journal of Immunology Research*, vol. 2014, no. 149185, 2014.
- [65] Y. Wu and B. P. Zhou, "TNF- $\alpha$ /NF- $\kappa$ B/Snail pathway in cancer cell migration and invasion," *British Journal of Cancer*, vol. 102, pp. 639-644, 2010.
- [66] J. J. O'Shea, D. M. Schwartz, A. V. Villarino, M. Gadina, I. B. McInnes and A. Laurence, "The JAK-STAT pathway: impact on human disease and therapeutic intervention," *Annual Review of Medicine*, vol. 66, pp. 311-328, 2015.
- [67] J. K. Riley, K. Takeda, S. Akira and R. D. Schreiber, "Interleukin-10 receptor signaling through the JAK-STAT pathway: requirement for two distinct receptor-derived signals for anti-inflammatory action," *Journal of Biological Chemistry*, vol. 274, no. 23, pp. 16513-16521, 1999.
- [68] E. S. Acuner-Ozababacan, B. H. Engin, E. Guven-Maiorov, G. Kuzu, S. Muratcioglu, A. Baspinar, Z. Chen, C. Van Waes, A. Gurosy, O. Keskin and R.

- Nussinov, "The structural network of Interleukin-10 and its implications in inflammation and cancer," *BMC Genomics*, vol. 15, no. Suppl 4, 2014.
- [69] M. Esquivel-Velazquez, P. Ostoa-Saloma, M. I. Palacios-Arreola, K. E. Nava-Castro, J. I. Castro and J. Morales-Montor, "The role of cytokines in breast cancer development and progression," *Journal of Interferon & Cytokine Research*, vol. 35, no. 1, pp. 1-16, 2015.
- [70] S.-Q. Qui, S. J. H. Waaijer, M. C. Zwager, E. G. E. de Vries, B. van der Vergt and C. P. Schroder, "Tumor-associated macrophages in breast cancer: Innocent bystander or important player?," *Cancer Treatment Reviews*, vol. 70, pp. 178-189, 2018.
- [71] M. Liguori, G. Solinas, G. Germano, A. Manovani and P. Allavena, "Tumor-associated macrophages as incessant builders and destroyers of the cancer stroma," *Cancers (Basel)*, vol. 3, no. 4, pp. 3740-3761, 2011.
- [72] S. D. Jayasingam, M. Citartan, T. H. Thang, A. A. M. Zin, K. Cheen Ang and E. W. Cheng, "Evaluating the polarization of tumor-associated macrophages into M1 and M2 phenotypes in human cancer tissue: technicalities and challenges in routine clinical practice," *Frontiers in Oncology*, vol. 9, no. 1512, 2020.
- [73] J. M. Houthuijzen and J. Jonkers, "Cancer-associated fibroblasts as key regulators of the breast cancer tumor microenvironment," *Cancer and Metastasis Reviews*, vol. 37, pp. 577-597, 2018.
- [74] C. Jotzu, E. Alt, G. Welte, J. Li, B. T. Hennessy, E. Devarajan, S. Krishnappa, S. Pinilla, L. Droll and Y. H. Song, "Adipose tissue-derived stem cells differentiate into carcinoma-associated fibroblast-like cells under the influence of tumor-derived factors," *Analytical Cellular Pathology*, vol. 33, no. 2, pp. 61-79, 2010.
- [75] C. Guido, D. Whitaker-Menezes, C. Capparelli, R. Balliet, Z. Lin, R. G. Pestell, A. Howell, S. Aquila, S. Ando, U. Martinez-Outschoorn, F. Sotgia and M. P. Lisanti, "Metabolic reprogramming of cancer-associated fibroblasts by TGF- $\beta$  drives tumor growth," *Cell Cycle*, vol. 11, no. 16, pp. 3019-3035, 2012.
- [76] A. Aboussekhra, "Role of cancer-associated fibroblasts in breast cancer development and prognosis," *The International Journal of Developmental Biology*, vol. 55, pp. 841-849, 2011.

- [77] M. K. Wendt, T. M. Allington and W. P. Schiemann, "Mechanisms of epithelial-mesenchymal transition by TGF- $\beta$ ," *Future Oncology*, vol. 5, no. 8, pp. 1145-1168, 2010.
- [78] J. Zhou, X. H. Wang, Y. X. Zhao, C. Chen, X. Xu, Q. Sun, H. C. M. Wu, J. F. Sang, L. Su, X. Q. Tang, X. B. Shi, Y. Zhang, Q. Yu, Y. Z. Yao and W. J. Zhang, "Cancer-associated fibroblasts correlate with tumor-associated macrophages infiltration and lymphatic metastasis in triple negative breast cancer patients," *Journal of Cancer*, vol. 9, no. 24, pp. 4635-4641, 2018.
- [79] B. Dirat, L. Bochet, M. Dabek, D. Daviaud, S. Dauvillier, B. Majed, Y. Y. Wang, A. Muelle, B. Salles, S. Le Gonidec, I. Garrido, G. Escourrou, P. Valet and C. Muller, "Cancer-associated adipocytes exhibit an activated phenotype and contribute to breast cancer invasion," *Cancer Research*, vol. 71, no. 7, pp. 2455-2465, 2011.
- [80] J. A. Cho, H. Park, E. H. Lim and K. W. Lee, "Exosomes from breast cancer cells can convert adipose tissue-derived mesenchymal stem cells into myofibroblast-like cells," *International Journal of Oncology*, vol. 40, pp. 130-138, 2012.
- [81] J. Lee, B. S. Hong, H. S. Ryu, H. B. Lee, M. Lee, I. A. Park, J. Kim, W. Han, D. Y. Noh and G. H. M, "Transition into inflammatory cancer-associated adipocytes in breast cancer microenvironment requires microRNA regulatory mechanism," *PLoS One*, vol. 12, no. 3, 2017.
- [82] Q. Wu, B. Li, Z. Li, J. Li, S. Sun and S. Sun, "Cancer-associated adipocytes: key players in breast cancer progression," *Journal of Hematology & Oncology*, vol. 12, no. 95, 2019.
- [83] Y. Cao, "Adipocyte and lipid metabolism in cancer drug resistance," *The Journal of Clinical Investigation*, vol. 129, no. 8, pp. 3006-3017, 2019.
- [84] S. Beloribi-Djefafia, S. Vasseur and F. Guillaumond, "Lipid metabolic reprogramming in cancer cells," *Oncogenesis*, vol. 5, no. 189, 2016.
- [85] S. Balaban, R. F. Shearer, L. S. Lee, M. van Geldermalsen, M. Schreuder, H. C. Shtein, R. Carins, K. C. Thomas, D. J. Fazakerley, T. Grewal, J. Holst, D. N. Saunders and A. J. Hoy, "Adipocyte lipolysis links obesity to breast cancer growth: adipocyte-derived fatty acids drive breast cancer cell proliferation and migration," *Cancer & Metabolism*, vol. 5, no. 1, 2017.

- [86] M. Chen and J. Huang, "The expanded role of fatty acid metabolism in cancer: new aspects and targets," *Precision Clinical Medicine*, vol. 2, no. 3, pp. 183-191, 2019.
- [87] Y. Y. Wang, C. Attane, D. Milhas, B. Dirat, S. Dauvillier, A. Guerard, J. Gilhodes, I. Lazar, N. Alet, V. Laurent, S. Le Gonidec, D. Biard, C. Herve, F. Bost, G. Sheng Ren, F. Bono, G. Escourrou, M. Prentki, L. Nieto and P. M. C. Valet, "Mammary adipocytes stimulate breast cancer invasion through metabolic remodeling of tumor cells," *JCI Insight*, vol. 2, no. 4, 2017.
- [88] R. A. Hegele, "Plasma lipoproteins: genetic influences and clinical implications," *Nature Reviews Genetics*, vol. 10, no. 2, pp. 109-121, 2009.
- [89] R. W. Mahley, T. L. Innerarity, S. C. J. Rall and K. H. Weisgraber, "Plasma lipoproteins: apolipoprotein structure and function," *Journal of Lipid Research*, vol. 25, no. 12, pp. 1277-1294, 1984.
- [90] A. Jonas and M. C. Phillips, "Lipoprotein structure," in *Biochemistry of Lipids, Lipoproteins, and Membranes (5th Edn.)*, Amsterdam, Boston: Elsevier, 2008, pp. 485-506.
- [91] J. E. Vance and K. Adeli, "Assembly and secretion of triacylglycerol-rich lipoproteins," in *Biochemistry of Lipids, Lipoproteins, and Membranes (5th Edn.)*, Amsterdam, Boston: Elsevier, 2008, pp. 507-531.
- [92] H. Heid, S. Rickelt, R. Zimbelmann, S. Winter, H. Schumacher, Y. Dorflinger, C. Kuhn and W. W. Franke, "On the formation of lipid droplets in human adipocytes: the organization of the perilipin–vimentin cortex," *PLoS One*, vol. 9, no. 2, 2014.
- [93] R. W. Mahley, "Apolipoprotein E: cholesterol transport protein with expanding role in cell biology," *Science*, vol. 240, no. 4852, pp. 622-630, 1988.
- [94] W. J. Schneider, "Lipoprotein receptors," in *Biochemistry of Lipids, Lipoproteins, and Membranes (5th Edn.)*, Amsterdam, Boston: Elsevier, 2008, pp. 555-578.
- [95] S. Tiwari and S. A. Siddiqi, "Intracellular trafficking and secretion of VLDL," *Arteriosclerosis, Thrombosis, and Vascular Biology*, vol. 32, no. 5, pp. 1079-1086, 2012.
- [96] C. J. Fielding and P. E. Fielding, "Dynamics of lipoprotein transport in the circulatory system," in *Biochemistry of Lipids, Lipoproteins and Membranes (5th Edn.)*, Amsterdam, Boston: Elsevier, 2008, pp. 533-553.

- [97] J. L. Goldstein and M. S. Brown, "The LDL Receptor," *Arteriosclerosis, Thrombosis, and Vascular Biology*, vol. 29, no. 4, pp. 431-438, 2009.
- [98] M. Ouimet, T. J. Barrett and E. A. Fisher, "HDL and reverse cholesterol transport: basic mechanisms and their roles in vascular health and disease," *Circulation Research*, vol. 124, no. 10, 2019.
- [99] M. C. Phillips, "Molecular mechanisms of cellular cholesterol efflux," *Journal of Biological Chemistry*, vol. 289, no. 35, pp. 24020-24029, 2014.
- [100] I. Tabas, "Consequences of cellular cholesterol accumulation: basic concepts and physiological implications," *The Journal of Clinical Investigation*, vol. 110, no. 7, pp. 905-911, 2002.
- [101] H. Wong and M. C. Schotz, "The lipase gene family," *Journal of Lipid Research*, vol. 43, no. 7, pp. 993-999, 2002.
- [102] G. S. Richmond and T. K. Smith, "Phospholipases A1," *International Journal of Molecular Sciences*, vol. 12, no. 1, pp. 588-612, 2011.
- [103] I. Ishii, N. Fukushima, X. Ye and J. Chun, "Lysophospholipid receptors: signaling and biology," *Annual Review of Biochemistry*, vol. 73, pp. 321-354, 2004.
- [104] G. B. Mills and W. H. Moolenaar, "The emerging role of lysophosphatidic acid in cancer," *Nature Reviews Cancer*, vol. 3, no. 8, pp. 582-591, 2003.
- [105] W. A. Hide, L. Chan and W. H. Li, "Structure and evolution of the lipase superfamily," *Journal of Lipid Research*, vol. 33, no. 2, pp. 167-178, 1992.
- [106] H. van Tilbeurgh, A. Roussel, J. M. Lalouel and C. Cambillau, "Lipoprotein lipase molecular model based on the pancreatic lipase x-ray structure: consequences for heparin binding and catalysis," *Journal of Biological Chemistry*, vol. 269, no. 6, pp. 4626-4633, 1994.
- [107] R. J. Brown and D. J. Rader, "Lipases as modulators of atherosclerosis in murine models," *Current Drug Targets*, vol. 8, pp. 1307-1319, 2007.
- [108] B. Perret, L. Mabile, L. Martinez, F. Terce, R. Barbaras and X. Collet, "Hepatic lipase: structure/function relationship, synthesis, and regulation," *Journal of Lipid Research*, vol. 43, no. 8, pp. 1163-1169, 2002.

- [109] H. Jansen, A. J. M. Verhoeven and E. J. G. Sijbrands, "Hepatic lipase: a pro- or anti-atherogenic protein," *Journal of Lipid Research*, vol. 43, no. 8, pp. 1352-1362, 2002.
- [110] K. Hirata, H. L. Dichek, J. A. Cioffi, S. Y. Choi, N. J. Leeper, L. Quintana, G. S. Kronmal, A. D. Cooper and T. Quertermous, "Cloning of a unique lipase from endothelial cells extends the lipase gene family," *Journal of Biological Chemistry*, vol. 274, no. 20, pp. 14170-14175, 1999.
- [111] K. Preiss-Landl, R. Zimmerman, G. Hammerle and R. Zechner, "Lipoprotein lipase: the regulation of tissue specific expression and its role in lipid and energy metabolism," *Current Opinion in Lipidology*, vol. 13, no. 5, pp. 471-481, 2002.
- [112] N. B. Kuemmerle, E. Rysman, P. S. Lombardo, A. J. Flanagan, B. C. Lipe, W. A. Wells, J. R. Pettus, H. M. Froehlich, V. A. Memoli, P. M. Morganelli, J. V. Swinnen, L. A. Timmerman, C. L. C. J. Fricano, B. L. Eisenberg, W. B. Coleman and W. B. Kinlaw, "Lipoprotein lipase links dietary fat to solid tumor cell proliferation," *Molecular Cancer Therapeutics*, vol. 10, no. 3, pp. 427-436, 2011.
- [113] N. Griffon, E. C. Budreck, C. J. Long, U. C. Broedl, D. H. L. Marchadier, J. M. Glick and D. J. Rader, "Substrate specificity of lipoprotein lipase and endothelial lipase: studies of lid chimeras," *Journal of Lipid Research*, vol. 47, no. 8, pp. 1803-1811, 2006.
- [114] J. C. Cohen, "Endothelial lipase: direct evidence for a role in HDL metabolism," *The Journal of Clinical Investigation*, vol. 111, no. 3, pp. 318-321, 2003.
- [115] M. Merkel, R. H. Eckel and I. J. Goldberg, "Lipoprotein lipase, genetics, lipid uptake, and regulation," *Journal of Lipid Research*, vol. 43, no. 12, pp. 1997-2006, 2002.
- [116] J. E. A. Braun and D. L. Severson, "Regulation of the synthesis, processing and translocation of lipoprotein lipase," *Biochemical Journal*, vol. 287, no. 2, pp. 337-347, 1992.
- [117] R. Arora, A. V. Nimonkar, D. Baird, C. Wang, C. H. Chiu, P. A. Horton, S. Hanrahan, R. Cubbon, S. Weldon, W. R. Tschantz, S. Mueller, R. Brunner, P. Lehr, P. Meier, J. Ottl, A. Voznesensky, P. Pandey, T. M. Smith, A. Stojanovic, A. Flyer and J. W. Trauger, "Structure of lipoprotein lipase in complex with GPIHBP1," *PNAS*, vol. 116, no. 21, pp. 10360-10365, 2019.

- [118] C. K. Hayne, H. Yumerefendi, L. Cao, J. W. Gauer, M. J. Lafferty, B. Kuhlman, D. A. Erie and S. B. Neher, "We FRET so you don't have to: new models of the lipoprotein lipase dimer," *Biochemistry*, vol. 57, no. 2, pp. 241-254, 2018.
- [119] M. H. Doolittle, N. Ehrhardt and M. Peterfy, "Lipase maturation factor 1 (Lmf1): structure and role in lipase folding and assembly," *Current Opinion in Lipidology*, vol. 21, no. 3, pp. 198-203, 2010.
- [120] R. A. Hegele, "Multidimensional regulation of lipoprotein lipase: impact on biochemical and cardiovascular phenotypes," *Journal of Lipid Research*, vol. 57, no. 9, pp. 1601-1607, 2016.
- [121] G. Birrane, A. P. Beigneux, B. Dwyer, B. Stack-Logue, K. K. Kristensen, O. L. Francone, L. G. Fong, H. D. T. Mertens, C. Q. Pan, M. Ploug, S. G. Young and M. Meiyappan, "Structure of the lipoprotein lipase-GPIHBP1 complex that mediates plasma triglyceride hydrolysis," *Proceedings of the National Academy of Sciences of the United States of America*, vol. 116, no. 5, pp. 1723-1732, 2019.
- [122] C. M. Allan, M. Larsson, R. S. Jung, M. Ploug, A. Bensadoun, A. P. Beigneux, L. G. Fong and S. G. Young, "Mobility of "HSPG-bound" LPL explains how LPL is able to reach GPIHBP1 on capillaries," *Journal of Lipid Research*, vol. 58, no. 1, pp. 216-225, 2017.
- [123] M. C. Jong, M. H. Hofker and L. M. Havekes, "Role of apoCs in lipoprotein metabolism," *Arteriosclerosis, Thrombosis and Vascular Biology*, vol. 19, no. 3, pp. 472-484, 1999.
- [124] M. R. Krauss, P. N. Herbet, R. I. Levy and D. S. Frederickson, "Further observations on the activation and inhibition of lipoprotein lipase by apolipoproteins," *Circulation Research*, vol. 33, pp. 403-411, 1973.
- [125] T. S. Tengku-Muhammad, A. Cryer and D. P. Ramji, "Synergism between interferon gamma and tumour necrosis factor alpha in the regulation of lipoprotein lipase in the macrophage J774.2 cell line," *Cytokine*, vol. 10, no. 1, pp. 38-48, 1998.
- [126] H. Wang and R. H. Eckel, "Lipoprotein lipase: from gene to obesity," *The American Journal of Physiology-Endocrinology and Metabolism*, vol. 297, no. 2, pp. 271-288, 2009.

- [127] S. Lanza-Jacoby, S. C. Lansey, E. E. Miller and M. P. Cleary, "Sequential changes in the activities of lipoprotein lipase and lipogenic enzymes during tumor growth in rats," *Cancer Research*, vol. 44, no. 11, pp. 5062-5067, 1984.
- [128] J. R. Mead and D. P. Ramji, "The pivotal role of lipoprotein lipase in atherosclerosis," *Cardiovascular Research*, vol. 55, no. 2, pp. 261-269, 2002.
- [129] S. A. Irvine, P. Foka, S. A. Rogers, J. R. Mead and D. P. Ramji, "A critical role for the SP1-binding sites in the transforming growth factor- $\beta$ -mediated inhibition of lipoprotein lipase gene expression in macrophages," *Nucleic Acids Research*, vol. 33, no. 5, pp. 1423-1434, 2005.
- [130] Y. Essaji, Y. Yang, C. J. Albert, D. A. Ford and R. J. Brown, "Hydrolysis products generated by lipoprotein lipase and endothelial lipase influence macrophage cell signalling pathways," *Lipids*, vol. 48, no. 8, pp. 769-778, 2013.
- [131] S. Jansson, K. Aaltonen, P. O. Bendahl, A. K. Falck, M. Karlsson, K. Pietras and L. Ryden, "The PDGF pathway in breast cancer is linked to tumour aggressiveness, triple-negative subtype and early recurrence," *Breast Cancer Research and Treatment*, vol. 169, no. 2, pp. 231-241, 2018.
- [132] A. A. Farooqi and Z. H. Siddik, "Platelet-derived growth factor (PDGF) signalling in cancer: rapidly emerging signalling landscape," *Cell Biochemistry and Function*, vol. 33, no. 5, pp. 257-265, 2015.
- [133] M. P. Pinto, W. W. Dye, B. M. Jacobsen and K. B. Horwitz, "Malignant stroma increases luminal breast cancer cell proliferation and angiogenesis through platelet-derived growth factor signaling," *BMC Cancer*, vol. 14, no. 1, 2014.
- [134] N. Thyagarajan, J. D. Marshall, A. T. Pickett, C. Schumacher, Y. Yang, S. L. Christian and R. J. Brown, "Transcriptomic analysis of THP-1 macrophages exposed to lipoprotein hydrolysis products generated by lipoprotein lipase," *Lipids*, vol. 52, no. 3, pp. 189-205, 2017.
- [135] L. Wang, R. Gill, T. L. Pedersen, L. J. Higgins, J. W. Newman and J. C. Rutledge, "Triglyceride-rich lipoprotein lipolysis releases neutral and oxidized FFAs that induce endothelial cell inflammation," *Journal of Lipid Research*, vol. 50, no. 2, pp. 204-213, 2009.
- [136] S. L. Figenschau, E. Knutsen, I. Urbarova, C. Fenton, B. Elston, M. Perander, E. S. Mortensen and K. A. Fenton, "ICAM1 expression is induced by

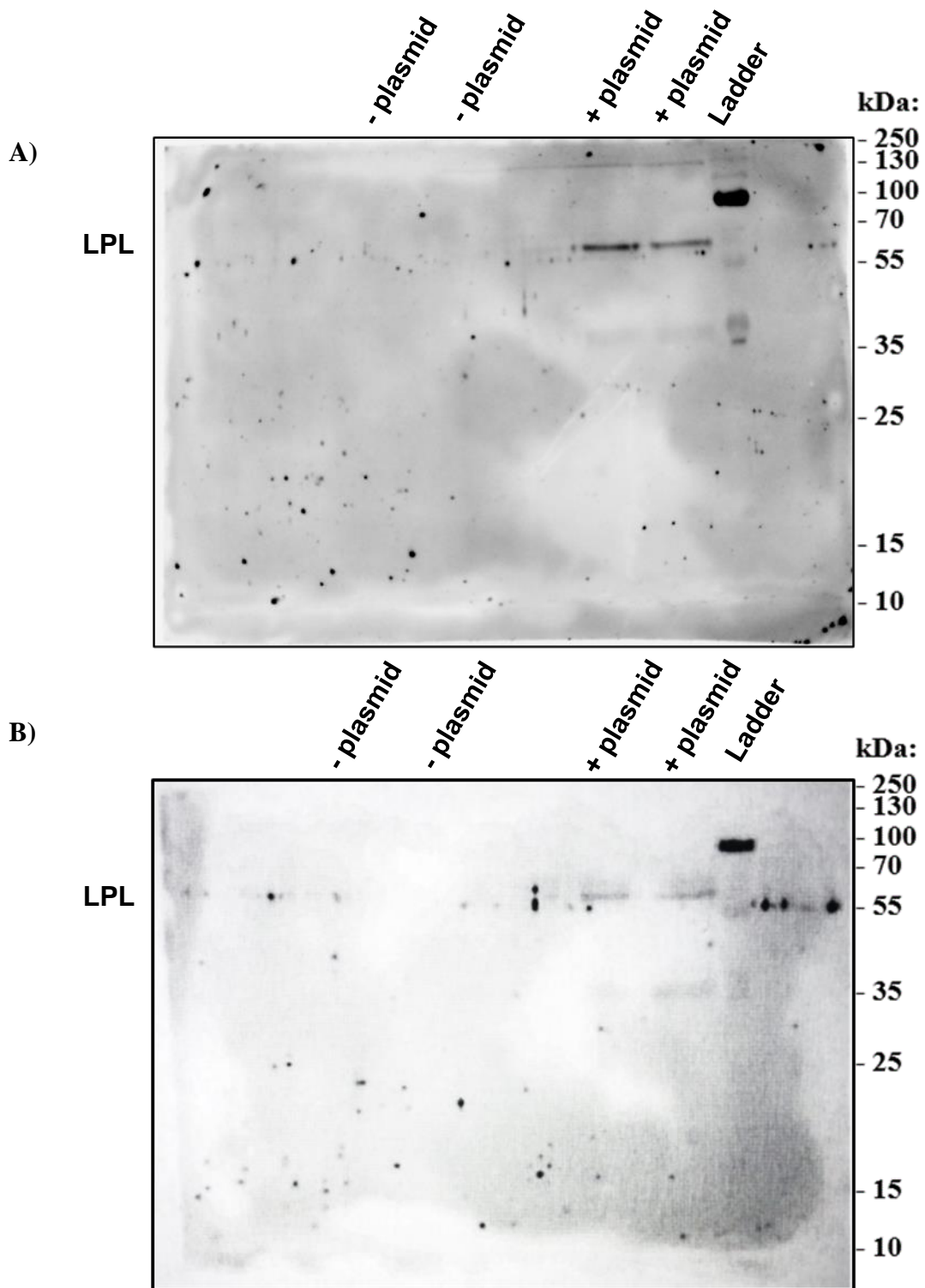
proinflammatory cytokines and associated with TLS formation in aggressive breast cancer subtypes," *Scientific Reports*, vol. 9, no. 11720, 2018.

- [137] C. F. Semenkovich, S. H. Chen, M. Wims, C. C. Luo, W. H. Li and L. Chan, "Lipoprotein lipase and hepatic lipase mRNA tissue specific expression, developmental regulation, and evolution," *Journal of Lipid Research*, vol. 30, no. 3, pp. 423-431, 1989.
- [138] C. A. Schneider, W. S. Rasband and K. W. Eliceiri, "NIH Image to ImageJ: 25 years of image analysis," *Nature Methods*, vol. 9, no. 7, pp. 671-675, 2012.
- [139] R. Lehner and R. Verger, "Purification and characterization of a porcine liver microsomal triacylglycerol hydrolase," *Biochemistry*, vol. 36, no. 7, pp. 1861-1868, 1997.
- [140] M. S. Pitts, J. N. McShane, M. C. Hoener, S. L. Christian and M. D. Berry, "TAAR1 levels and sub-cellular distribution are cell line but not breast cancer subtype specific," *Histochemistry and Cell Biology*, vol. 152, pp. 155-166, 2019.
- [141] Q. Cao, H. Ruan, K. Wang, Z. Song, L. Bao, T. Xu, H. Xiao, C. Wang, G. Cheng, J. Tong, X. Meng, D. Liu, H. Yang, K. Chen and X. Zhang, "Overexpression of PLIN2 is a prognostic marker and attenuates tumor progression in clear cell renal cell carcinoma," *International Journal of Oncology*, vol. 53, no. 1, pp. 137-147, 2018.
- [142] K. S. Lucenay, I. Doostan, C. Karakas, T. Bui, Z. Ding, G. B. Mills, K. K. Hunt and K. Keyomarsi, "Cyclin E associates with the lipogenic enzyme ATP-citrate lyase to enable malignant growth of breast cancer cells," *Cancer Research*, vol. 76, no. 8, pp. 2406-2418, 2016.
- [143] S. M. Houten, S. Violante, F. V. Ventura and R. J. A. Wanders, "The biochemistry and physiology of mitochondrial fatty acid  $\beta$ -oxidation and its genetic disorders," *Annual Review of Physiology*, vol. 78, pp. 23-44, 2016.
- [144] J. D. Marshall, E. R. Courage, R. F. Elliot, M. N. Fitzpatrick, A. D. Kim, A. F. Lopez-Clavijo, B. A. Woolfrey, M. Ouimet, M. J. O. Wakelam and R. J. Brown, "THP-1 macrophage cholesterol efflux is impaired by palmitoleate through Akt activation," *PLoS One*, vol. 15, no. 5, 2020.
- [145] Q. Qu, F. Zeng, X. Liu, Q. J. Wang and F. Deng, "Fatty acid oxidation and carnitine palmitoyltransferase I: emerging therapeutic targets in cancer," *Cell Death & Disease*, vol. 7, no. 2226, 2016.

- [146] B. D. Manning and A. Toker, "AKT/PKB Signaling: Navigating the Network," *Cell*, vol. 169, pp. 381-405, 2017.
- [147] A. R. Clark and A. Toker, "Signalling specificity in the akt pathway in breast cancer," *Biochemical Society Transactions*, vol. 42, no. 5, pp. 1349-1355, 2014.
- [148] T. Porstmann, C. R. Santos, B. Griffiths, M. Cully, M. L. S. Wu, J. R. Griffiths, Y. L. Chung and A. Schulze, "SREBP activity is regulated by mtorc1 and contributes to akt-dependent cell growth," *Cell Metabolism*, vol. 8, no. 3, pp. 224-236, 2008.
- [149] B. Sun, G. Wang, H. Liu, P. Liu, W. O. Twal, H. Cheung, S. L. Carroll, S. P. Ethier, E. E. Mevers, C. J. T. Roberts, C. Chen, Q. Li, L. Wang, M. Yang and J. J. Zhao, "Oridonin inhibits aberrant AKT activation in breast cancer," *Oncotarget*, vol. 9, no. 35, pp. 23878-23889, 2018.
- [150] M. Cully, H. You, A. J. Levine and T. W. Mak, "Beyond PTEN mutations: the PI3K pathway as an intergrator of multiple inputs during tumorigenesis," *Nature Reviews: Cancer*, vol. 6, no. 3, pp. 184-192, 2006.
- [151] Riss, T. L., R. A., Moravec, A. L. Niles, S. Duellman, H. A. Benink, T. J. Worzella and L. Minor, Cell viability assays, Eli Lilly & Company and the National Center for Advancing Translational Sciences, 2004.
- [152] T. Inaba, M. Kawamura, T. Gotoda, K. Harada, M. Shimada, J. Ohsuga, H. Shimano, Y. Akanuma, Y. Y and N. Yamada, "Effects of platelet-derived growth factor on the synthesis of lipoprotein lipase in human monocyte-derived macrophages," *Arteriosclerosis, Thrombosis, and Vascular Biology*, vol. 15, pp. 522-528, 1995.
- [153] N. Todorovic-Rakovic and J. Milovanovic, "Interleukin-8 in breast cancer progression," *Journal of Interferon & Cytokine Research*, vol. 33, no. 10, pp. 563-570, 2013.
- [154] S. Nagai and M. Toi, "Interleukin-4 and breast cancer," *Breast Cancer*, vol. 7, no. 3, pp. 181-186, 2000.
- [155] M. Metzemaekers, V. Vanheule, R. Janssens, S. Struyf and P. Proost, "Overview of the mechanisms that may contribute to the non-redundant activities of interferon-inducible CXC chemokine receptor 3 ligands," *Frontiers in Immunology*, vol. 8, no. 1970, 2018.
- [156] K. J. Baker, A. Houston and E. Brint, "IL-1 family members in cancer; two sides to every story," *Frontiers in Immunology*, vol. 10, no. 1197, 2019.

- [157] M. K. Sgagias, A. Kasid and D. N. J. Danforth, "Interleukin-1 alpha and tumor necrosis factor-alpha (TNF alpha) inhibit growth and induce TNF messenger RNA in MCF-7 human breast cancer cells," *Molecular Endocrinology*, vol. 5, no. 11, pp. 1740-1747, 1991.
- [158] O. Kourko, K. Seaver, N. Odoardi, S. Basta and K. Gee, "IL-27, IL-30, and IL-35: a cytokine triumvirate in cancer," *Frontiers in Oncology*, vol. 9, no. 969, 2019.
- [159] Y. Liu, A. Beyer and R. Aebersold, "On the dependency of cellular protein levels on mRNA abundance," *Cell*, vol. 165, pp. 535-550, 2016.
- [160] O. Ben-Zeev, G. Stahnke, G. Liu, R. C. Davis and M. H. Doolittle, "Lipoprotein lipase and hepatic lipase: the role of asparagine-linked glycosylation in the expression of a functional enzyme," *Journal of Lipid Research*, vol. 35, no. 9, pp. 1511-1523, 1994.
- [161] M. E. Monaco, "Fatty acid metabolism in breast cancer subtypes," *Oncotarget*, vol. 8, no. 17, pp. 29487-29500, 2017.

## **Appendix I: Supplementary data**



**Supplemental Figure 1: Western blot to detect LPL protein expression, additional replicates**

HEK-293 cells were transfected with or without LPL plasmid. Heparinized media and cell lysates were collected from both groups. (A & B) Western blot of heparinized media from transfected cells to detect LPL.

**Supplemental Table 1: Summarized data from the cytokine array analysis of MDA-MB-231 breast cancer cell supernatant from cells treated with total lipoprotein hydrolysis products generated by LPL or mock heparinized media**

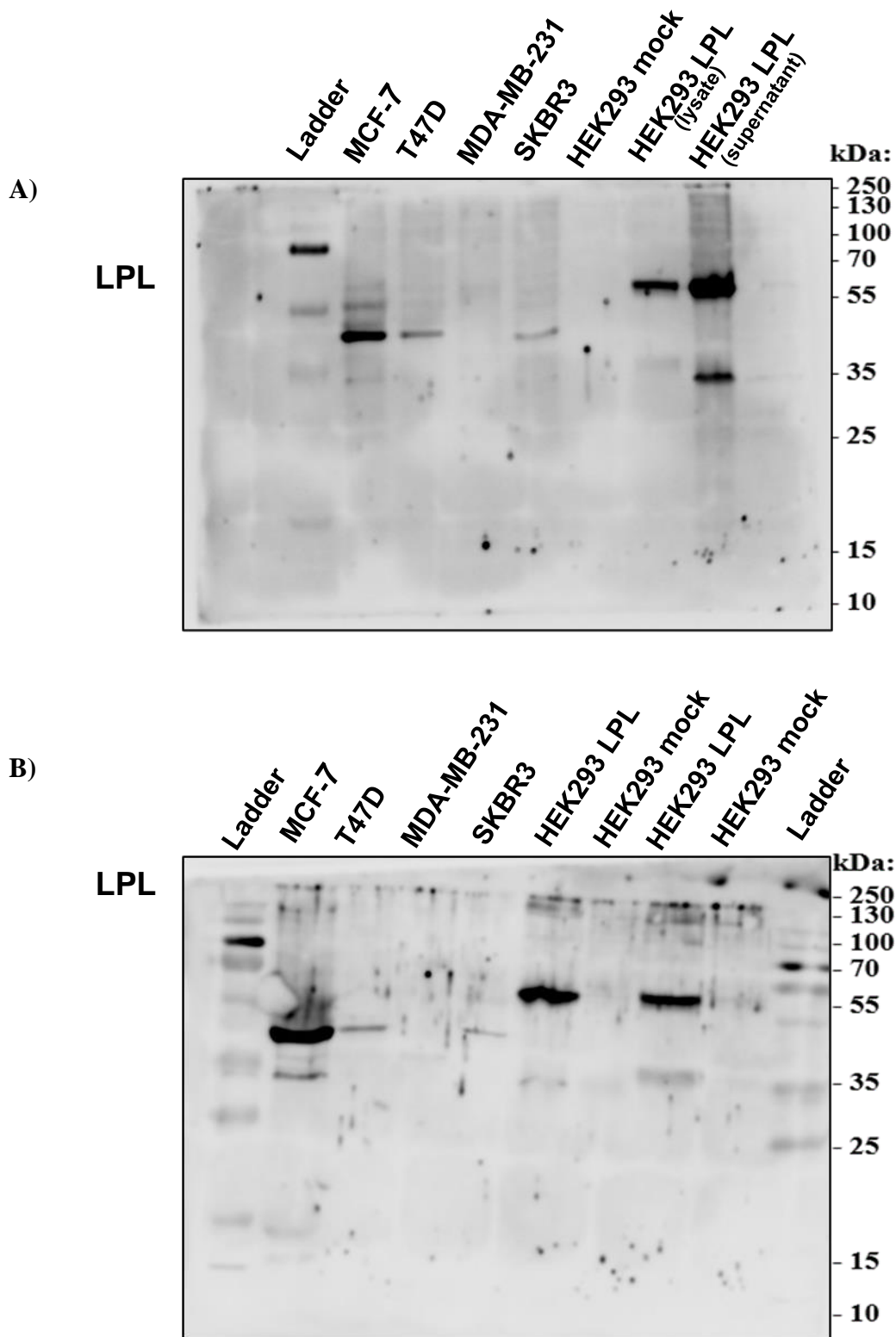
SAMPLE	Mock per Average Reference		HP per Average Reference		p-value
	Avg	SD	Avg	SD	
Reference	0.950452	0.055559	0.953179	0.020938	n/a
CCL1/I-309	0.002923	0.001715	0.00624	0.002456	0.063775
CCL2	0.011846	0.010441	0.020225	0.008817	0.174054
MIP-1 $\alpha$ /MIP-1 $\beta$	0.001949	0.001752	0.003635	0.002608	0.202592
CCL5/RANTES	0.013301	0.006824	0.026532	0.008626	0.052802
CD40 Ligand	0.00416	0.003823	0.007663	0.004511	0.181447
C5/C5a	0.00159	0.001576	0.00502	0.002307	0.050303
<b>CXCL1/GRO<math>\alpha</math></b>	0.436649	0.03717	0.4987	0.025919	<b>0.038336</b>
CXCL10/IP-10	0.003282	0.001735	0.005583	0.001978	0.102238
Reference	1.096387	0.108829	0.996837	0.045558	n/a
<b>CXCL11</b>	0.003493	0.001742	0.006369	0.001382	<b>0.044258</b>
CXCL12	0.017889	0.009789	0.029356	0.015059	0.165432
G-CSF	0.087605	0.02504	0.127237	0.047882	0.136407
GM-CSF	0.184296	0.054862	0.264802	0.065704	0.08932
<b>ICAM-1/CD54</b>	0.043449	0.003583	0.069594	0.003416	<b>0.000397</b>
IFN- $\gamma$	0.003994	0.002276	0.008816	0.003819	0.066761
IL-1 $\alpha$ /IL-1F1	0.006876	0.003323	0.014043	0.005391	0.060787
IL-1 $\beta$	0.000997	0.001727	0.003194	0.001282	0.075807
IL-1ra/IL-1F3	0.004068	0.002967	0.005553	0.004094	0.31889
IL-2	0.002934	0.001532	0.004124	0.002828	0.278309
<b>IL-4</b>	0.00082	0.001254	0.00385	0.001562	<b>0.029384</b>
IL-5	0.002128	0.001158	0.004195	0.002418	0.126306
<b>IL-6</b>	0.407422	0.024457	0.684525	0.111108	<b>0.006746</b>
<b>IL-8</b>	0.847102	0.126748	1.110999	0.069154	<b>0.016999</b>
IL-10	0.002555	0.003001	0.006672	0.002081	0.061304
IL-12 p70	0.001291	0.001163	0.004422	0.002864	0.077107
IL-13	0.004397	0.002036	0.004406	0.001417	0.497568
IL-16	0.004305	0.002177	0.004166	0.001735	0.467478
IL-17A	0.001796	0.002658	0.002771	0.003413	0.358145
IL-17E	0.005732	0.003186	0.009331	0.002505	0.099444
IL-18/IL-1F4	0.025771	0.02144	0.044171	0.030125	0.218669
IL-21	0.003497	0.002588	0.008043	0.002939	0.057365
IL-27	0.001828	0.001514	0.00408	0.002209	0.109497
IL-32 $\alpha$	0.002749	0.002199	0.004744	0.001876	0.148966
Reference	0.953161	0.065582	1.049984	0.035963	n/a
MIF	0.239509	0.033918	0.291352	0.040565	0.082351

Serpin E1	0.445025	0.049865	0.516378	0.079239	0.128646
<b>TNF-<math>\alpha</math></b>	0.000478	0.000519	0.003487	0.002399	<b>0.050487</b>
TREM-1	0.001584	0.001741	0.002483	0.002743	0.328329
Negative control	0	0	0	0	0

**Supplemental Table 2: Summarized data from the cytokine array analysis of MCF-7 breast cancer cell supernatant from cells treated with total lipoprotein hydrolysis products generated by LPL or mock heparinized media**

SAMPLE	Mock per Average Reference		HP per Average Reference		p-value
	Avg	SD	Avg	SD	
Reference	1.00043	0.057629	0.907397	0.040549	n/a
CCL1/I-309	0.003309	0.000982	0.002601	0.002784	0.349666
CCL2	0.002225	0.000643	0.001396	0.000704	0.103345
MIP-1 $\alpha$ /MIP-1 $\beta$	0.002369	0.000778	0.002946	0.002479	0.360191
CCL5/RANTES	0.02281	0.004577	0.026126	0.002375	0.16389
CD40 Ligand	0.00311	0.00088	0.002868	0.001128	0.391923
C5/C5a	0.000591	0.000714	0.000194	0.000335	0.216054
CXCL1/GRO $\alpha$	0.005208	0.001158	0.003293	0.003138	0.188845
CXCL10/IP-10	0.001066	0.000214	0.000968	0.000949	0.434755
Reference	1.004453	0.02834	1.049637	0.055163	n/a
CXCL11	0.002127	0.000959	0.002253	0.001391	0.451848
CXCL12	0.026887	0.010009	0.028842	0.006204	0.393984
G-CSF	0.002664	0.001061	0.003366	0.003653	0.382609
GM-CSF	0.000753	0.000829	0.001471	0.000345	0.119076
ICAM-1/CD54	0.00462	0.000895	0.004581	0.001316	0.483942
IFN- $\gamma$	0.003062	0.001484	0.003034	0.001641	0.491629
<b>IL-1<math>\alpha</math>/IL-1F1</b>	0.003896	0.001379	0.001428	0.001456	<b>0.050014</b>
IL-1 $\beta$	0.000666	0.000582	8.15E-05	0.000141	0.083259
IL-1ra/IL-1F3	0.004386	0.001791	0.003609	0.002779	0.352375
IL-2	0.001522	0.000268	0.00185	0.000664	0.235452
IL-4	0.001144	7.73E-05	0.0009	0.000848	0.323091
IL-5	0.001068	0.000988	0.000749	0.000659	0.332636
IL-6	0.001459	0.00057	0.000623	0.000571	0.073685
IL-8	0.006884	0.00051	0.006323	0.001782	0.313747
IL-10	0.000358	0.00062	9.03E-05	0.000156	0.254355
IL-12 p70	0.000872	0.000511	0.000282	0.00028	0.077161
IL-13	0.003947	0.000929	0.002174	0.003049	0.194885
IL-16	0.003731	0.001926	0.00171	0.001638	0.119244
IL-17A	0.001968	0.001707	0.000324	0.000464	0.091333
IL-17E	0.00589	0.002098	0.007295	0.003553	0.293543
IL-18/IL-1F4	0.020425	0.005493	0.025998	0.007984	0.187792
IL-21	0.001046	0.000976	0.00138	0.001793	0.39548
<b>IL-27</b>	0.001147	0.000797	0.000145	0.000127	<b>0.048985</b>
IL-32 $\alpha$	0.002628	0.000393	0.002047	0.003131	0.382814
Reference	0.995117	0.033912	1.042966	0.016252	n/a
MIF	0.158458	0.04234	0.18721	0.060633	0.268792

Serpin E1	0.075094	0.018996	0.07988	0.016548	0.379314
TNF- $\alpha$	0.001012	0.001182	0.000625	0.000816	0.332269
TREM-1	0.000703	0.001218	0.000129	0.000223	0.233475
Negative control	0	0	0	0	0



**Supplemental Figure 2: Western blot to detect LPL protein expression in breast cancer cell lysates, additional replicates**

Recombinant human LPL from HEK-293 cell transfection was used as a positive control. Aberrantly expressed LPL was detected in the cell lysates of MCF-7, T47D, and SKBR3 cells. LPL was not detected in the MDA-MB-231 cell lysate.